THESIS FOR THE DEGREE OF DOCTOR OF PHILOSOPHY

On Rate-Dependency of Gothenburg Clay

Mats Olsson

"If we knew what we were doing,
it would not be called research, would it…"

Albert Einstein

Department of Civil and Environmental Engineering
Division of GeoEngineering
CHALMERS UNIVERSITY OF TECHNOLOGY
Gothenburg, Sweden 2013

On Rate-Dependency of Gothenburg Clay

MATS OLSSON

ISBN 978-91-7385-911-0

Doktorsavhandling vid Chalmers tekniska högskola

Ny serie nr 3592

ISSN 0346-718X

Department of Civil and Environmental Engineering

Division of GeoEngineering

Chalmers University of Technology

SE-412 96 Göteborg

Sweden

Telephone + 46 (0)31 772 10 00

www.chalmers.se

Chalmers reproservice

Gothenburg, Sweden 2013

On Rate-Dependency of Gothenburg Clay
MATS OLSSON
Department of Civil and Environmental Engineering
Division of GeoEngineering
Chalmers University of Technology

ABSTRACT

Long-term settlements in clay constitute a major engineering challenge in areas with deep deposits of soft clay. This dissertation aims to extend the understanding and theoretical framework of rate-dependent soil behaviour, so that uncertainties in predictions of long-term settlements are significantly reduced. This is first done by looking at the basic behaviour of soft soils and some existing advanced constitutive models. The research comprised of the development of a new rate-dependent model called MAC-s which was implemented in COMSOL Multiphysics. A focus of the latter development was the prediction of the coefficient of lateral earth pressure at rest, K_0, during creep and unloading. In order to help validate the K_0 value, i.e. the ratio between the horizontal and vertical effective stress at normal consolidated conditions, a novel K_0-triaxial cell was developed and tested on samples of soft Gothenburg clay. The simulations of oedometer and undrained triaxial tests with the new model are in good agreement with experimental data. The test results from the K_0-triaxial cell indicate that the normally consolidated K_0 value of soft Gothenburg clay is in the range of 0.50-0.55, which does not match the commonly used empirical relations, based on the index properties of the clay.

More experimental tests should be performed to validate the model formulation, and gather comprehensive data on K_0 values for soft soils.

Keywords: Soft clay, creep, anisotropy, K_0-triaxial cell, destructuration.

ACKNOWLEDGMENTS

The work presented in this thesis was conducted at the Division of GeoEngineering at Chalmers University of Technology, under the supervision of Professor Claes Alén. Financial sponsors were Trafikverket, SBUF, NCC AB and Chalmers University of Technology, who are greatly acknowledged for their support.

I would like to thank my supervisor Professor Claes Alén for initiating this project and for his great interest and guidance during this project. I would also like to thank Professor Minna Karstunen and Professor Göran Sällfors for all their support and interesting discussions during the project.

I would also like to thank Dr Jelke Dijkstra for his valuable and interesting remarks and discussions, especially about the laboratory equipment. I would also like to thank Peter Hedborg and Aaro Pirhonen with all the help in the laboratory and my employer, NCC, for giving me the opportunity to dedicate the last three years to this project. I would also like to express my appreciation to all my colleagues and friends for their support and encouragement.

Last but not least, I would like to express my deepest gratitude and love to my family, Anna-Karin, Thea & Hugo, for their love, patience and support, and for always showing me what is important in life.

Gothenburg, November 2013
Mats Olsson

TABLE OF CONTENTS

LIST OF NOTATIONS

The main notations used in this dissertation is given below and is also described in the re section too.

Roman letters

C_c	compression index
C_c^*	reconstituted compression index defined as e^*_{100}-e^*_{1000}
$C_{\alpha e}$	creep index
$C_{\alpha ei}$	intrinsic creep index
D	elastic stiffness matrix
e	void ratio
e_0	initial void ratio
e^*_{100}	intrinsic void ratio at a vertical effective stress of 100 kPa
e^*_{1000}	intrinsic void ratio at a vertical effective stress of 1000 kPa
E	young's modulus
E^*	modified Young´s modulus
I_v	Void index
k	hydraulic conductivity
K_0	coefficient of lateral earth pressure
K_0^{nc}	coefficient of lateral earth pressure in the NC-region
K´	effective Bulk Modulus of soil
m	shape factor for the NCS surface
M	slope of the Critical state line
M_c	value of M in triaxial compression
M_e	value of M in triaxial extension
M_{MC}	Mohr-Coulomb failure surface
p´	mean effective stress
p_c	size of yield curve in p-q space
p_{ci}	size of intrinsic yield curve in p-q space
p^{eq}	equivalent mean effective stress

q	deviatoric stress ($q= \sigma'_v- \sigma'_h$ in triaxial stress space)
r, r_s	creep number or Time resistance number
r_{si}	intrinsic creep number
R	time resistance
s'	the average value σ'_v and σ'_h $(\sigma'_v+\sigma'_h)/2$
t	the difference between σ'_v and σ'_h $(\sigma'_v-\sigma'_h)/2$
w_L	liquid limit
w_N	natural water content
w_p	plasticity limit

Greek letters

α	scalar rotation of yield function
α_0	initial α value
α_e	anisotropy factor in elastic region
α_{zz}	deviatoric fabric tensor where subscript indicate direction
$\boldsymbol{\alpha}_d$	deviatoric fabric tensor
β_k	Change of hydraulic conductivity w.r.t. strain
ε_a	axial strain
ε_{zz}	strain where the subscript indicate the direction
ε_v	volumetric strain
ε_d	deviatoric strain
ε_v^c	volumetric creep strain
ε_v^p	volumetric plastic strain
ε_d^c	deviatoric creep strain
ε_d^p	volumetric plastic strain
η	stress ratio
η_0	initial stress ratio

θ	value of Lodes angle
κ^*	modified swelling index
λ_i	slope of the intrinsic normal compression line
λ^*	modified compression index
λ_i^*	intrinsic modified compression index
μ^*	modified creep index (SSC creep index)
ν'	Poisson's ratio
ν^*	modified Poisson's ratio
ξ	rate of destructuration
ξ_d	rate of destructuration by deviatoric strain
ξ_v	rate of destructuration by volumetric strain
σ'_{zz}	effective stress where the subscript indicate the direction
σ'_1	major principal effective stress
σ'_2	intermediate principal effective stress
σ'_3	minor principal effective stress
σ'_h	horizontal effective stress
σ'_v	vertical effective stress
σ'_c	apparent preconsolidation stress
σ'_{vc}	vertical apparent preconsolidation stress
τ	reference time
ϕ'	friction angle
ϕ'_{cs}	critical state friction angle
χ	amount of bonding
χ_0	initial amount of bonding
ω	rate of rotation
ω_d	rate of rotation by deviatoric strain
ω_d^*	modified rate of rotation by deviatoric strain ($\omega_d^* = \omega_v \cdot \omega_d$)
ω_v	rate of rotation by volumetric strain

Abbreviations

CRS	Constant Rate of Strain
ICL	Intrinsic Compression Line
IL	Incremental Loading
LMN	Lade & Matsouka-Nakai
MAC-s	Modified Anisotropic Creep model with structure
MCC	Modified Cam-Clay model
NC	Normal Consolidated
NCS	Normal Compression Surface
n-SAC	non-associated creep model for Structured Anisotropic Clay
OCR	Over Consolidation Ratio OCR=σ'_c/σ'_0
SSC	Soft Soil Creep
SCL	Sedimentation Compression Line

1 INTRODUCTION

1.1 Background

Long-term settlements in clay constitute a major engineering challenge in road design and construction in areas with deep deposits of soft clay. Soil improvement or the construction of building foundations or embankments can be quite complicated and expensive in such areas. Construction costs need to be balanced against high maintenance costs. In order to do this optimally, there is a need to predict long-term settlement with a high degree of accuracy.

However, predicting long-term settlement is not an easy task. Today there are numerous different numerical tools to help the engineer to predict the long-term settlement. Even though the numerical tools have become more refined and involve possibilities for representing the complex soil behaviour in increasingly detailed manner, the engineer needs to balance this, against the quality of the soil properties that have been determined.

An improved understanding of the rate-dependency or creep behaviour of soft clays and exploiting this in the formulation of the constitutive model in a numerical program give possibilities to better predictions for complex situations. These advanced models needs to be complemented with proper input data in order to really benefit from their performance.

In addition to the creep parameters the coefficient of lateral earth pressure at rest, K_0, is very important to establish since it will greatly affect the stress paths of the soil when loaded or unloaded. The present practice in Sweden is to use an empirical relation to the liquid limit to estimate the values to be used. In order to improve the predictions of both vertical and horizontal displacement using constitutive models implemented in finite element

software, an improved knowledge of the earth pressure coefficient, K_0, is needed.

1.2 Objectives and limitations

The aim of this research is to extend the mechanical characterization, understanding and theoretical framework of rate-dependent soil behaviour, so that uncertainties in predictions of long-term settlements are significantly reduced. In order to achieve this aim the following objectives are formulated

- To construct a new K_0-triaxial device in order to more accurately obtain representative values of K_0 for soft soils as function of stress and its evolution with time.
- To develop a constitutive model, or adjust an existing model, which includes the necessary formulations for creep, anisotropy and structure explicitly.
- To implement the model in user friendly finite element software and validate the model using laboratory experiments.
- To describe necessary laboratory experiments that need to be conducted to establish proper input parameters for the model and how to evaluate them.

The formulation of the constitutive model is restricted to incorporate monotonic loading, i.e. cyclic and dynamic loading conditions are not considered. The model is validated using experimental data from laboratory tests of natural soil samples, which are acquired in the Gothenburg area.

2 BEHAVIOUR OF SOFT SOILS

This chapter aims to describe some important aspects of soft soil behaviour i.e. compressibility, strain rate relations, creep, anisotropy, destructuration and other relevant phenomena. It will not give a full description of all aspects, but aims merely to give an overview of the topic. This chapter includes issues which are necessary to derive soil data to calibrate, and perhaps modify, the material models discussed in more detail in this thesis.

The literature survey in this thesis is a complement to the literature survey presented in the Licentiate Thesis, see Olsson (2010).

2.1 Introduction

Between the time a soil is sedimented or deposited and the time it is encountered in connection with some human activity, it is most likely that it has been altered as a result of the action of some post-depositional processes. These processes could be physical, chemical and/or biological, Mitchell & Soga (2005). If the sediment is comparatively young, this probably means that it is not in equilibrium in its current environment, since it is exposed rather recently to new conditions of stresses, chemistry, temperature and other factors.

It is essential to have an understanding of changes caused by the post-depositional processes in order to be able to understand the soil properties and interpreting the soil profile data.

The behaviour of a soft soil, such as soft plastic clays, is very much influenced by the sedimentation and post-depositional processes. Depending on the mineralogy of the sediment and the conditions of the new environment, i.e. stresses, chemistry etc, the soil will behave differently. These factors, especially the compressibility of the soil, have

been studied by numerous researchers e.g. Terzaghi (1954), Roscoe et al. (1958), Bjerrum (1967), Sällfors (1975), Mesri & Godlewski (1977), Graham et al. (1983), Leroueil et al. (1985), Larsson (1986), Burland (1990), Länsivaara (1999), Karstunen et al. (2005) to name but a few.

2.2 Yielding of clays

Yielding of clays has been an interest of research for many years for numerous researchers. An implication of this is that there is a number of different ways of defining the yield stress, e.g. Casagrande (1936), Burmister (1951), Schmertmann (1953), Sällfors (1975), Graham et al. (1983).

Normally, the yield stress is defined from tests that are compressed one-dimensionally in horizontally constrained conditions. A unified definition of the yield stress does not exist, as implied above, and normally the evaluated yield stress for one-dimensional tests is inside the dotted box in Figure 2.1, i.e. in the region of where the compression curve get steeper.

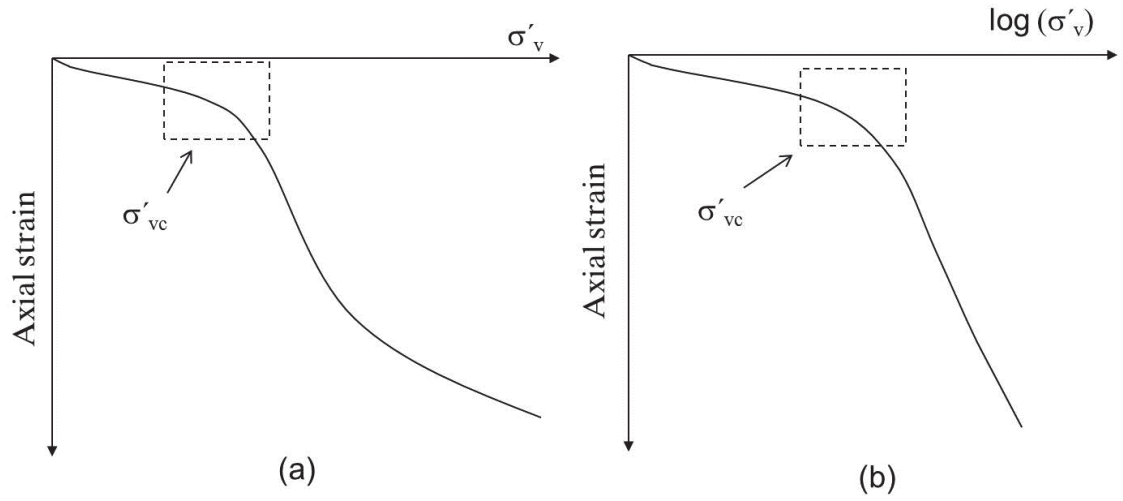

Figure 2.1. Region of yield stress (a) linear and (b) log scale of stress.

This implies that when speaking about yield stress or yield surface and the shape of the surface, it is very important to emphasize the method used to define it.

In Sweden it is very common to use the Sällfors method to evaluate the σ'_{vc} from constant rate of strain, CRS, tests with a strain rate of 0.7%/hr, see Sällfors (1975), were you construct a isosceles triangle according to Figure 2.2.

Yielding of clays in compression has been, and still is determined, more or less from one dimensional oedometer test only, such as incremental loading, IL, or CRS tests with different strain rates. From these test the classical compression and swelling parameters are established and that originally to be used for one dimensional calculations.

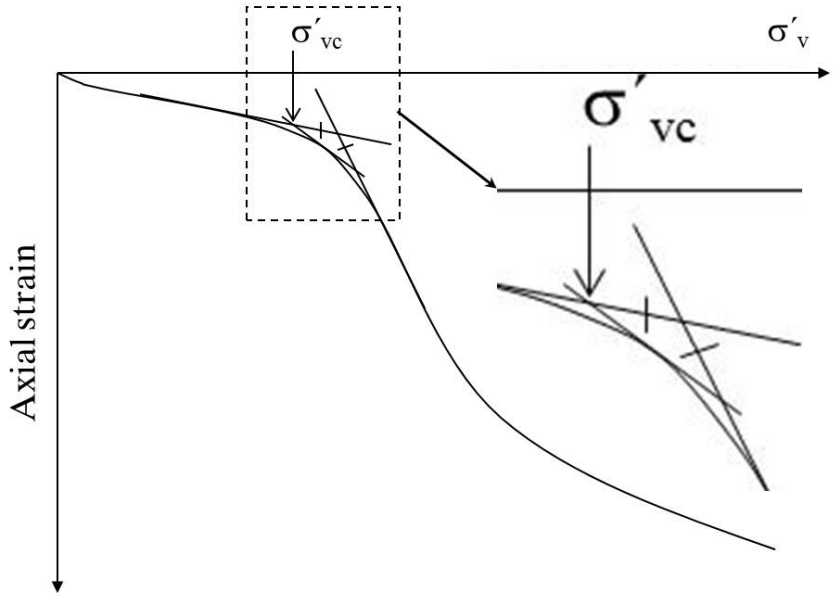

Figure 2.2. Evaluation of preconsolidation pressure from CRS oedometer test according to Sällfors method, Olsson (2010).

2.2.1 Effect of strain rate with respect of the yield surface

The response of soft clay is very strain-rate dependent, as shown by e.g. Leroueil et al. (1985) and Claesson (2003), and demonstrated in Figure 2.3 and Figure 2.4.

As shown in Figure 2.3 and Figure 2.4 the strain rate dependency is most evident in the normally consolidated region, i.e. when the stress state has past the preconsolidation pressure. Furthermore, based on Figure 2.3 and Figure 2.4, the higher the strain-rates conducted on the sample the higher the apparent preconsolidation pressure and excess pore-pressure for the tests.

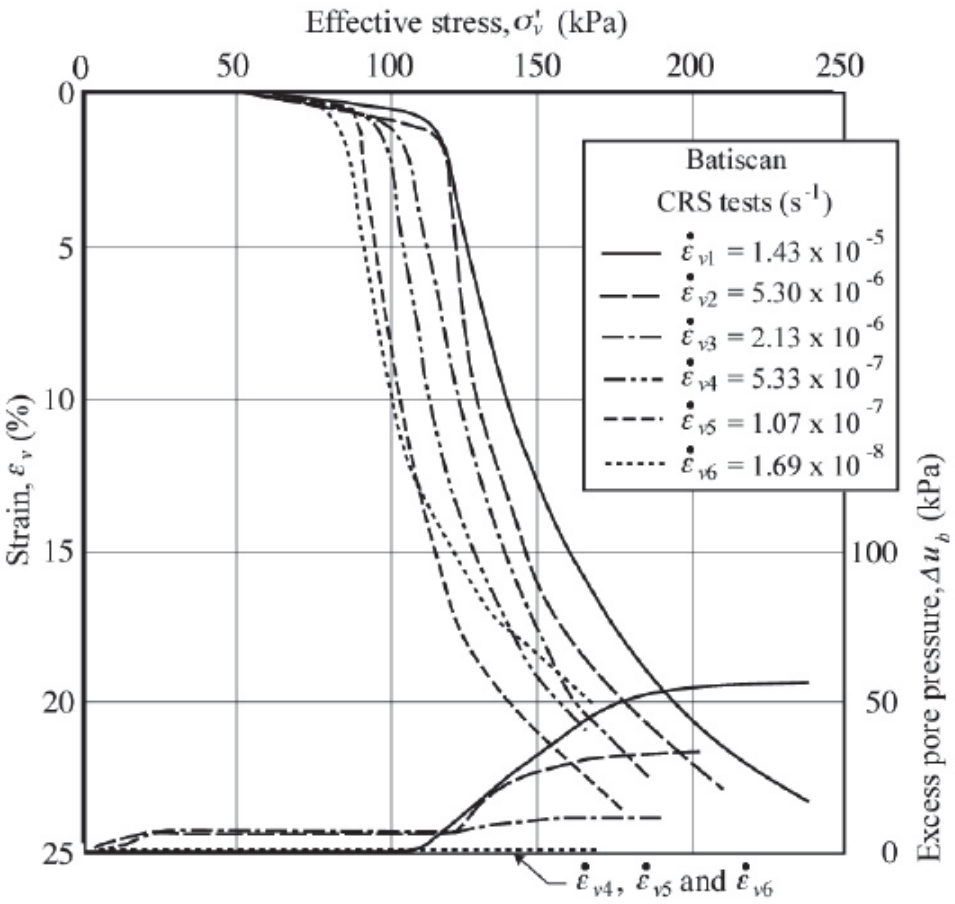

Figure 2.3. CRS oedometer tests on Batiscan clay, Leroueil (2006).

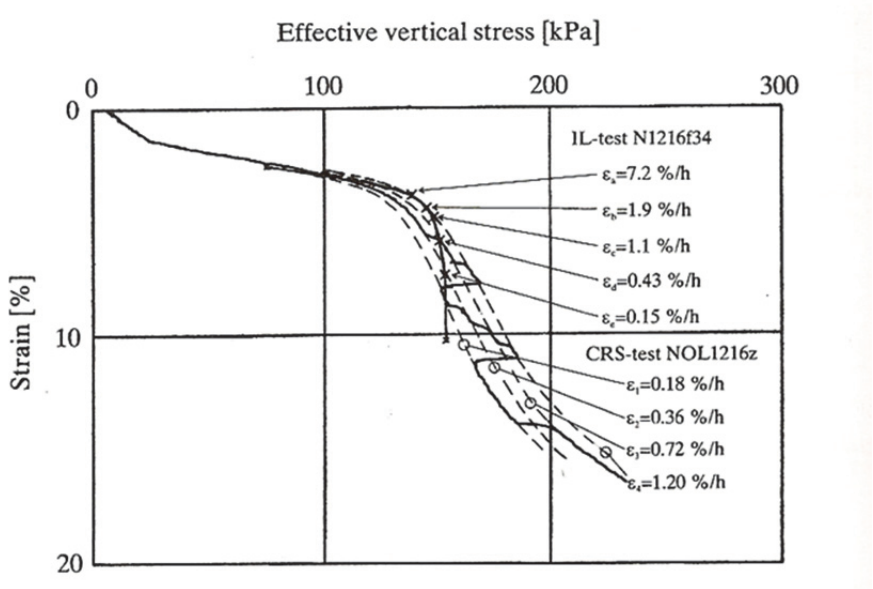

Figure 2.4. CRS oedometer test with different strain rates for a clay sample from Nol, just North of Gothenburg, Claesson (2003).

2.2.2 The shape of the yield surface for anisotropic consolidated clays

The shape of the yield surface for soft soils is not only strain rate dependent but also temperature dependent shown by e.g. Tidfors (1987) and Boudali (1995). In Figure 2.5 the effect of strain rate and temperature on the yield curves are shown.

An extensive laboratory investigation was conducted on Bäckebol clay by Larsson (1981). This laboratory study included both triaxial tests and plane strain tests to study the behaviour and shape of the yield surface. The test results from both triaxial and plane strain tests are given in Figure 2.6. Further examples, involving a large number of different clays is shown in Figure 2.7 compiled by Länsivaara (1999).

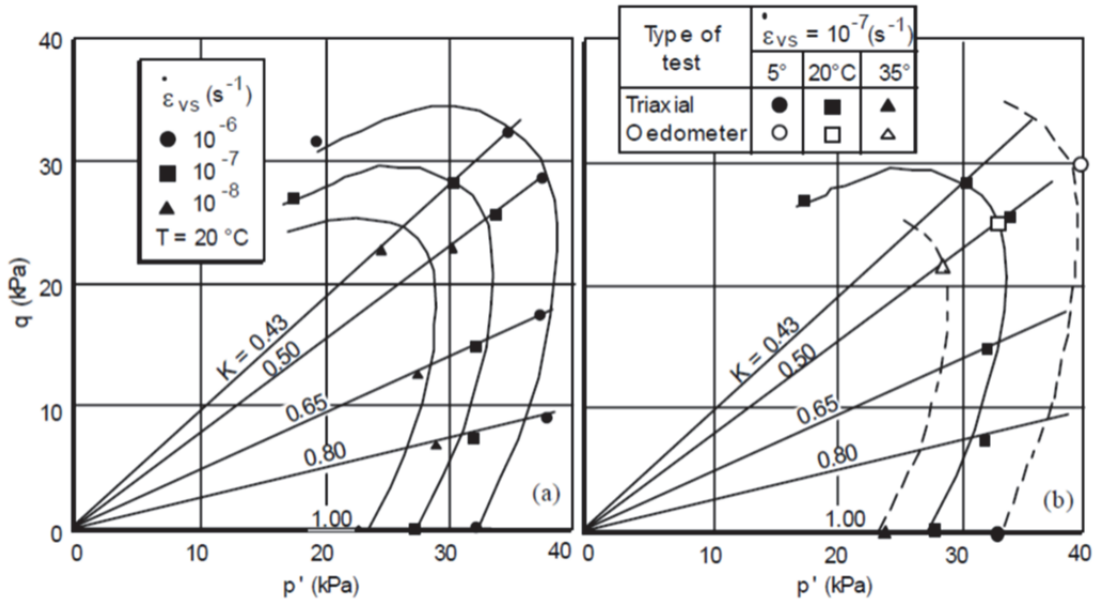

Figure 2.5. Variation of the yield curve of Berthierville clay with (left) strain rate and (right) temperature, Leroueil (2006).

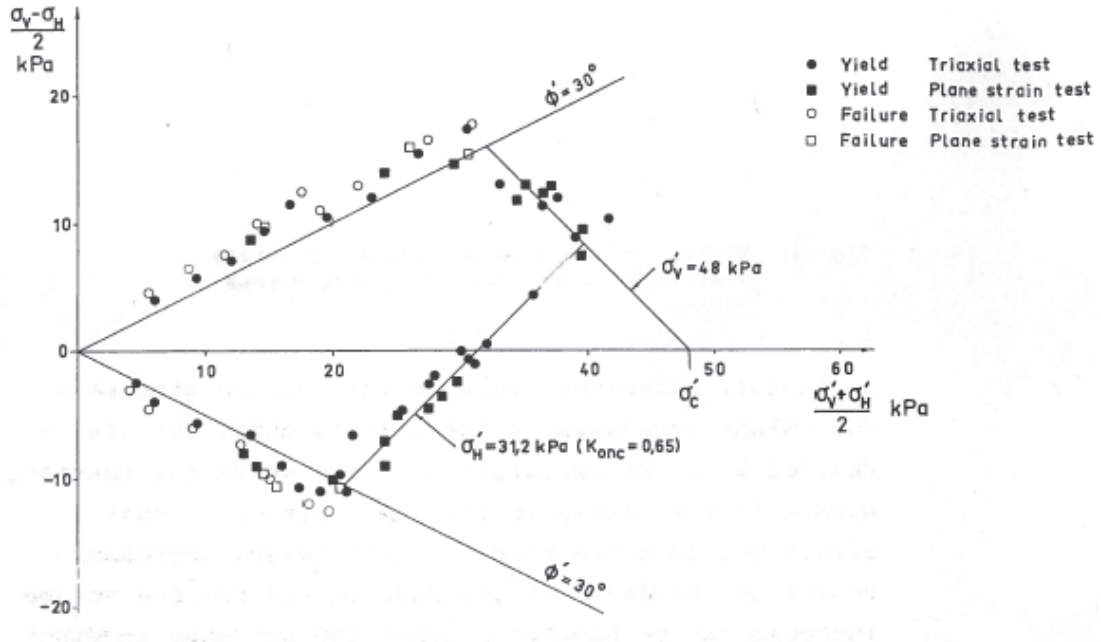

Figure 2.6. Experimental yield points for Bäckebol clay, Larsson (1981).

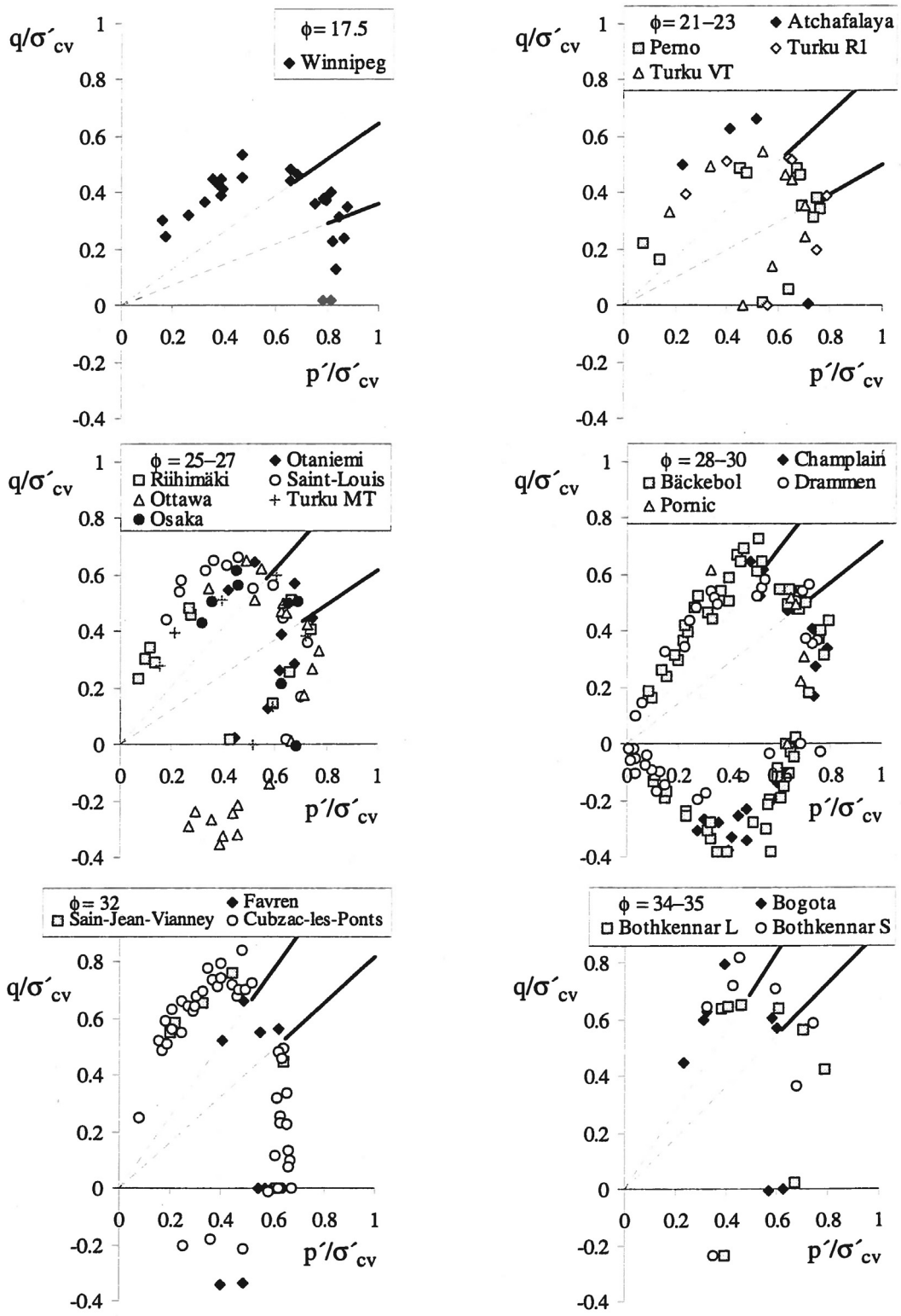

Figure 2.7. Experimental yield curves of different natural clays collected and presented by Länsivaara (1999).

2.2.3 The shape of yield surface in deviatoric plane

When it comes to implementation of constitutive models to numerical codes, the projection of the model in the deviatoric plane is an important issue. It is quite common in soil mechanics to adopt the Mohr-Coulomb failure criterion, and normally this is combined with some procedure to avoid the singularities in the corners. To avoid these corner effects a smooth failure surface could be used as suggested by e.g. Matsuoka & Nakai (1974) or Lade (1977).

Kirkgard (1988) and Kirkgard & Lade (1993) conducted an extensive laboratory study of the three dimensional behaviour of natural normally consolidated clay known as the San Francisco Bay mud. A number of tests in this study were performed in a true triaxial apparatus and some results are shown in Figure 2.8, compared with Drucker-Prager and Mohr-Coulomb failure criteria and LMN dependence criteria according to Bardet (1990). As could be seen in Figure 2.8 the LMN dependence with a friction angle of 30.6 degrees fits reasonably well, while Drucker-Prager failure criterion overestimates the strengths in all directions except for triaxial compression. The Mohr-Coulomb failure criteria underestimate the strengths of tests performed with values of θ [1] between 0 and 90 degrees.

[1] θ values defined according to Kirkgard & Lade (1993).

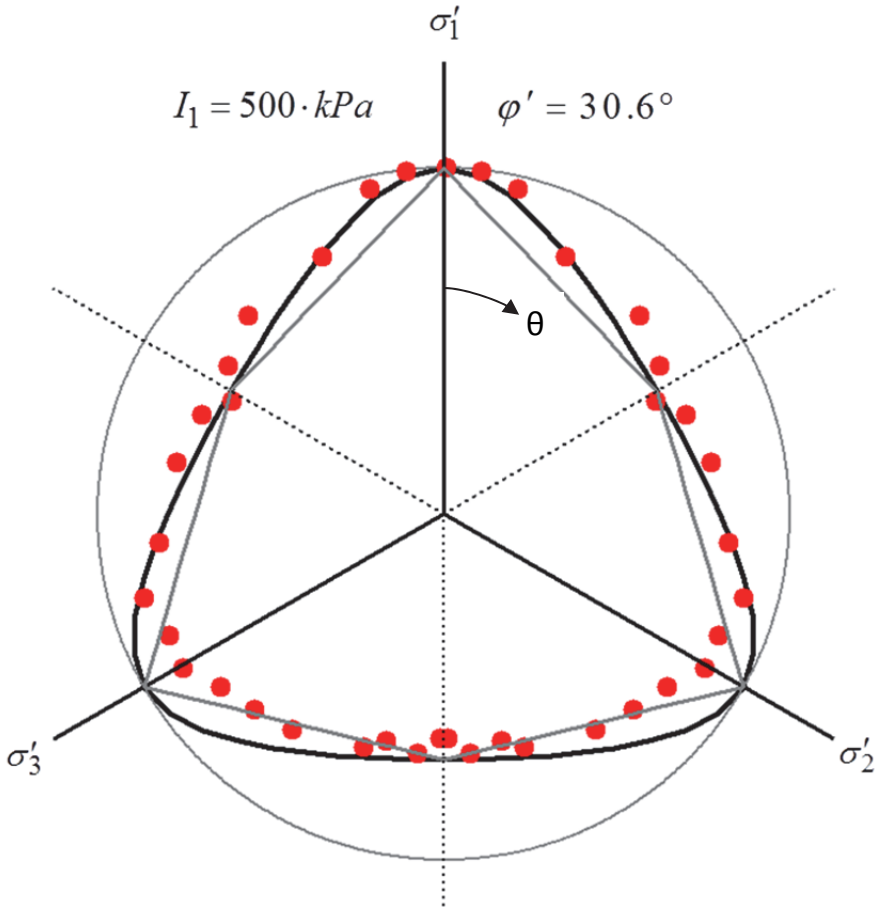

Figure 2.8. Failure surface for San Francisco Bay Mud in deviatoric plane compared with Drucker-Prager and Mohr-Coulomb failure criteria and LMN dependence criteria, data from Kirkgard & Lade (1993).

Similar studies with true triaxial apparatus have been done e.g. Nakai et al. (1986) and Callisto & Calabresi (1998), and they showed similar results, i.e. a curved shape failure surface in the deviatoric plane.

2.3 Structure of natural soil

The structure of a soil is composed of a fabric and interparticle force system that reflect all facets of the soil composition, history, present state and environment, Mitchell & Soga (2005).

Burland (1990) introduced the concept of intrinsic properties of clays, The intrinsic properties of clays relate to a situation in which the clay is reconstituted at a water content of between w_L and 1.5 w_L and then

reconsolidated, preferably one-dimensionally. The intrinsic parameters determined for reconstituted clays are termed ‘intrinsic’ properties since they are independent of the state of the soil. By comparing the intrinsic properties with the natural properties of the soil it is possible to assess structure and bonding of the natural soil.

Burland (1990) also introduced two lines called sedimentation compression line, SCL, and intrinsic compression line, ICL, and a new normalizing parameter called the void index, I_v. The void index aims to aid the correlations of compression characteristics of various clays. The void index is based on the intrinsic properties according to eq. (2.1).

$$I_v = \frac{e - e^*_{100}}{e^*_{100} - e^*_{1000}} = \frac{e - e^*_{100}}{C^*_c} \tag{2.1}$$

where e^*_{100} and e^*_{1000} are the intrinsic void ratios corresponding to the vertical effective stress 100 kPa and 1000 kPa respectively. In Figure 2.9 two standard incremental oedometer tests are plotted with the void index, I_v, against vertical effective stress for Gothenburg clay from a depth of 5 m.

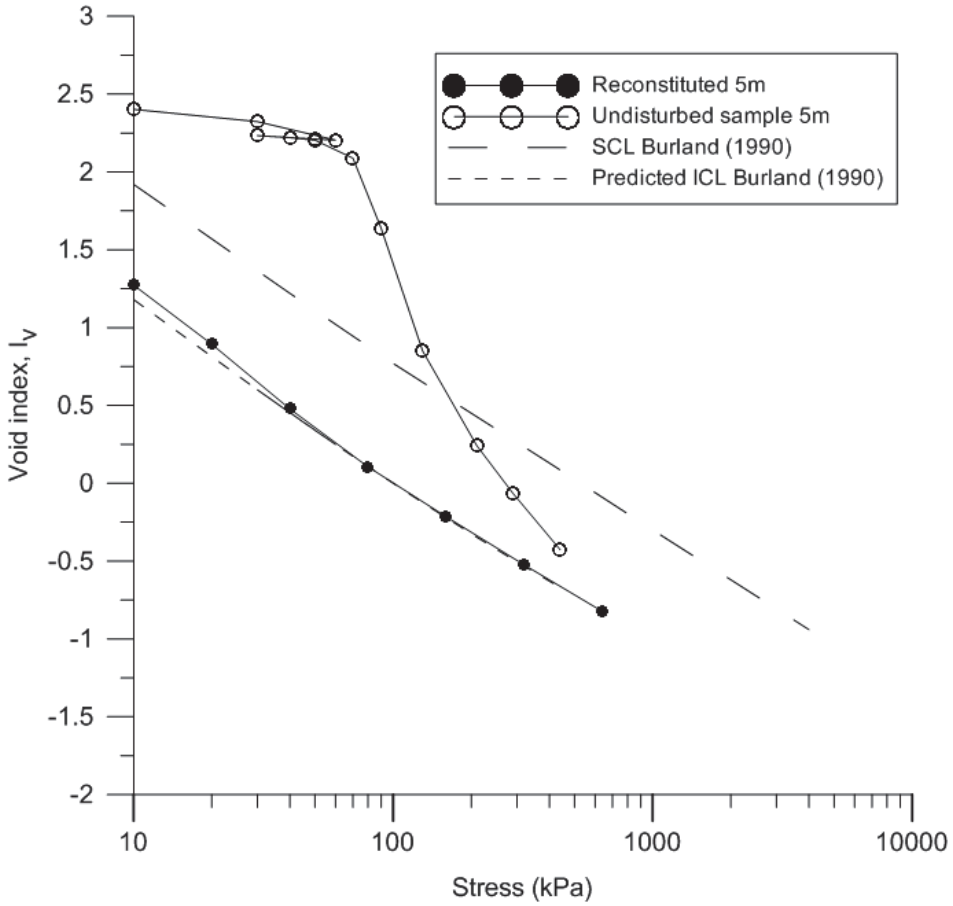

Figure 2.9. Oedometer tests on undisturbed and reconstituted Gothenburg clay from 5 m depth (w_L=65% and w_p=31%), compared with the ICL and SCL from Burland (1990).

The result in Figure 2.9 implies that the Gothenburg clay has quite a lot of structure since after passing the preconsolidation pressure the compression curve is considerably steeper than the SCL and it falls towards the ICL.

The sedimentation compression line, SCL, normally lies well above the intrinsic compression line, ICL, and this means that this soil is more brittle and sensitive than the reconstituted soil. This is also demonstrated in Figure 2.10 were two standard incremental oedometer tests were performed for a sample from a depth of 6.5 m of Bothkennar clay, Burland (1990). Here the void ratio is plotted against vertical effective stress including the SCL and the predicted ICL.

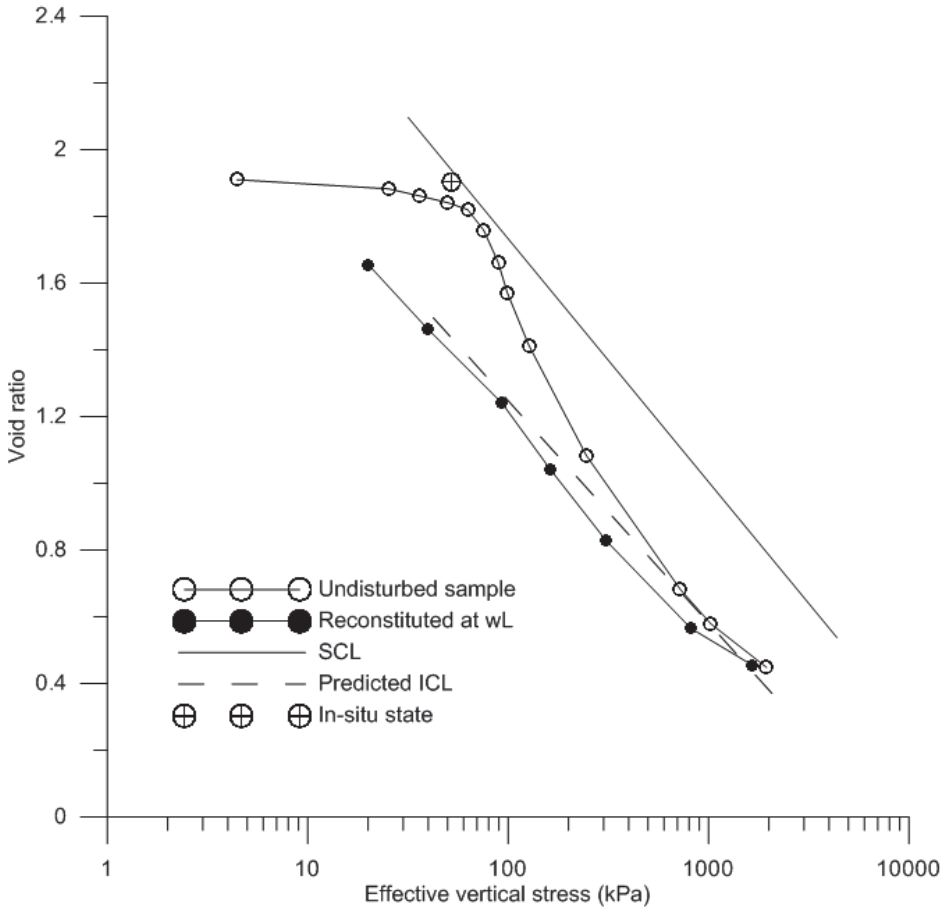

Figure 2.10. Oedometer tests on undisturbed and reconstituted Bothkennar clay from 6.5 m depth,(w_L=85.4%, w_p=41%), data from Burland (1990).

As could be seen from Figure 2.10 at a given void ratio the effective overburden pressure carried by the undisturbed clay sample is about five times the pressure that can be resisted by the corresponding reconstituted clay sample. This is due to the fabric and soil structure developed during sedimentation and post-depositional processes.

2.4 Development of horizontal stress, K_0

The ratio between horizontal and vertical effective stress is defined by the coefficient of earth pressure at rest, $K_0 = \sigma'_h / \sigma'_v$. Values of K_0 for normally consolidated clays are generally in the range of 0.3 - 0.75. Jaky (1944) defined an equation, see eq. (2.2), that is based on the effective stress critical friction angle, ϕ', measured in triaxial compression tests.

$$K_0 = (1 - \sin\phi') \cdot \frac{1 + \frac{2}{3}\sin\phi'}{1 + \sin\phi'} \tag{2.2}$$

In a later paper, Jaky (1948) dropped the fraction term from eq. (2.2) and the equation became what is normally used today and called the Jaky's equation, see eq. (2.3).

$$K_0 = 1 - \sin\phi' \tag{2.3}$$

Although there are a number of published papers and reports that suggest that there is a correlation between the K_0 and liquid limit or plasticity index, a comprehensive collection of data by Kulhawy & Mayne (1990) for 135 clay soils indicates little correlation. According to Mitchell & Soga (2005) this is not surprising, since K_0 is a parameter that is dependent on structure, composition and history, and not only the Atterbergs limits that is only dependent on the composition.

Since the response of a soil is very much dependent on its history, most clay soils exhibit some apparent over-consolidation. This overconsolidation could come from creep effects and/or unloading that have occurred e.g. from erosion. Thus, the K_0 coefficient for an over-consolidated soil K_0^{oc} is greater than for a normal consolidated soil K_0^{nc}, and it varies with the OCR. For over-consolidated clays Schmidt (1966) proposed the following eq. (2.4).

$$K_0 = K_0^{nc} \cdot OCR^{1.2 \cdot \sin(\phi')} \tag{2.4}$$

This equation has been modified by other researchers, and numerous equations have been proposed to represent both unloading and reloading, see e.g. Kulhawy & Mayne (1990) and Kullingsjö (2007).

Nadarajah (1973) studied the K_0 value during an oedometer test in Kaolin clay, and the result from one test is presented in Figure 2.11. The specimen

was initially consolidated to a vertical effective stress of 50 kPa and then additional load steps where applied to a vertical effective stress to 550 kPa. Subsequently, the specimen was unloaded to a vertical effective stress of 80 kPa.

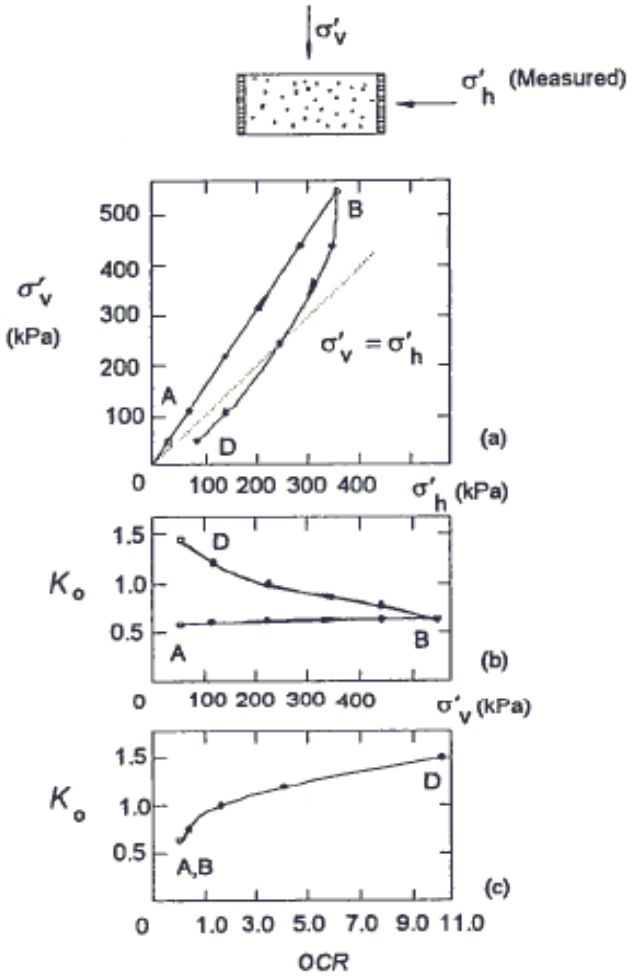

Figure 2.11. Oedometer test on Kaolin clay, Nadarajah (1973).

Figure 2.11 shows the influence of loading and unloading. It could be seen that during loading the K_0 value is more or less constant, but it increases for unloading and reaches a K_0 value of about 1.5 at a vertical effective stress of 50 kPa.

2.5 Undrained behaviour

The undrained shear strength of clays is probably the most commonly determined parameter for soft soils from different tests, both in field and laboratory.

The undrained behaviour of soft clay is influenced by the development of excess pore pressure. Depending on the stress or strain path and/or strain rate the sample will experience, it will exhibit a corresponding undrained shear strength. For lightly over- consolidated clays, i.e. an OCR of about 1.3, typical results for undrained compression and extension triaxial tests of Gothenburg clay for undisturbed clay samples is shown in Figure 2.12 for two different depths.

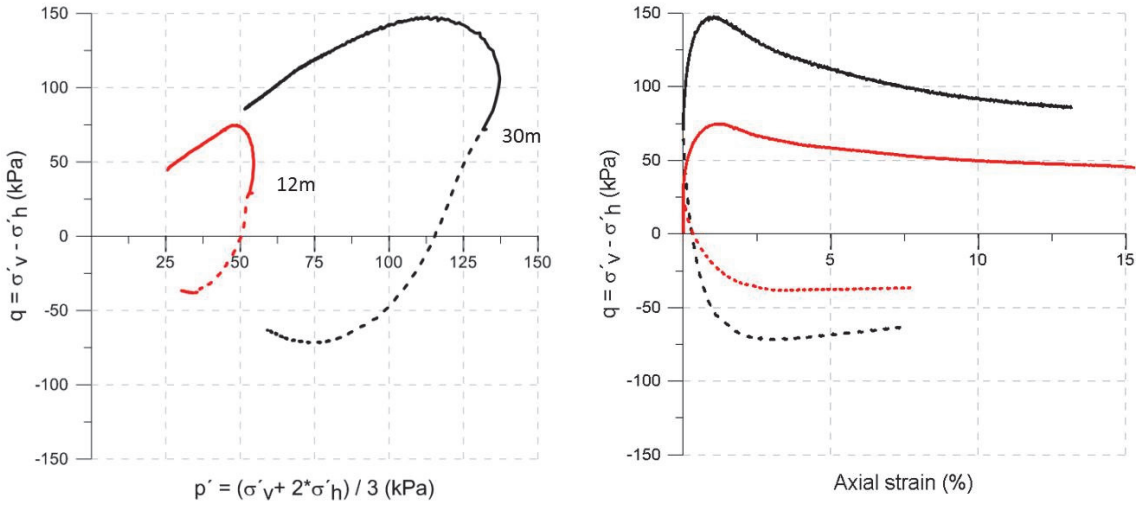

Figure 2.12. Typical results from compression and extension triaxial tests in p´- q space of natural soft Gothenburg clay for samples from two different depths (12m and 30m) with a deformation rate of 0.01 mm/min and a sample height of 100 mm.

The test results in Figure 2.12 suggest a critical friction angle of about 35 degrees at large strains and a friction angle of about 30-32 degrees at peak of deviatoric stress.

Normally, a clay sample at a certain over-consolidation ratio will, if compressed under undrained conditions, either contract or dilate. This is demonstrated in Figure 2.13 for undrained compression tests on reconstituted Boston Blue Clay.

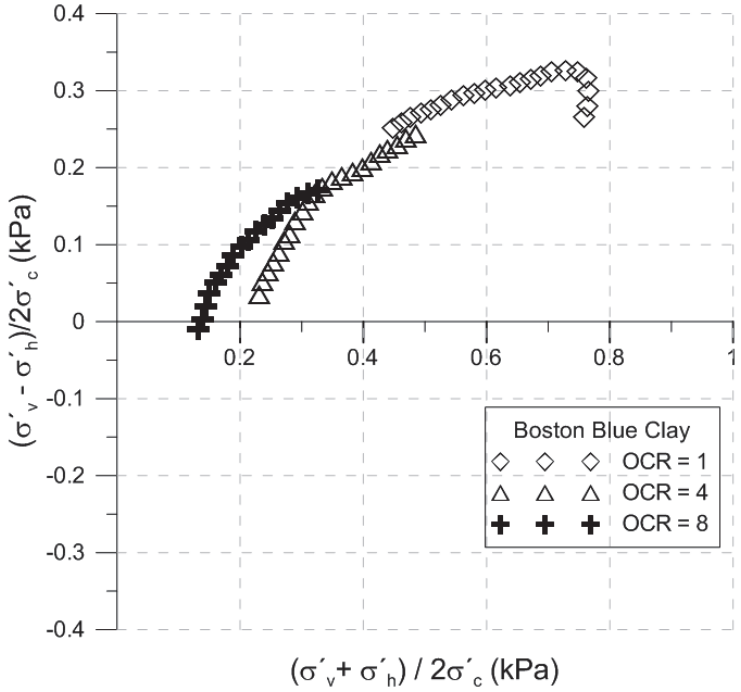

Figure 2.13. Stress paths for reconstituted Boston Blue Clay for different OCR values, data from Pestana (1994).

As could be seen from Figure 2.13 the soil tends to contract for low OCR and dilate for higher OCR. The test results also indicate a critical state friction angle of about 30-32 degrees.

2.6 Rate dependency

If a clay sample is undergoing different strain rates, it will exhibit different stress and strain paths. The behaviour of rate-dependency of clays has been observed by numerous researchers and demonstrated by e.g. Leroueil & Marques (1996), Sheahan et al. (1996) and Länsivaara (1999).

For undrained triaxial compression test, the peak strength varies with the strain rate, i.e. the faster the strain rate the higher the peak strength, see Figure 2.14 for typical behaviour of strain rate effects in p´- q plot. This is more noticeable for lightly over - consolidated clays with low OCR than for over - consolidated clays with high OCR values as shown by e.g. Sheahan et al. (1996). This difference in stress-strain path in undrained triaxial compression tests is similar to the results found in the one-dimensional oedometer tests, see Figure 2.3 and Figure 2.4.

In Figure 2.15 results from undrained triaxial compression test with varying strain rates are presented by Länsivaara (1999).

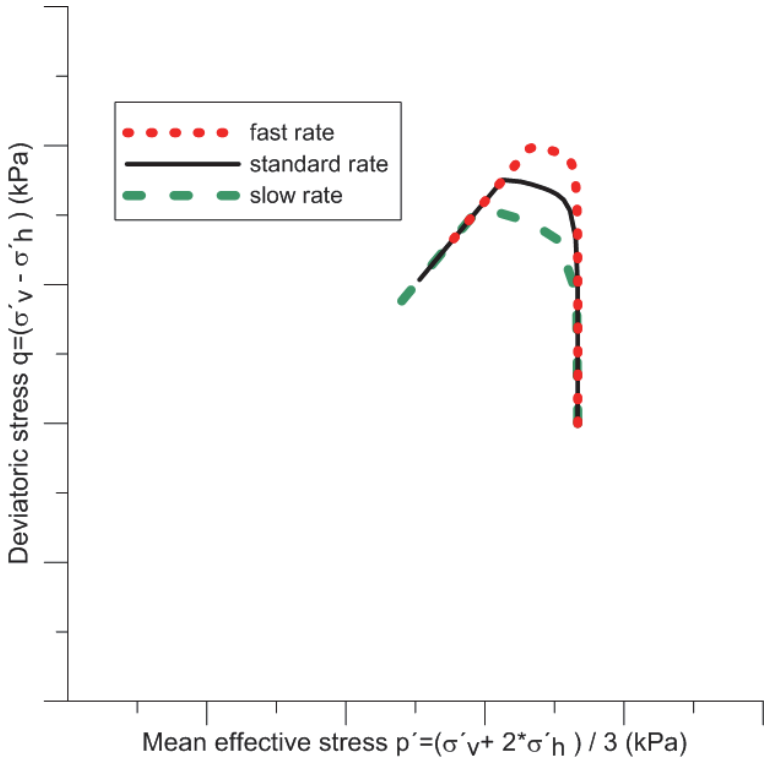

Figure 2.14. Typical strain rate effects for normally consolidated clays.

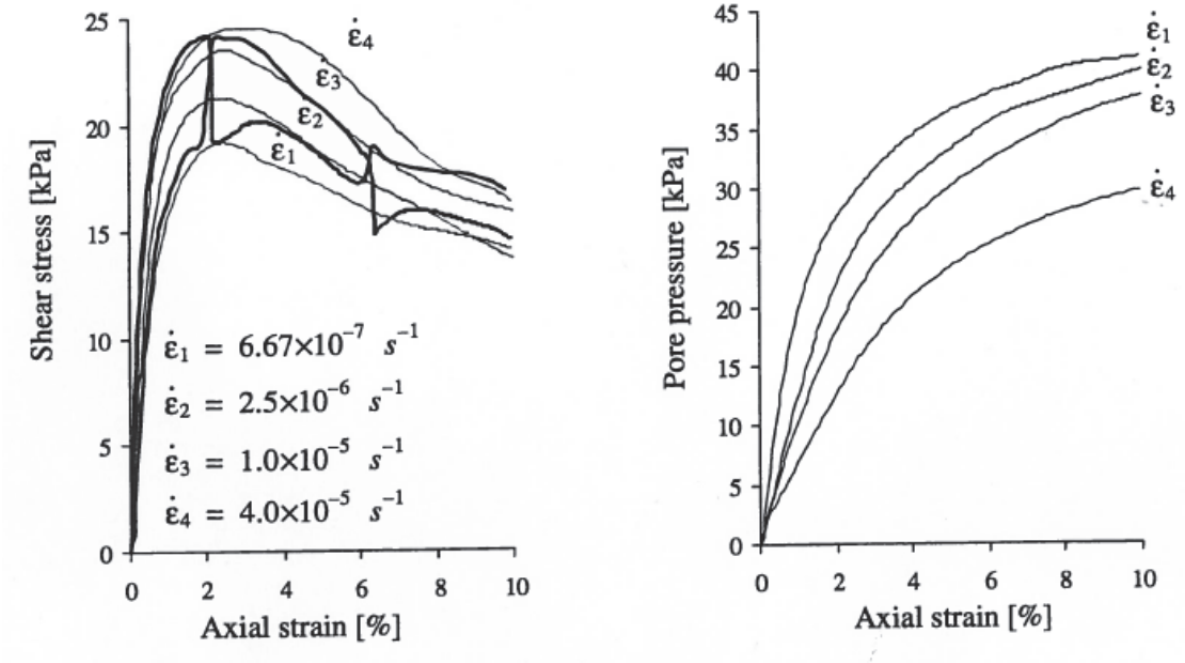

Figure 2.15. The effect of strain rate in undrained triaxial compression tests, Länsivaara (1999)

In Figure 2.15 six different tests are presented. Four tests are conducted with different strain rates and two tests are conducted with varying strain rates. The results demonstrate the rate - dependency of lightly over - consolidated clays. The peak strength obtained from a soil sample tested in laboratory corresponds to a certain strain rate and it is most likely that this strain rate is very different from the strain rate in in-situ or during construction work. This means that a constitutive model that cannot capture the strain rate dependency, is most likely not able to capture the behaviour in-situ or during construction work either.

3 CONSTITUTIVE MODELS

This chapter discusses some of the existing material models that include creep effects. This chapter starts with the basic critical state models, and then describes how these models have been extended to include the effect of creep, especially for soft soils such as clays.

3.1 Invariants

The constitutive models described in this thesis are often presented in general stress space by the following definitions.

Stress vector $\boldsymbol{\sigma}$ is defined as eq. (3.1) and the mean effective stress, p´, as eq. (3.2).

$$\boldsymbol{\sigma} = \begin{Bmatrix} \sigma'_{xx} \\ \sigma'_{yy} \\ \sigma'_{zz} \\ \sigma'_{xy} \\ \sigma'_{xz} \\ \sigma'_{yz} \end{Bmatrix} \tag{3.1}$$

$$p' = \frac{I_1}{3} = \frac{\left(\sigma'_{xx} + \sigma'_{yy} + \sigma'_{zz}\right)}{3} \tag{3.2}$$

where I_1 is the first invariant of stress. The deviatoric stress vector is defined according to eq. (3.3).

$$\boldsymbol{\sigma}_d = \begin{Bmatrix} \sigma'_{xx} - p' \\ \sigma'_{yy} - p' \\ \sigma'_{zz} - p' \\ \sqrt{2}\sigma'_{xy} \\ \sqrt{2}\sigma'_{xz} \\ \sqrt{2}\sigma'_{yz} \end{Bmatrix} \tag{3.3}$$

The normally used invariant $q = \sqrt{3J_2}$ where $J_2 = \frac{1}{2}\{\boldsymbol{\sigma}_d\}^T \{\boldsymbol{\sigma}_d\}$ is the second deviatoric stress invariant.

For anisotropy a definition of a so-called fabric or "rotation" tensor is essential. If the fabric tensor is defined as $\boldsymbol{\alpha}$, a new set of stress tensors could be defined.

$$\mathbf{s}^{\alpha} = \boldsymbol{\sigma} - \frac{1}{3}\boldsymbol{\sigma} \cdot \mathbf{I} \cdot \boldsymbol{\alpha} \tag{3.4}$$

where $\mathbf{I}$ is the unit matrix. This stress tensor becomes very important when modeling anisotropic behaviour of materials[2].

Defining the modified second stress invariant using the vector notation and considering fabric will take the following form according to eq. (3.5).

$$J_2^{\alpha} = \frac{1}{2}\{\boldsymbol{\sigma}_d - p' \cdot \boldsymbol{\alpha}_d\}^T \{\boldsymbol{\sigma}_d - p' \cdot \boldsymbol{\alpha}_d\} \tag{3.5}$$

where $\boldsymbol{\alpha}_d$ is the deviatoric fabric tensor defined according to eq. (3.6)

$$\boldsymbol{\alpha}_d = \begin{Bmatrix} \alpha_{xx} - 1 \\ \alpha_{yy} - 1 \\ \alpha_{zz} - 1 \\ \sqrt{2}\alpha_{xy} \\ \sqrt{2}\alpha_{xz} \\ \sqrt{2}\alpha_{yz} \end{Bmatrix} \tag{3.6}$$

The deviatoric strain vector and second deviatoric strain invariant are defined in analogous manner, see eq. (3.7) and eq. (3.8). For more detailed description of invariants see e.g. Potts & Zdravkovic (1999) or Nordal (2008).

[2] Note that $\alpha_{xx} + \alpha_{yy} + \alpha_{zz} = 3$

$$\boldsymbol{\varepsilon}_d = \begin{Bmatrix} \varepsilon_{xx} - I_1^{\varepsilon} \\ \varepsilon_{yy} - I_1^{\varepsilon} \\ \varepsilon_{zz} - I_1^{\varepsilon} \\ \sqrt{2}\varepsilon_{xy} \\ \sqrt{2}\varepsilon_{xz} \\ \sqrt{2}\varepsilon_{yz} \end{Bmatrix} = \begin{Bmatrix} \varepsilon_{xx} - I_1^{\varepsilon} \\ \varepsilon_{yy} - I_1^{\varepsilon} \\ \varepsilon_{zz} - I_1^{\varepsilon} \\ \gamma_{xy} / \sqrt{2} \\ \gamma_{xz} / \sqrt{2} \\ \gamma_{yz} / \sqrt{2} \end{Bmatrix} \tag{3.7}$$

$$J_2^{\varepsilon} = \frac{1}{2} \cdot \boldsymbol{\varepsilon}_d{}^T \cdot \boldsymbol{\varepsilon}_d \tag{3.8}$$

3.2 Critical State models

The concepts of critical state soil mechanics were developed by Roscoe et al. (1958) and Schofield & Wroth (1968). The critical state concept implies that when a soil is sheared, it eventually tends to an ultimate condition in which plastic shearing could continue indefinitely without any change in volume or effective stresses, Wood (1990).

The first critical state models were the Cam-Clay models developed at the University of Cambridge by Roscoe and co-workers. The original Cam-Clay formulation was presented by Roscoe & Schofield (1963) and Schofield & Wroth (1968). The Modified Cam-Clay formulation that is often used today, was put forward by Roscoe & Burland (1968).

3.2.1 Modified Cam-Clay

The Modified Cam-Clay (MCC) model was developed by Roscoe & Burland (1968) as an extension of the original Cam-Clay. This formulation is often used in numerical predictions and also very often used as a reference model when implementing new constitutive soil models. The Modified Cam-Clay formulation gives an elliptical shaped yield surface in p´- q space, see Figure 3.1, where the yield surface, f, is defined as eq. (3.9).

$$f = q^2 - M^2 \cdot (p_c - p') \cdot p' = 0 \tag{3.9}$$

where $M = \frac{6 \cdot \sin(\varphi')}{3 \pm \sin(\varphi')}$, and a negative sign is used for compression and positive sign for extension to define the critical state stress ratio, see Figure 3.1. The original MCC model used a constant value of the critical state parameter, M, corresponding to triaxial compression.

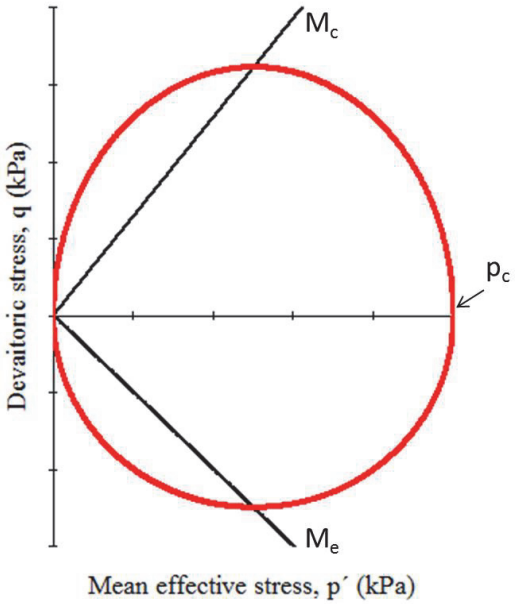

Figure 3.1. The shape of the Modified Cam-Clay (MCC) models yield surface with different critical state parameter M for compression and extension.

3.2.2 S-CLAY1S model

The S-CLAY1S model is an extension of the S-CLAY1 model that is based on ideas by Wheeler (1997), and then extended to its current form by Wheeler et al. (1999), Koskinen et al. (2002), Wheeler et al. (2003) and Karstunen et al. (2005).

The S-CLAY1 model is an extension of the Modified Cam-Clay model, with anisotropy represented by an inclined yield surface that is controlled by a rotational law to represent the change of the anisotropy during plastic straining. It should also be noted that Dafalias (1986) presented a very

similar model with a anisotropic yield surface using the rotated ellipse in p´-q space, but without any comparison with experimental data.

The extension of the S-CLAY1 model to its current form, i.e. to the S-CLAY1S model, incorporates the influence of bonding and destructuration. This is done by introducing an intrinsic yield surface that corresponds to a totally remoulded soil, i.e. no structure or bonds exist.

A short description of the mathematical formulation of the S-CLAY1S model in general stress space is given below.

3.2.2.1 Elastic behaviour

The elastic behaviour of the S-CLAY1S model is the same as for the Modified Cam-Clay model, where the elastic bulk modulus, K´, is defined according to eq. (3.10).

$$K' = \frac{1+e}{\kappa} p' \tag{3.10}$$

where κ is the slope of swelling line, p' is mean effective stress and e is the current void ratio. The shear modulus, G, is calculated based on the bulk modulus, eq. (3.10), and the assumption of a constant Poisson´s ratio, ν', according to eq. (3.11).

$$G = \frac{3(1-2\nu')}{2(1+\nu')} \cdot K' \tag{3.11}$$

3.2.2.2 Yield function

The natural and intrinsic yield surface in the S-CLAY1S model can be expressed in three dimensional stress space according to eq. (3.12) and has been visualized in p´-q space and principal stress space in Figure 3.2. The intrinsic yield surface is based on the formulation by Gens & Nova (1993). The intrinsic yield surface has the same shape and inclination, but differs in size with respect to the natural yield surface i.e. the yield surface, f, of the bonded soil.

$$f = \frac{3}{2}\left[\{\mathbf{s}\}^T\{\mathbf{s}\}\right] - \left[M^2 - \frac{3}{2}\{\boldsymbol{\alpha}_d\}^T\{\boldsymbol{\alpha}_d\}\right]\cdot(p_c - p')\cdot p' = 0 \tag{3.12}$$

where $\mathbf{s} = \boldsymbol{\sigma}_\mathbf{d} - p'\cdot\boldsymbol{\alpha}_\mathbf{d}$ and p_c is the preconsolidation pressure at the hydrostatic axis, see Figure 3.2, $\boldsymbol{\sigma}_d$ and $\boldsymbol{\alpha}_d$ are the deviatoric stress tensor and the deviatoric fabric tensor respectively.

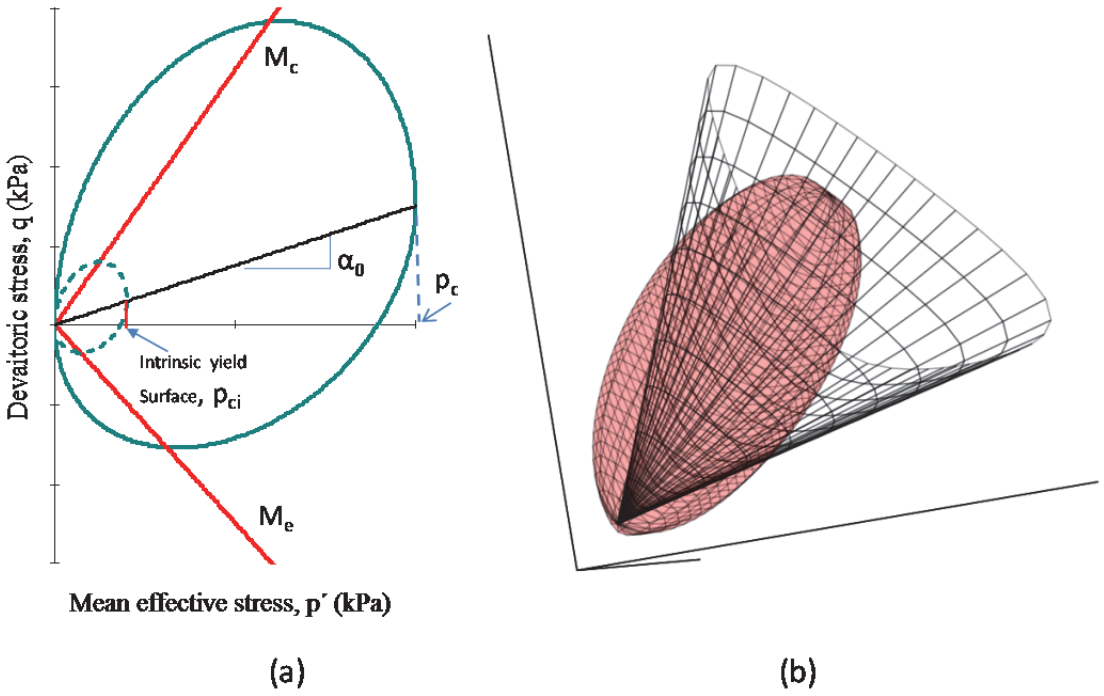

Figure 3.2. Visualisation in (a) p-q space and in (b) principal stress space for the S-CLAY1S model with the Matsouka-Nakai failure criteria.

In Figure 3.2 the S-CLAY1S model is plotted with the Matsouka-Nakai (MN) failure criteria while in the original S-CLAY1S model the Drucker-Prager failure criteria was used. The latest implementation of the S-CLAY1S model in to a finite element code was done by Sivasithamparam (2012). Sivasithamparam (2012) used a Lode dependency with a formulation from Sheng et al. (2000) that give a smooth failure surface in the deviatoric plane, similar to the MN failure criteria.

The S-CLAY1S model assumes an associated flow rule i.e. the yield surface and plastic potential is the same.

3.2.2.3 Hardening laws

The S-CLAY1S model incorporates three different hardenings laws. The first hardening law is controlling the change in the size of the intrinsic yield surface with respect to the plastic volumetric strains ($\Delta\varepsilon_v^p$), similar to that of Modified Cam-Clay, according to eq. (3.13).

$$\Delta p_{ci} = \frac{v \cdot p_{ci}}{\lambda_i - \kappa} \cdot \Delta\varepsilon_v^p \tag{3.13}$$

where v is specific volume, λ_i is the slope of the intrinsic normal compression line and κ is the slope of the swelling line in the compression plane.

The second hardening law is describing the rotation of the yield surface, i.e. the evolution of the anisotropy due to plastic straining, according to eq. (3.14).

$$\Delta\boldsymbol{\alpha}_d = \omega\left(\left[\frac{3\boldsymbol{\eta}}{4} - \boldsymbol{\alpha}_d\right] \cdot \langle\Delta\varepsilon_v^p\rangle + \omega_d\left[\frac{\boldsymbol{\eta}}{3} - \boldsymbol{\alpha}_d\right] \cdot \Delta\varepsilon_d^p\right) \tag{3.14}$$

where $\boldsymbol{\eta}$ is the generalised stress ratio, defined as $\boldsymbol{\eta} = \boldsymbol{\sigma}_d / p'$, and ε_d^p is the plastic deviatoric strain. The new soil constants ω and ω_d controls the rate at which $\boldsymbol{\alpha}_d$ heads towards its current target value.

The third hardening law describes the degradation of bonding in the soil and is defined by an intrinsic yield surface. The size of the intrinsic yield surface is related to the natural yield surface by a parameter χ which determines the current degree of bonding according to eq. (3.15).

$$p_c = (1+\chi) \cdot p_{ci} \tag{3.15}$$

where p_{ci} is the intrinsic preconsolidation pressure, see Figure 3.2. The degradation of bonding is associated with volumetric and deviatoric plastic strains and formulated according to eq. (3.16).

$$\Delta\chi = -\xi\chi\left(\left|\Delta\varepsilon_v^p\right| + \xi_d\left|\Delta\varepsilon_d^p\right|\right) \tag{3.16}$$

where ξ and ξ_d are soil constants controlling the rate of degradation.

3.2.3 Discussion

Even though the advanced model such as the S-CLAY1S, described above, could capture many of the important aspects of natural soil behaviour of normally consolidated and lightly over-consolidated clays, it does not include the effects of creep or strain-rate effects that could be of great importance.

Section 3.3 discusses some of the existing models that include creep effects.

3.3 Advanced constitutive models incorporating creep

Since the 1970´s a number of different constitutive models, two and three dimensional, that include the effect of creep have been proposed e.g. Runesson (1978), Adachi & Oka (1982), Vermeer et al. (1998), Leoni et al. (2008), Grimstad & Degago (2010), Yin & Karstunen (2011).

Normally creep or viscous models are split into two classes. Either they follow Perzyna´s theory of overstress, see Perzyna (1963), or they could be placed under the category of non-stationary flow surface theory or similar, see e.g. Liingaard et al. (2004).

The first anisotropic three dimensional model that included creep effect is the model by Sekiguchi & Ohta (1977) that assumes a fixed anisotropy and has problems with corner effects. In the parallel Runesson (1978) proposed a three dimensional creep model using an anisotropic yield surface as a rotated ellipse in p´-q space.

None of the creep models described below uses the Perzyna´s theory of overstress, since the parameters to describe the creep behaviour in overstress models tend to be non-physical and need a cumbersome calibration. The creep models described in the following make use of conventional soil parameters with a physical meaning, which are relatively easy to evaluate and obtain. The only parameters that could be discussed and needs further development are the destructuration parameters for the S-CLAY1S.

Below a short description of some of the most recently developed and relevant material models for this thesis are given.

3.3.1 Isotropic Soft Soil Creep model

The isotropic Soft Soil Creep (SSC) model was developed by Vermeer and his co-workers, see Vermeer et al. (1998). It is based on the one dimensional theory by Buisman (1936) and extended to general state of stress and strain. In this model a new stress measure called p^{eq} is used, defined as eq. (3.17).

$$p^{eq} = p' + \frac{q^2}{M^2 p'} \tag{3.17}$$

where M is a shape parameter as shown in Figure 3.3. In fact this expression gives the ellipse of the Modified Cam-Clay introduced by Roscoe & Burland (1968). The failure is represented by the Mohr-Coulomb failure surface, M_{MC} in Figure 3.3.

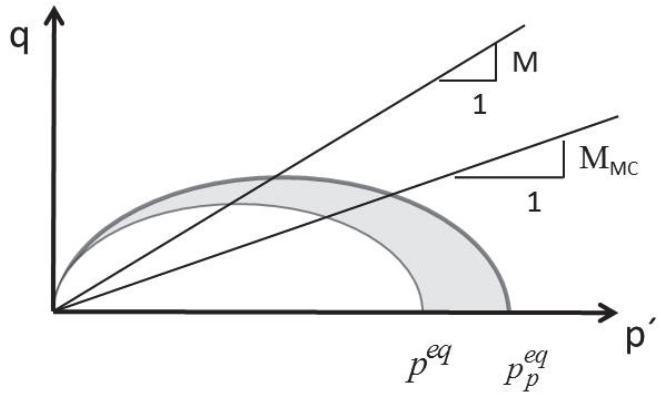

Figure 3.3. Diagram of p^{eq} for the Soft Soil Creep model in a p-q plane.

The volumetric strain rate is formulated according to eq. (3.18).

$$\dot{\varepsilon}_v^c = \frac{\mu^*}{\tau}\left(\frac{p^{eq}}{p_p^{eq}}\right)^{\frac{\lambda^*-\kappa^*}{\mu^*}} \tag{3.18}$$

where λ^* and κ^* are the modified compression index and modified swelling index, respectively, evaluated from a "$\ln p' - \varepsilon_v$" plot, and μ^* is the modified creep index. τ is the reference time, normally chosen to be 1 day since the parameters evaluated come from incremental oedometer tests with 1 day duration of each load increment. The preconsolidation pressure p_p^{eq} evolves with volumetric creep strains ε_v^c according to eq. (3.19).

$$p_p^{eq} = p_{p0}^{eq} \cdot \exp\left(\frac{\varepsilon_v^c}{\lambda^* - \kappa^*}\right) \tag{3.19}$$

In this formulation there is no true yield surface since the soil will always have permanent creep deformation, even if the creep strain would be extremely small for high values of OCR. Therefore, the reference surface is

called normal compression surface instead of a yield surface for this type of models. When approaching the normal compression surface from high OCR, the normal compression surface represents the region of where large viscoplastic strains will occur, i.e. there is no sudden transition between elastic to elastic-viscoplastic regions.

The SSC model has an assumption of constant contours of volumetric creep strains and this is a major drawback, since it would reproduce unrealistic creep strains for, more or less, all stress paths.

For more information about this model the reader is referred to Stolle et al. (1997), Vermeer et al. (1998), Vermeer & Neher (1999), Stolle et al. (1999) and Brinkgreve et al. (2011).

3.3.2 Anisotropic Creep Model (ACM)

The Anisotropic Creep Model developed by Leoni et al. (2008) combines the ideas of the Soft Soil Creep model and S-CLAY1 model, i.e. the S-CLAY1S model without structure. It adopts the rotated ellipsoid, see Figure 3.4, which is similar to the S-CLAY1S, without the intrinsic yield surface, as the normal compression surface of the model.

The Anisotropic Creep Model has of two hardening laws, one that controls the size of the normal compression surface similar to eq. (3.19) and one that controls the rotation of the normal compression surface analogous to eq. (3.14) with a small differences, namely the rotational law is controlled by the volumetric and deviatoric creep strains for the Anisotropic Creep Model. This would imply that the normal compression surface would start to rotate, i.e. change inclination, due to creep strains at all stress states, in contrast to the S-CLAY1S model.

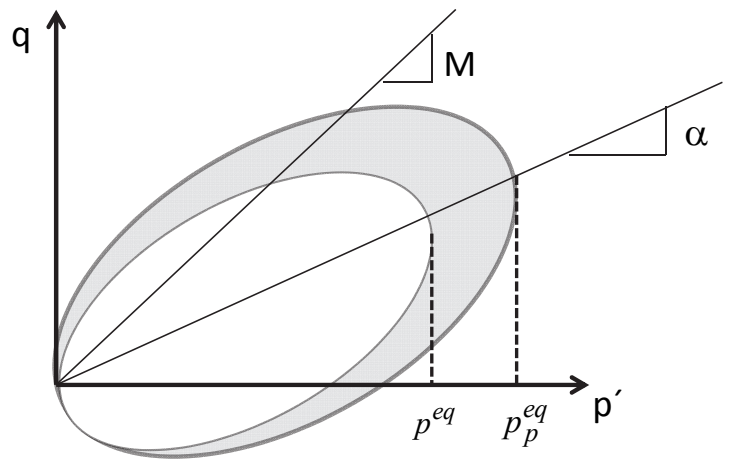

Figure 3.4. Anisotropic Creep Model.

The normal compression surface of the Anisotropic Creep Model is formulated according to eq. (3.20).

$$p^{eq} = p' + \frac{3}{2} \cdot \frac{\{\boldsymbol{\sigma}_d - p' \cdot \boldsymbol{\alpha}_d\}^T \{\boldsymbol{\sigma}_d - p' \cdot \boldsymbol{\alpha}_d\}}{p'\left(M^2 - \frac{3}{2}\{\boldsymbol{\alpha}_d\}^T \{\boldsymbol{\alpha}_d\}\right)} \tag{3.20}$$

The Anisotropic Creep Model also has the same drawback that is mentioned for the SSC model, i.e. it assumes constant contours of volumetric creep strains.

3.3.3 n-SAC model

The n-SAC model (non-associated creep model for Structured Anisotropic Clay) was developed by Grimstad & Degago (2010) and is an extension of the S-CLAY1S model. The n-SAC model incorporates not just four different hardening rules, but also a non-associated flow rule is used. It also makes use of the rotated ellipsoid as a reference surface similar to the ACM model, see Figure 3.4. A major difference in the n-SAC model compared to the ACM model is the formulation of the (visco) plastic multiplier, presented by Grimstad et al. (2008), Grimstad (2009) and Grimstad & Degago (2010). The formulation by Grimstad et al. (2008), where eq. (3.21) is used to represent the visco-plastic multiplier, implies that one could also model creep swelling. For oedometer condition in the

normal consolidated region the new visco-plastic multiplier will be identical for the approaches used in SSC model.

$$\dot{\lambda} = \frac{1}{r_{si} \cdot \tau} \cdot \left(\frac{p^{eq}}{(1+\chi) \cdot p'_{ci}} \right)^{r_{si} \cdot \left(\lambda_i^* - \kappa^* \right)} \cdot \frac{M_c^2 - \alpha_0^2}{M_c^2 - \eta_0^2} \tag{3.21}$$

where M_c is critical state line in compression, α_0 is the inclination of the potential surface in K_0^{NC} loading and η_0 is the stress path corresponding to K_0^{NC} loading. The parameter r_{si} is the intrinsic creep parameter, defined in Figure 3.5. The isotropic hardening of the intrinsic reference stress is defined according to eq. (3.22).

$$\frac{dp'_{ci}}{d\lambda} = \frac{p'_{ci}}{\lambda_i^* - \kappa^*} \frac{\partial Q}{\partial p'} \tag{3.22}$$

In the n-SAC model the equivalent stress is calculated from eq. (3.23) and the plastic potential according to eq. (3.24).

$$p^{eq} = p' + \frac{3}{2} \cdot \frac{\{\boldsymbol{\sigma}_d - p' \cdot \boldsymbol{\beta}_d\}^T \{\boldsymbol{\sigma}_d - p' \cdot \boldsymbol{\beta}_d\}}{p' \left(M^2 - \frac{3}{2} \{\boldsymbol{\beta}_d\}^T \{\boldsymbol{\beta}_d\} \right)} \tag{3.23}$$

where $\boldsymbol{\beta}_d$ is the deviatoric rotational vector.

$$Q = p' + \frac{3}{2} \cdot \frac{\{\boldsymbol{\sigma}_d - p' \cdot \boldsymbol{\alpha}_d\}^T \{\boldsymbol{\sigma}_d - p' \cdot \boldsymbol{\alpha}_d\}}{p' \left(M^2 - \frac{3}{2} \{\boldsymbol{\alpha}_d\}^T \{\boldsymbol{\alpha}_d\} \right)} - p_Q^{eq} = 0 \tag{3.24}$$

The n-SAC model uses similar hardening laws that are used in the S-CLAY1S model for both rotation law and destructuration, see Grimstad & Degago (2010) for details.

In addition to the hardening laws, Grimstad & Degago (2010) also define a creep limit dependent on either t_{max} or OCR_{max}, i.e. if t_{max} or OCR_{max} is reached no more creep will occur. Grimstad & Degago (2010) also defines the initial structure according to eq. (3.25).

$$\chi_0 = \frac{r_{si} - r_{s,\min}}{r_{s,\min}} \tag{3.25}$$

where r_{si} is the intrinsic time resistance number and $r_{s,min}$ is the minimum time resistance number measured, see Figure 3.5.

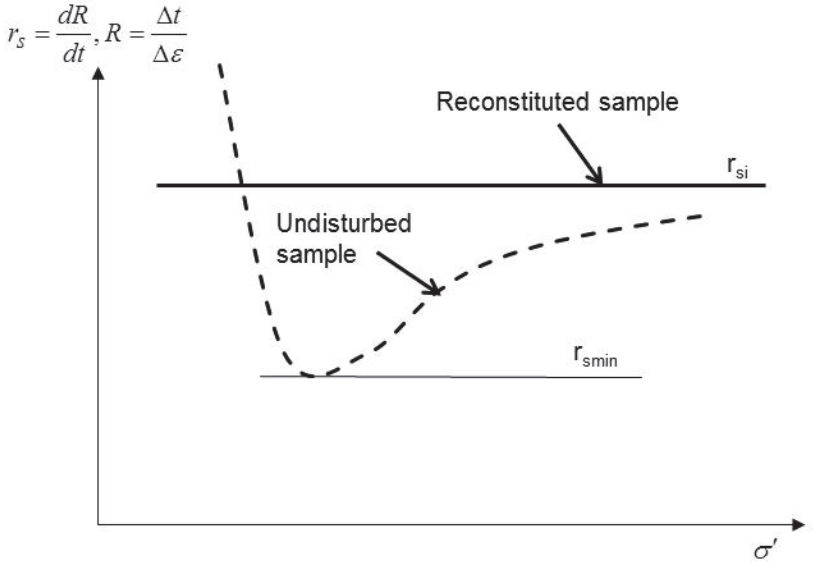

Figure 3.5. Determination of creep parameters according Grimstad & Degago (2010).

See Grimstad & Degago (2010) for more information regarding the n-SAC model.

3.3.4 CREEP-SCLAY1S model

The CREEP-SCLAY1S model is an extension of the S-CLAY1S model described in section 3.2.2 that incorporates creep effects. This model has been implemented by Sivasithamparam et al. (2013) in the finite element code Plaxis BV. The model make use of the equivalent mean stress similar to the Anisotropic Creep Model, see eq. (3.20), and the visco-plastic multiplier presented by Grimstad et al. (2008). The visco-plastic multiplier is then expressed as eq. (3.26).

$$\dot{\lambda} = \frac{\mu_i^*}{\tau} \cdot \left(\frac{p^{eq}}{(1+\chi) \cdot p'_{ci}} \right)^{\frac{(\lambda_i^* - \kappa^*)}{\mu_i^*}} \cdot \frac{M_c^2 - \alpha_0^2}{M_c^2 - \eta_0^2} \tag{3.26}$$

where α_0 is the inclination of the reference surface in K_0^{NC} loading and η_0 is the stress path corresponding to K_0^{NC} loading. M_c is the slope of critical state line in triaxial compression and μ_i^* is the intrinsic creep index.

The model uses the same three hardening laws described for the S-CLAY1S model, see eq. (3.13) - (3.15), with the only difference being that the plastic strains in S-CLAY1S are replaced by the creep strains in the CREEP-SCLAY1S model.

The CREEP-SCLAY1S model also makes use of the Lode angle dependency, similarly to S-CLAY1S with the formulation by Sheng et al. (2000), see eq. (3.27).

$$M(\theta) = M_c \left(\frac{2\beta^4}{1+\beta^4+\left(1-\beta^4\right)\sin 3\theta} \right)^{\frac{1}{4}} \tag{3.27}$$

where $\beta=M_e/M_c$. It should be noticed that eq. (3.27) does not satisfy the convexity requirement when $\beta < 0.6$.

3.3.5 Discussion

The constitutive models described above incorporate many of the important aspects of soft soil behaviour. These constitutive models are capable of capturing strain rate - dependency, especially the n-SAC model and CREEP-SCLAY1S model, since these models also are capable of capturing “creep swelling” behaviour, due to the formulation of the visco-plastic multiplier. This makes it possible to go above the so-called failure line i.e. into the “dry side”.

Using the formulation of SSC model or ACM and looking at how the creep strain components are calculated in general stress space, see eq. (3.28), it is

clear that these models will have numerical problems when approaching critical state, M.

$$\dot{\varepsilon}_{ij}^{c} = \frac{\varepsilon_{v}^{c}}{\frac{\partial p'_{eq}}{\partial p'}} \cdot \frac{\partial p'_{eq}}{\partial \sigma'_{ij}} \tag{3.28}$$

The value of $\frac{\partial p'_{eq}}{\partial p'} \to 0$ when $q / p' \to M$, which implies that eq. (3.28) goes to infinity when approaching critical state. In the implementation of the model this is controlled by using a Mohr-Coulomb failure criterion with zero dilatancy that has a smaller inclination than the critical state M. However, this implies that these models are restricted to stress states below the failure line.

The n-SAC model and CREEP-SCLAY1S model use the rotated ellipse in p´-q space as a normal compression surface. By using the new visco-plastic multiplier that allows you to go above the critical state line, as in the original MCC model, it would imply that these models would also suffer from predicting unrealistic high values of undrained shear strength for overconsolidated soils, as often stated for the MCC model.

To use these constitutive models, n-SAC and CREEP-SCLAY1S models, as a base and improve the normal compression surface to better represent experimental findings for the overconsolidated state, i.e. the dry-side, would be a major improvement. The models do not include any form of anisotropy in the linear elastic region and neither are they capable of capturing small strain stiffness or hysteretic effects. So, these features would also need further research.

4 DEVELOPMENT OF AN ANISOTROPIC CREEP MODEL

In this chapter a new anisotropic creep model is developed and implemented in to the COMSOL Multiphysics v4.3a finite element program. This chapter gives a detailed description of the mathematical formulation in general stress space and discusses the implementation of the model.

4.1 Introduction

The modified anisotropic creep model with structure will from here on be called the MAC-s model (Modified Anisotropic Creep model with structure). It is based on the CREEP-SCLAY1S model and the n-SAC model developed by Karstunen et al. (2005) and Grimstad & Degago (2010), respectively. The difference between the MAC-s model and the CREEP-SCLAY1S model is that the new model has a different normal compression surface (NCS), but it uses the CREEP-SCLAY1S normal compression surface as the plastic potential surface. The normal compression surface is a simplified form of the MIT-S1 model, see Figure 4.3. The main intention of the new material model is to capture the “dry side” or the overconsolidated state better than the existing creep models and to give more flexibility to change the shape of the normal compression surface.

4.2 Mathematical formulation of the constitutive model

This creep model is based on the extension from one-dimensional formulation to a general three-dimensional constitutive model by Vermeer et al. (1998). The difference is that this constitutive model does not adopt the Modified Cam-Clay (MCC) type of ellipses as described in the following sections.

4.2.1 Elastic parameters

The MAC-s model makes use of the same type of stress dependent formulation for the elastic parameters as the Modified Cam-Clay type of models i.e. the tangent bulk modulus is defined according to eq. (4.1).

$$K' = \frac{p'}{\kappa^*} \tag{4.1}$$

where κ^* is the slope of swelling line and p' is mean effective stress. The shear modulus, G, is calculated based on the bulk modulus with the assumption of a constant Poisson´s ratio, ν', according to eq. (3.11).

$$G = \frac{3(1-2\nu')}{2(1+\nu')} \cdot K' \tag{4.2}$$

The model also incorporates a simplified form of transversely isotropic material according to Graham & Houlsby (1983) that uses only one extra parameter instead of the three extra you need for fully define a transversely isotropic material. Using the procedure described by Graham & Houlsby (1983) the elastic stiffness matrix, D, is defined as eq. (4.3).

$$D = \frac{E^*}{(1+\nu^*)(1-2\nu^*)} \cdot \begin{bmatrix} \alpha_e^2(1-\nu^*) & \alpha_e^2\nu^* & \alpha_e\nu^* & & & \\ \alpha_e^2\nu^* & \alpha_e^2(1-\nu^*) & \alpha_e\nu^* & & & \\ \alpha_e\nu^* & \alpha_e\nu^* & 1-\nu^* & & & \\ & & & \alpha_e^2(1-2\nu^*) & & \\ & & & & \alpha_e(1-2\nu^*) & \\ & & & & & \alpha_e(1-2\nu^*) \end{bmatrix} \tag{4.3}$$

where $E_v = E^*$, $E_h = \alpha_e^2 E^*$, $\nu_{vv} = \nu^* / \alpha_e$, $\nu_{vh} = \nu*$ and $2G_{vh} = \alpha_e E^* / (1+\nu^*)$ and for clarity all zeros are left out.

A detailed description regarding the transformation described above could be found in Graham & Houlsby (1983). The FE software used, COMSOL Multiphysics v.4.3a, to implement the MAC-s model gives the user the options from full anisotropic, orthotropic and isotropic linear elasticity in addition to the simplified transversely isotropic material described above.

The effect of the parameter α_e in eq. (4.3) is shown in Figure 4.1 for typical undrained tests on clay which has been reconsolidated to a stress state lower than the preconsolidation pressure.

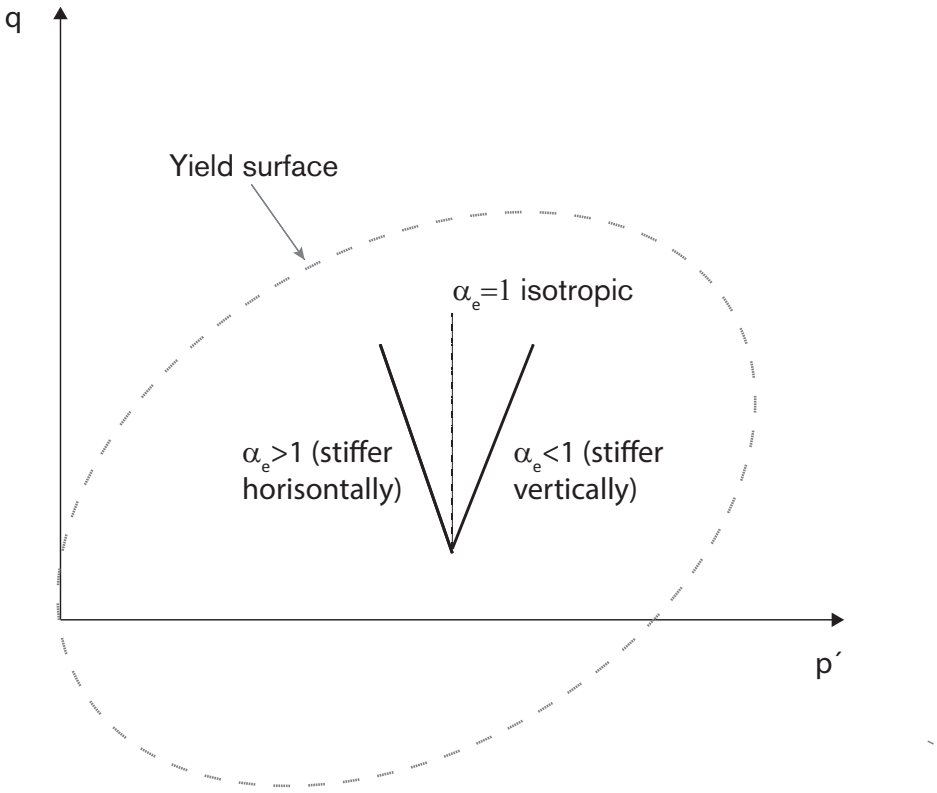

Figure 4.1. Schematic illustration for the elastic stress paths for different α_e-values in undrained shear test.

4.2.2 Normal compression and plastic potential surface

The normal compression surface, F, of the new anisotropic creep model in general stress space is defined according to eq. (4.4).

$$F = \frac{1}{2}(\mathbf{s})^T(\mathbf{s}) - p'^2 \cdot \left(1 - \left(\frac{p'}{p_c}\right)^m\right) \cdot \left(\mathrm{M}^2 - \frac{1}{2}\boldsymbol{\alpha}_\mathbf{d}{}^T \boldsymbol{\alpha}_\mathbf{d}\right) \tag{4.4}$$

where $\mathbf{s} = \boldsymbol{\sigma}_d - p' \cdot \boldsymbol{\alpha}_d$ and the exponent m in eq. (4.4) controls the shape, slenderness, of the normal consolidation surface. Using the same procedure as presented in Chapter 3 i.e. using the equivalent mean stress, p_{eq}, the normal compression surface is formulated according to eq. (4.5).

$$p_{eq} = \frac{p'}{\left[1 - \frac{\frac{1}{2}\{\boldsymbol{\sigma}_d - p' \cdot \boldsymbol{\alpha}_d\}^T \{\boldsymbol{\sigma}_d - p' \cdot \boldsymbol{\alpha}_d\}}{p'^2 \cdot \left(\mathrm{M}^2 - \frac{1}{2}\{\boldsymbol{\alpha}_\mathbf{d}\}^T \{\boldsymbol{\alpha}_\mathbf{d}\}\right)}\right]^{\frac{1}{m}}} \tag{4.5}$$

The plastic potential that is used for this model has the same shape as the CREEP-SCLAY1S model, i.e. the rotated ellipsoid according to eq. (4.6).

$$p_Q^{eq} = p' + \frac{3}{2} \cdot \frac{\{\boldsymbol{\sigma}_d - p' \cdot \boldsymbol{\alpha}_d\}^T \{\boldsymbol{\sigma}_d - p' \cdot \boldsymbol{\alpha}_d\}}{p'\left(M^2 - \frac{3}{2}\{\boldsymbol{\alpha}_d\}^T \{\boldsymbol{\alpha}_d\}\right)} \tag{4.6}$$

The normal compression surface makes use of the same hardening laws as described in section 4.2.3. The main reason of using the rotated ellipsoid as the plastic potential is that critical state is fulfilled at failure, furthermore Karstunen & Koskinen (2008) showed that the strain paths predicted by the S-CLAY1 model correspond well with experimental findings.

A visualization of the new normal compression surface, NCS, in general stress space compared with the plastic potential surface is presented in Figure 4.2a, and in Figure 4.2b only the new normal compression surface is presented to better visualize the deviatoric plane. Figure 4.3 shows a comparison of the new normal compression surface and the plastic potential surface in p´-q. In Figure 4.4 the influence of different α_0 and m values are displayed.

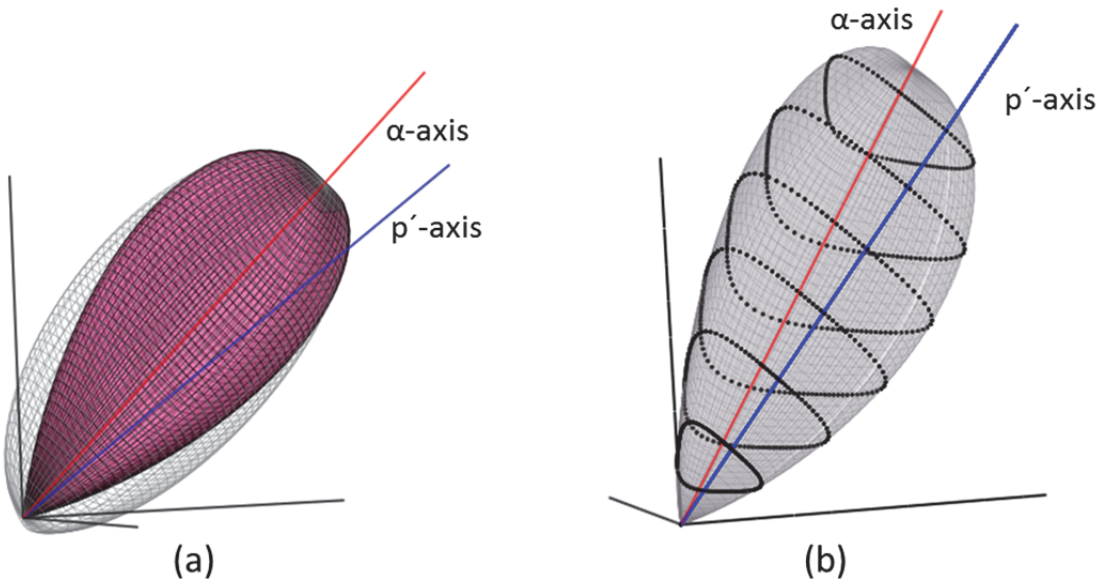

Figure 4.2. Visualisation of (a) for NCS (solid colour) and plastic potential surface (grey mesh) and (b) visualization of NCS only.

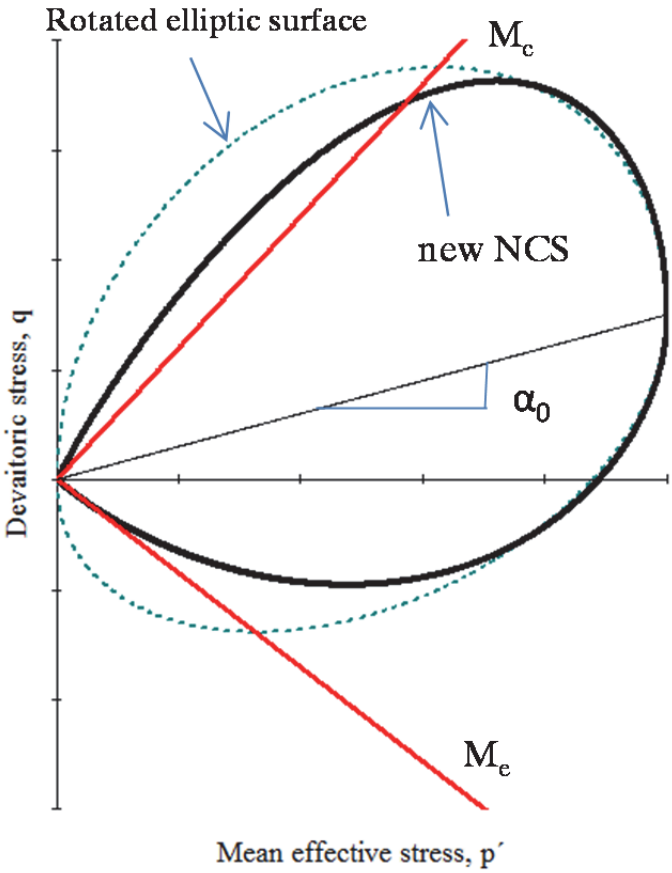

Figure 4.3. The NCS (solid line) of the MAC-s model with m=0.4 compared with plastic potential surface (dotted line) in p´-q plot together with the failure criteria.

The MAC-s model makes use of the visco-plastic multiplier as Grimstad et al. (2008) presented in the n-SAC model, see eq. (4.7).

$$\dot{\lambda} = \frac{1}{r_{si} \cdot \tau} \cdot \left(\frac{p^{eq}}{(1+\chi) \cdot p'_{ci}} \right)^{r_{si} \cdot \left(\lambda_i^* - \kappa^* \right)} \cdot \frac{M_c^2 - \alpha_0^2}{M_c^2 - \eta_0^2} \tag{4.7}$$

where M_c is critical state line in compression and α_0 , see eq. (4.17), is the rotation of the potential surface in K_0^{NC} loading and η_0 is the stress path corresponding to K_0^{NC} loading. It should be mentioned, that when implementing the creep model into COMSOL one makes use of either the Ordinary Differential Equation (ODE) feature or the new creep feature in version 4.3a or later. This means, when using these features in COMSOL, the visco-plastic multiplier is automatically obtained as described for the n-SAC model.

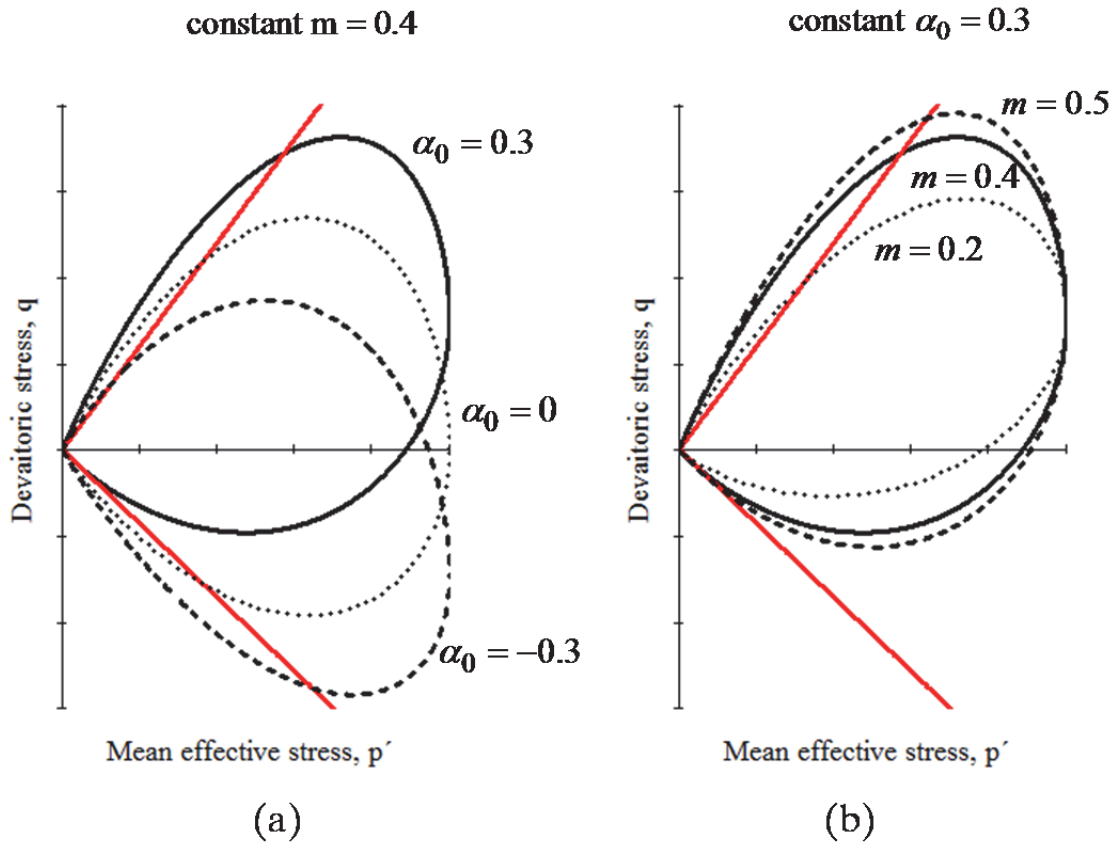

Figure 4.4. (a) The influence of the initial anisotropy and (b) the influence of different m values on the shape of NCS of the MAC-s model.

The MAC-s model also incorporates structure or bonding, as described for the S-CLAY1S model, based on the formulation by Gens & Nova (1993). The intrinsic reference surface has the same shape and inclination, but differs in size with respect to the normal compression surface i.e. the surface of the bonded soil, see Figure 4.5.

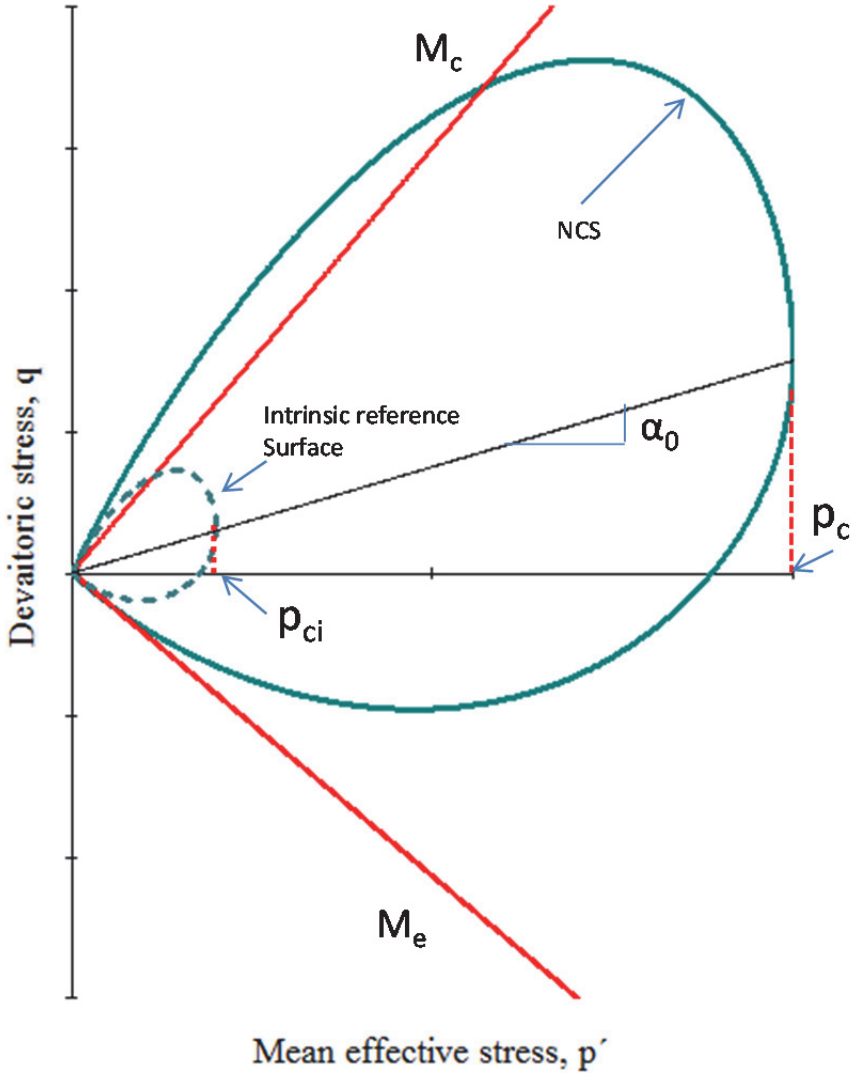

Figure 4.5. Visualisation in p´-q space of the NCS of the MAC-s model including the intrinsic reference surface and the failure criteria.

4.2.3 Hardenings laws

The MAC-s model incorporates three different hardening laws. The hardening laws are the same as for the CREEP-SCLAY1S model with

some small differences and are presented below for the sake of completeness.

The first hardening law is controlling the change in the size of the intrinsic reference surface with respect to the volumetric creep strains (ε_v^c), similar to that of Modified Cam-Clay, according to eq. (3.13).

$$p_{ci} = p_{ci0} \exp\left(\frac{\varepsilon_v^c}{\lambda_i^* - \kappa^*} \right) \tag{4.8}$$

where λ_i^* and κ^* are the modified compression index and modified swelling index respectively, evaluated from a "$\ln p' - \varepsilon_v$" plot. The parameter p_{ci0} is the initial preconsolidation pressure at the hydrostatic axis and the subscript "i" means the intrinsic parameter.

The second hardening law is describing the rotation of the reference surface, i.e. the evolution of the anisotropy, due to creep strains similarly to eq. (3.14).

$$d\boldsymbol{\alpha}_d = \left(\omega_v \left[\frac{3\boldsymbol{\eta}}{4} - \boldsymbol{\alpha}_d \right] \cdot \langle d\varepsilon_v^c \rangle + \omega_d^* \left[\frac{\boldsymbol{\eta}}{3} - \boldsymbol{\alpha}_d \right] \cdot d\varepsilon_d^c \right) \tag{4.9}$$

where $\boldsymbol{\eta}$ the generalised stress ratio, defined as $\boldsymbol{\eta} = \boldsymbol{\sigma}_d / p'$, and ε_d^c is the deviatoric creep strain. The new soil constants ω_v and ω_d^* controls the absolute rate at which $\boldsymbol{\alpha}_d$ heads towards its current target value. The $\langle\rangle$ are the Macaulay brackets and means that $\langle \varepsilon_v^c \rangle = d\varepsilon_v^c$ for $\mathrm{d}\varepsilon_v^c \geq 0$ and $\langle \varepsilon_v^c \rangle = 0$ for $\mathrm{d}\varepsilon_v^c \leq 0$.

It should be noted that the original form of eq. (4.9) is formulated with the parameter ω_v outside the outer parenthesis as eq. (3.14) this implies that the parameter ω_d^* should be seen as the product of the two, i.e.

$\omega_d^* = \omega_v \cdot \omega_d$, in this model. This is done to give the possibility to switch off either the volumetric or the deviatoric contribution in the rotational law if necessary.

The third hardening law describes the degradation of bonding in the soil and is defined by an intrinsic reference surface, based on the formulation by Gens & Nova (1993). The intrinsic reference surface has the same shape and inclination, but differs in size with respect to the normal compression surface i.e. the normal compression surface of the bonded soil. The size of the intrinsic reference surface is related to the normal compression surface by a parameter χ which determines the current degree of bonding according to eq.(3.15).

$$p_c = (1+\chi) \cdot p_{ci} \tag{4.10}$$

where p_{ci} is the intrinsic preconsolidation pressure at the hydrostatic axis, see Figure 4.5. The degradation of bonding is associated with volumetric and deviatoric creep strains and formulated according to eq. (3.16).

$$d\chi = -\chi\left(\xi_v \left|d\varepsilon_v^c\right| + \xi_d \left|d\varepsilon_d^c\right|\right) \tag{4.11}$$

where ξ_v and ξ_d are additional soil constants controlling the rate of degradation.

A small difference between the hardening laws for CREEP-SCLAY1S and the MAC-s model could be seen by comparing the equations above with eq. (3.14) and eq. (3.16). The difference is that in the MAC-s model there is no parameter that controls the total rate of either rotation of the normal compression surface or degradation of structure. Instead there is a parameter each for volumetric and deviatoric creep strains that controls the rate of rotation of the normal compression surface and degradation of structure.

4.3 Lode Angle dependency

In the proposed creep model the so-called LMN dependence by Bardet (1990) is used. The LMN dependency is based on failure surfaces of Lade & Duncan (1975) and Matsuoka & Nakai (1974). The parameter M in eq. (4.5) and eq. (4.6) has been made a function of the Lode angle as described below. This formulation gives a smooth failure surface compared to the Mohr-Coulomb failure surface, see Figure 4.6 for comparison.

LMN dependency is formulated according to eq. (4.12).

$$f(\theta) = \frac{\sqrt{3}}{2} \cdot \frac{\beta}{\sqrt{\beta^2 - \beta + 1}} \cdot \frac{1}{\cos(\Phi)} \tag{4.12}$$

where

$$\Phi = \begin{Bmatrix} \frac{1}{6}\cos^{-1}\left(-1 + \frac{27}{2}\frac{\beta^2(1-\beta)^2}{\left(\beta^2 - \beta + 1\right)^3} \cdot \sin^2(3\theta) \right) \text{ if } \theta \le 0 \\ \frac{\pi}{3} - \frac{1}{6}\cos^{-1}\left(-1 + \frac{27}{2}\frac{\beta^2(1-\beta)^2}{\left(\beta^2 - \beta + 1\right)^3} \cdot \sin^2(3\theta) \right) \text{ if } \theta > 0 \end{Bmatrix}$$

and β is related to the friction angle according to eq. (4.13) or eq. (4.14) and the Lode angle is defined as eq. (4.15)

$$\beta = \frac{3 - \sin(\phi')}{3 + \sin(\phi')} \tag{4.13}$$

Another option is to us the relation between the M parameter in compression and extension as eq. (4.14) to give more flexibility.

$$\beta = \frac{M_e}{M_c} \tag{4.14}$$

$$\theta_\alpha = \frac{1}{3}\sin^{-1}\left(\frac{3\sqrt{3}}{2}\cdot\frac{J_3^\alpha}{\left(J_2^\alpha\right)^{3/2}}\right) \tag{4.15}$$

where the α-term means that the Lode angle is defined on the α-line, i.e. $\boldsymbol{\sigma}_d - \boldsymbol{\alpha}_d p' = 0$, instead of on the isotropic axis. The LMN dependency has a more complex analytical expression than other formulations of the Lode angle dependences, but is satisfying the convexity requirement.

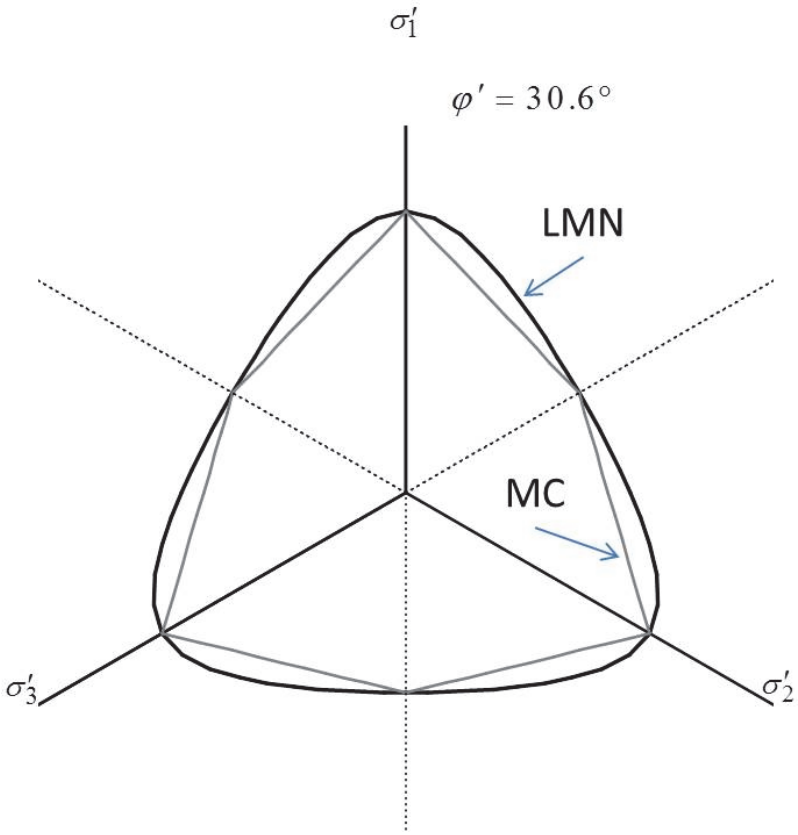

Figure 4.6. Failure surface in the deviatoric plane. LMN dependence compared with the Mohr-Coulomb (MC) failure surface.

4.4 Evaluation of model parameters

For the new anisotropic creep model there are a maximum of 15 parameters to define when structure and anisotropy is included. Some of these could be established by some simple assumptions as described in the following. In Table 4.1 an overview of the parameters used in the model

and a short description of tests that needs to be performed to obtain the proper values for the model parameters are given.

Some of the parameters described in Table 4.1 could also be determined with reasonable accuracy with certain assumptions, as briefly described below.

4.4.1 Initial condition, α_0, and rotation parameters, ω_v and ω^*_d.

In geomechanics it is commonly assumed, supported by a large amount of experimental data, that an estimate of the lateral earth pressure at rest corresponding to normally consolidated state of a soil, K_0^{NC}, is provided by Jaky´s formula according to eq. (4.16).

$$K_0^{NC} \approx 1 - \sin\phi' \tag{4.16}$$

where ϕ' is the critical state friction angle.

Wheeler et al. (2003) showed that by assuming that the soil has consolidated one-dimensionally, there is a theoretical link between K_0^{NC} and the initial rotation of the reference surface, α_0. By considering that in one-dimensional loading the ratio between deviatoric and volumetric irrecoverable strains is about 2/3, the initial inclination, α_0, could then be determined as eq. (4.17).

$$\alpha_0 = \frac{\eta_0^2 + 3\eta_0 - M_c^2}{3} \tag{4.17}$$

where $\eta_0 = 3(1 - K_0^{NC}) / (1 + 2K_0^{NC})$ and $M_c = 6 \cdot \sin\phi' / (3 - \sin\phi')$. Wheeler et al. (2003) also showed that the shear rotation parameter, ω_d, could be determined utilizing the assumption above. By setting dα=0 in eq. (3.14) and then combining with the flow rule of the plastic potential and eq. (4.17)

and after some algebraic manipulation the following expression is obtained.

$$\omega_d = \frac{3}{8} \cdot \frac{4M_c^2 - 4\eta_0^2 - 3\eta_0}{\eta_0^2 - M_c^2 + 2\eta_0} \tag{4.18}$$

As discussed above, parameter ω_d^* in the MAC-s model is the product of the two, i.e. ω_d and ω_v, and this gives $\omega_d^* = \omega_d \cdot \omega_v$.

The parameter, ω_v, controls rate of NCS to rotate due to volumetric creep strains. Determination of this parameter is not a straight forward task. A simple way of estimating a value for was presented by Zentar et al. (2002) where they relate it to the compression index, λ, and suggested typical values of $\omega_v = 10/\lambda - 15/\lambda$. These suggestions are based on simulation results.

Leoni et al. (2008) suggested that the parameter, ω_v, that controls the absolute rate of rotation could be estimated with a more theoretical approach. Leoni et al. (2008) assumed that the anisotropy is more or less erased when $\alpha_0 / \alpha = 10$, and furthermore that this typically occurs when the stress go two to three times over the original normal compression surface. Leoni et al. (2008) then presented the following expression.

$$\omega_v = \frac{1}{\lambda^*} \cdot \ln\left(\frac{10M_c^2 - 2\alpha_0\omega_d}{M_c^2 - 2\alpha_0\omega_d} \right) \tag{4.19}$$

The simplest and probably the most correct way of determining the rotational parameter, ω_v, would be to conduct model simulations of laboratory tests that involves a large amount of rotation e.g. an isotropic consolidation test or a undrained shearing in triaxial extension, as suggested by Pestana & Whittle (1999).

Table 4.1. An overview of the parameter used in the MAC-s model.

Test type	Parameter	Physical contribution/meaning
1-D compression test (triaxial, oedometer or CRS apparatus)	κ^* and λ_i^*	Modified swelling and intrinsic compression index evaluated from $\ln p' - \varepsilon_v$ plot
1-D reconstituted compression test	r_{si}	Intrinsic creep number $r_{si} = 1/\mu_i^*$
K_0-oedometer or K_0-triaxial measuring radial strains with unloading stage	ν_{ur}	Poisson´s ratio at un/reloading
	K_0^{NC}	K_0 for normal consolidated clay
Undrained triaxial shear tests: CK_0UC and CK_0UE at OCR≥1	M_c and M_e	Critical state slope of failure in compression and extension
	α_e	Elastic anisotropy factor
	m	Shape coefficient for of the NCS, typical value of m = 0.35-0.4
Drained/undrained triaxial tests in different stress paths	ω_v and ω_d^*	Control the volumetric and deviatoric rate of rotation of NCS
1-D reconstituted compression test	χ_0	Initial amount of bonding
Drained triaxial tests for different stress paths	ξ_v and ξ_d	Control the rate of degradation of bonding due to volumetric and deviatoric creep strains
	α_0	Initial inclination
1-D compression test or undrained triaxial test	σ'_{vc}	Vertical preconsolidation pressure

4.4.2 Destructuration parameters and the shape parameter m

The degradation of bonding with creep strains, called destructuration, is represented by three parameters. To determine the initial bonding, χ_0, of a natural soil there is according to Koskinen et al. (2002) two possible ways. The simplest procedure is to use the sensitivity of the soil, $\chi_0 = S_T - 1$. The second one is to conduct oedometer test on reconstituted soil samples and compare with undisturbed oedometer test to find and evaluate the intrinsic compression line, see Figure 4.7.

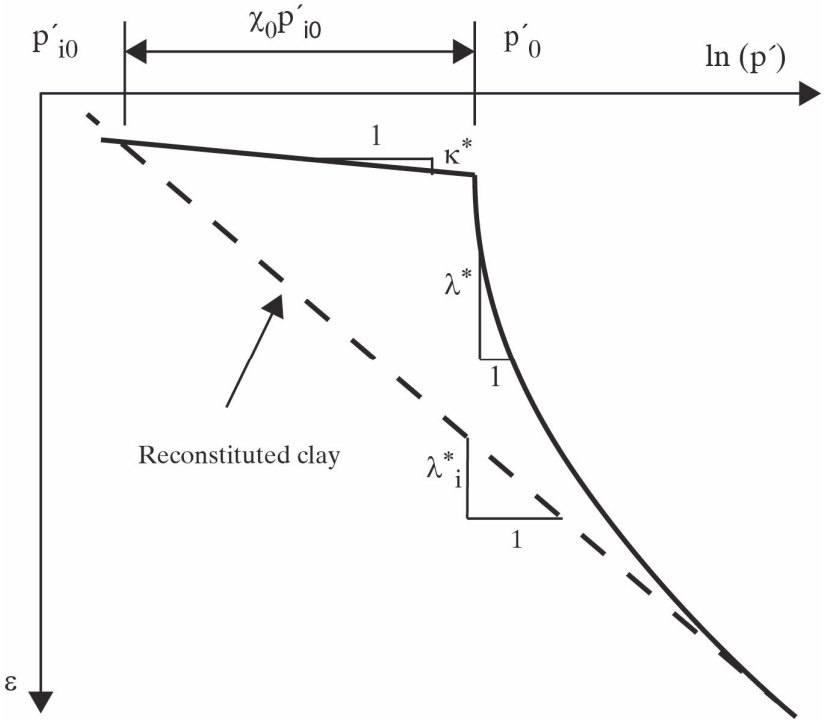

Figure 4.7. Definition of parameters when reconstituted sample compared with undisturbed sample is used.

Another approach to define the initial bonding of a clay was presented by Grimstad & Degago (2010) according to eq. (4.20).

$$\chi_0 = \frac{r_{si} - r_{s\min}}{r_{s\min}} \tag{4.20}$$

where r_{si} is the intrinsic creep number and r_{smin} is the minimum creep number evaluated from a least one incremental oedometer test.

To determine the values of the parameters ξ_v and ξ_d Koskinen et al. (2002) suggested a optimization procedure. This is conducted by simulating a triaxial test with a very low value of η so ξ_v could be estimated, i.e. where the shear strains were small and the effect of the parameter ξ_d is negligible. Then, with this estimated value of ξ_v, a simulation of a triaxial test with a high value of η is conducted to estimate the ξ_d value.

To determine the shape parameter *m* undrained triaxial test should be conducted for both compression and extension, and simulation of these tests should be conducted so the best fit of the critical state line is found.

4.5 Implementation

The FE software used to implement the new MAC-s model is COMSOL Multiphysics v.4.3a and v.4.3b. Here a short description of the implementation is done and the reader is referred to Olsson (2013) for a more complete description of the implementation of the creep model in to COMSOL.

The implementation of the model makes use of three different features in the structure of COMSOL, namely a Solid Mechanics, Darcy law and two Ordinary differential equation (ODE) features. The Solid Mechanics node offers the major features, i.e. all other features are linked to this, and the definition of the linear elastic properties and the relevant boundary conditions are set here. The Darcy law features controls the flow of water and relevant boundary conditions for this is set here in. The two ODE features contain the rotational hardening law and the creep strain contribution. The creep strain contribution can also be calculated with the new creep feature in version 4.3a.

4.6 Model simulations

Some common laboratory tests are simulated below to present the performance and capabilities of the new creep model. The parameters chosen for these simulations are just hypothetical even do they represent what would be typical for Gothenburg clays.

Input parameters used are summarized in Table 4.2 and the initial state variables were created from an initial vertical stress of 100 kPa and a K_0=0.6 and for the CRS oedometer simulations the simulated sample has been unloaded to a vertical effective stress of 10 kPa and the preconsolidation pressure is set to 100 kPa. For the triaxial simulations the OCR varies with different simulations and is stated in the plots of the results. The simulated test samples have a diameter of 50 mm and a sample height 20 mm for oedometer and 100 mm for the triaxial test.

Table 4.2. Input parameters for simulations.

ν_{ur}	ϕ'	κ^*	λ_i^*	r_{si}	τ	ω_v	ω_d^*
0.2	32°	0.015	0.1	1000	1[day]	200	170

χ_0	ξ_v	ξ_d	M_c	M_e	α_0	m
10	8	2	1.287	0.9	0.49	0.4

Note: Input parameters M_c, M_e, α_0 and ω_d^* is a function of friction angle ϕ'.

In Figure 4.8a two CRS tests are simulated with varying the destructuration parameter ξ_v and in Figure 4.8b three CRS tests are simulated with different strain rates. As could be seen from Figure 4.8a the influence of destructuration parameter ξ_v is very pronounced for the CRS simulations. A change, 4 to 8 in this case, gives very large difference in stiffness in the normal consolidated range. Another observation to be seen is that the

preconsolidation pressure does not change due the change of the destructuration parameter, ξ_v.

Figure 4.8b demonstrates that when simulating a CRS test with different strain rates, with the same set of soil parameters, the preconsolidation pressure increases with increasing strain rate and vice versa. However, when passing the preconsolidation pressure the stress-strain curves become parallel to each other. It can also be seen that when varying the strain rate, the stress-strain curve jumps between isotaches, i.e. following the stress - strain curve associated with the corresponding strain rates. The simulations of the CRS test results correspond to the general behaviour observed experimentally, discussed in Chapter 2.

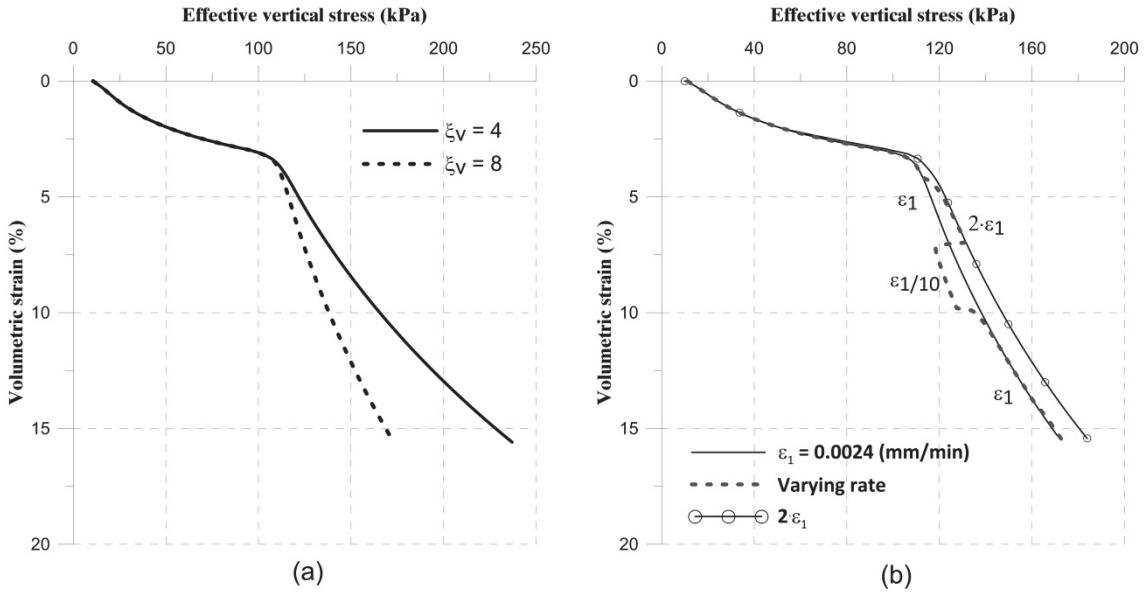

Figure 4.8. Simulated CRS tests conducted. (a) Effect of the destructuration parameters with a constant deformation rate of 0.0024 mm/min, ξ_v, and (b) effect of strain rate.

In Figure 4.9 and Figure 4.10 K_0- consolidated undrained triaxial tests are simulated, both compression and extension, were the dots in the figures represent the stresses at the start of shearing. These triaxial simulations are

conducted with different OCR values and with different values of the rotation parameter ω_v respectively.

For higher OCR values, based on Figure 4.9, once the normal compression surface is reached, there is an increase in the undrained shear strength, until at a certain point the critical state line is reached and then the undrained shear strength starts to decrease. For the undrained triaxial test performed with OCR=1.1 the results are similar to the simulations with higher OCR, and as stresses reach the normal compression surface there is a decreases in the undrained shear strength. The extension tests simulated have the same behaviour as the compression tests. However, the critical state line is influenced by the Lode angle dependency and therefore the simulated extension tests have a lower undrained shear strength than the compression tests.

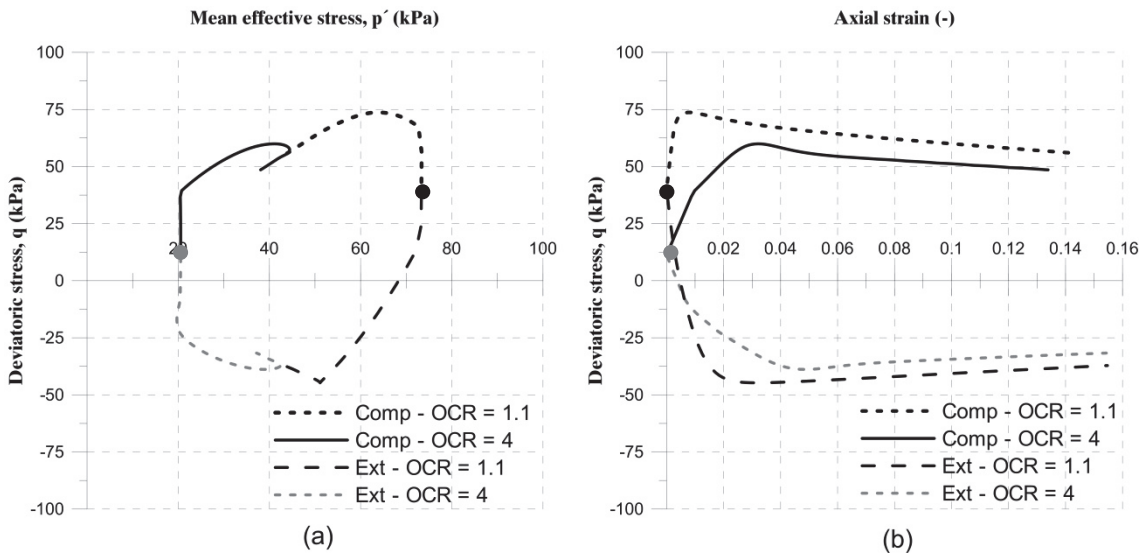

Figure 4.9. Simulations of K_0 Consolidated Undrained compression and extension triaxial tests with different OCR values with a constant deformation rate of 0.01 mm/min.

As seen in Figure 4.10, changing the parameter ω_v has very little influence on the results for an undrained compression test while in contrast it has a great influence on the extension test. This is to be expected since

significant rotation of NCS is experienced during such test, given the starting point of the shearing was K_0-consolidated to in-situ state. The value of the rotational parameter, ω_v, is also effecting the direction of stress path at the critical state line, i.e. if a low value is set the predicted undrained shear strength will increase and the opposite occurs if a high value is chosen. The value chosen are, as demonstrated in Figure 4.10, also affecting both the stress path and the apparent failure strength of the material.

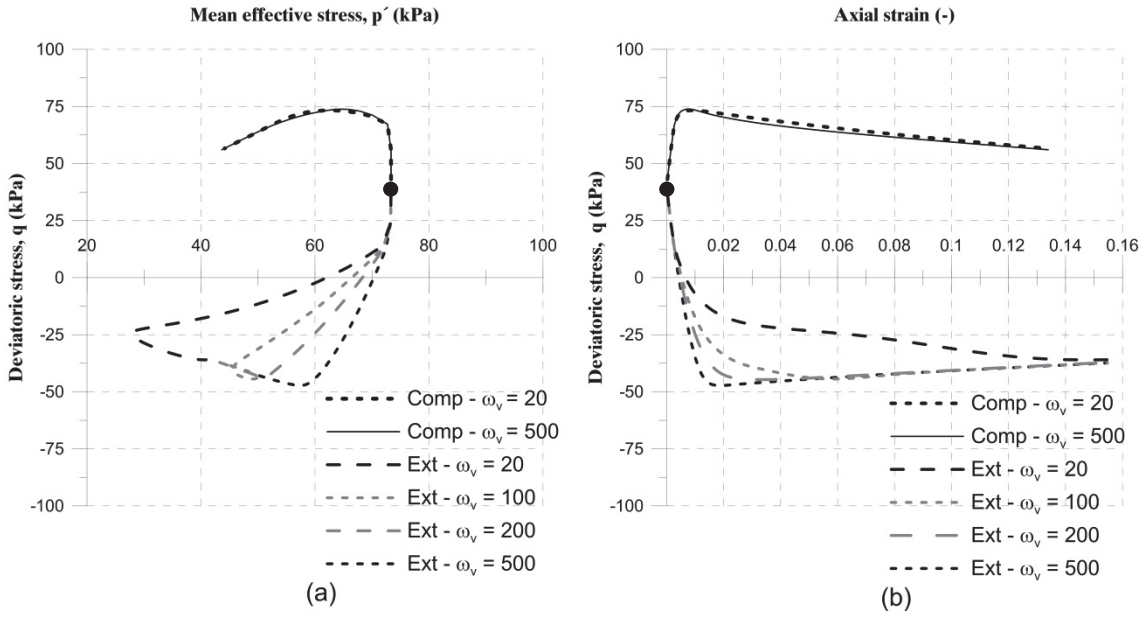

Figure 4.10. Simulations of K_0 Consolidated Undrained compression and extension triaxial tests with different values of ω_v with a constant deformation rate of 0.01 mm/min.

In Figure 4.11 simulation of three undrained triaxial test with different strain rates are shown. When the strain rate is changing, the resulting undrained shear strength is changed accordingly. It is also demonstrated in Figure 4.11 that the MAC-s model is capable of capturing the post peak strain rate variation. This is due to that the volumetric creep strains are not restricted to be positive only, as done in the ACM model.

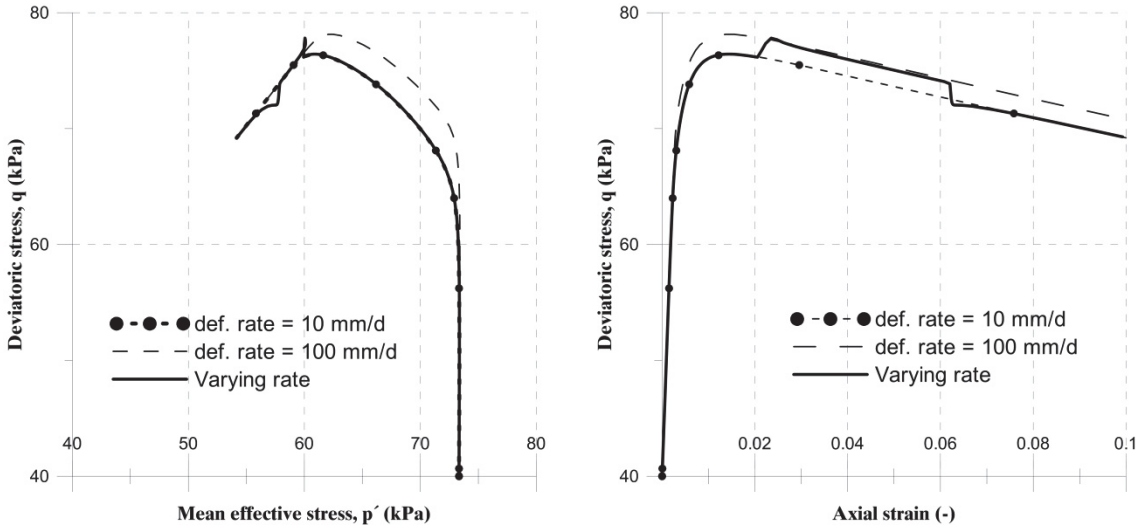

Figure 4.11. Simulations of undrained triaxial tests with different strain rates.

4.7 Discussion

The MAC-s model seems to be capable of capturing many of the important aspects of soft clay behaviour such as rate-dependency, destructuration and the effect of plastic anisotropy. It also seems to predict more reasonable stress paths and undrained shear strength for overconsolidated soils than the previous models. This is due to the new formulation of the normal consolidation surface, shown in Figure 4.3.

The new normal compression surface has the greatest influence on the overconsolidated part, and the new model also gives a possibility to change the appearance of the normal compression surface via the shape factor m, see Figure 4.4, giving the model additionally flexibility.

In Figure 4.12 and Figure 4.13 comparison between the MAC-s model and the CREEP-SCLAY1S model is performed for undrained triaxial test with an OCR = 4, for both compression and extension. It also includes a variation of the shape factor, m, for the MAC-s model and how it affects the stress and strain path.

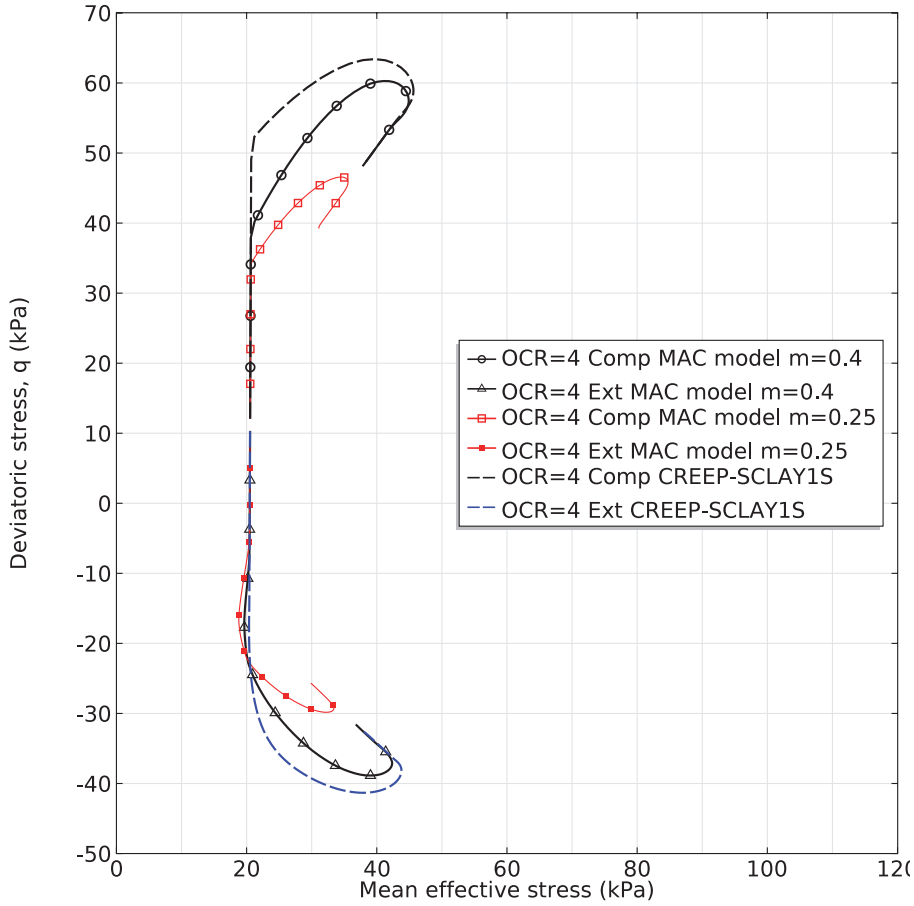

Figure 4.12. Comparison between the stress path predictions by the MAC-s model and the CREEP-SCLAY1S model for undrained triaxial test for OCR=4 with different values of the shape factor m.

Because of the shape of the new normal consolidation surface in the MAC -s model, it predicts yielding earlier than CREEP-SCLAY1S model, as demonstrated in Figure 4.12 and Figure 4.13. Hence the predicted peak undrained shear strength is lower than that predicted by the CREEP-SCLAY1S model. A smaller m value results in lower yielding and lower strength, but the stress – strain curve becomes parallel, see Figure 4.13.

The stress-strain curves, in Figure 4.13, shows that for the simulation with the greater *m* value (*m*=0.4) the residual stress-strain curves coincide with CREEP-SCLAY1S simulation at large strain. The two simulations fall down on the critical state line at more or less the same stress state. However, the MAC-s model is predicting larger strains before reaching the

peak strength compared to the CREEP-SCLAY1S model, and this due to the different formulation of the normal compression surface. The influence of the shape factor *m* is very evident: when using a lower *m* value, as stated above, the predicted peak strength is reduced.

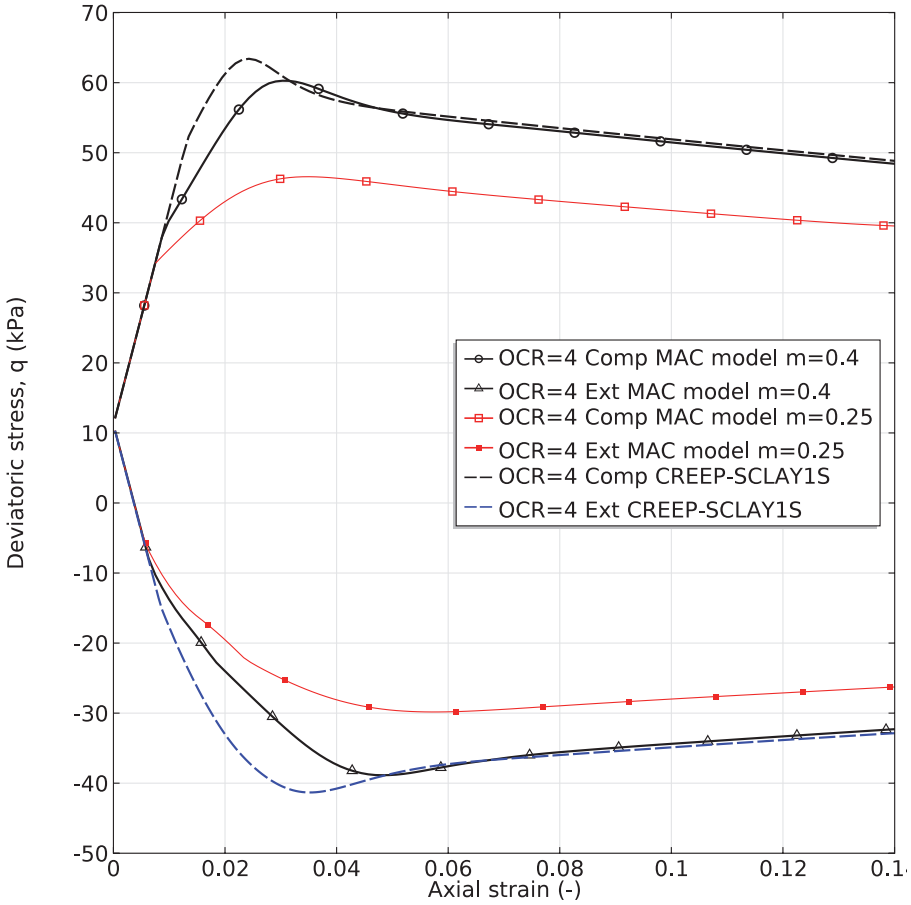

Figure 4.13. Comparison between the stress-strain predictions by the MAC-s model and the CREEP-SCLAY1S model for undrained triaxial test for OCR=4 with different values of the shape factor m.

In Chapter 5 and 6, a number of different laboratory test on Gothenburg clay are presented. Chapter 6 includes also some simulations with the new model compared to some selected laboratory tests in order to see how well the new model represents real soil behaviour.

5 NOVEL K_0-TRIAXIAL CELL

In this chapter a new K_0-triaxial cell will be presented. First some conventional techniques for establishing both compression and strength parameters for soft soils will briefly be discussed.

Empirical relations regarding the ratio of horizontal and vertical effective stress will be discussed and compared with results with the K_0-triaxial cell.

5.1 Introduction

The new K_0-triaxial cell presented in this chapter was developed mainly to establish the ratio between horizontal and vertical effective stress at normally consolidated conditions, i.e. the K_0^{nc} value without any ring friction.

A relatively extensive laboratory study was performed in order to have a better understanding of the creep behaviour of Gothenburg clay. In this chapter the test procedure of the traditional techniques for establishing consolidation and strength parameters for soft soil properties are briefly described and the experimental results are presented in Chapter 6.

5.2 Conventional techniques for soil testing

Conventionally soil properties, such as compression behaviour and strength, are typically determined based on a limited number of laboratory tests, such as Incremental loading oedometer (IL), CRS oedometer, triaxial test and the Bishop and Wesley triaxial cell. A detailed description of the equipment used in this thesis could be found in e.g. Persson (2004). In the following, the devices used in this work are briefly described.

5.2.1 **Incrementally loaded oedometer test**

IL oedometer tests are perhaps the oldest and most common type of soil test that has been used to determine mechanical soil properties. The set-up for an IL-oedometer is shown in Figure 5.1.

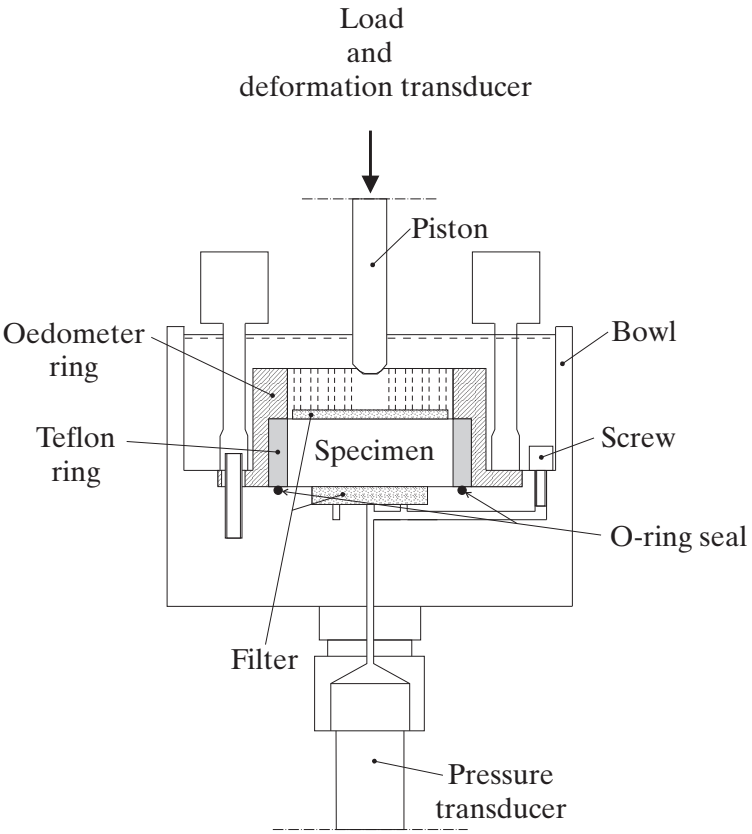

Figure 5.1. A schematic sketch of the used oedometer, Claesson (2003).

In the present study the main purpose of these tests was to study the creep behaviour of soft clays in the Gothenburg region.

The tests were performed on specimens with a diameter of 50 mm and a height of 20 mm. In order to minimize side friction during the test silicon grease is applied to the Teflon ring. The IL oedometer tests are loaded with a load increment ratio. Traditionally the load increment ratio is 1 for duration of 24 hours i.e. each load increment is equal to the previous load and applied for 24 hours. The drainage could either be two-sided or one sided, in the latter case drainage is only permitted on the top of the sample

and this enables measuring the pore water pressure at the bottom of sample.

5.2.2 Constant rate of strain oedometer tests

The Constant Rate of Strain (CRS) oedometer test is the most commonly used test in Sweden to determine the compression parameters for soft clays. Strictly speaking, the Swedish version of the test is a constant deformation rate test, rather than constant rate of strain.

The methodology used in Sweden was developed by Sällfors (1975) and the test equipment and procedure is very similar to the IL oedometer test, see Figure 5.1. The main difference is that the load is applied with a constant strain rate. In Sweden a rate of 0.0024 mm/min is used as a standard. This strain rate is a result from correlation of field tests and laboratory tests conducted by Sällfors (1975).

In the present study CRS oedometer tests are used to determine the compression properties such as preconsolidation pressure, constrained modulus, and the consolidation coefficient of vertical consolidation.

5.2.3 Bishop and Wesley triaxial test

The triaxial system used in this thesis is described in detailed by Menzies (1988) and in the GDS Advanced Digital Controller Handbook (2000). It is originally designed for stiff London clay, but extensively modified for testing soft clays. Figure 5.2 shows the triaxial cell setup with the advanced control units for the cell pressure, back pressure, axial load, data acquisition and the computer software.

The cell pressure and axial load control units are filled with paraffin oil and the back pressure control unit is filled with deionized water that has been de-aired in a vacuum chamber with a negative pressure of 0.9 bars.

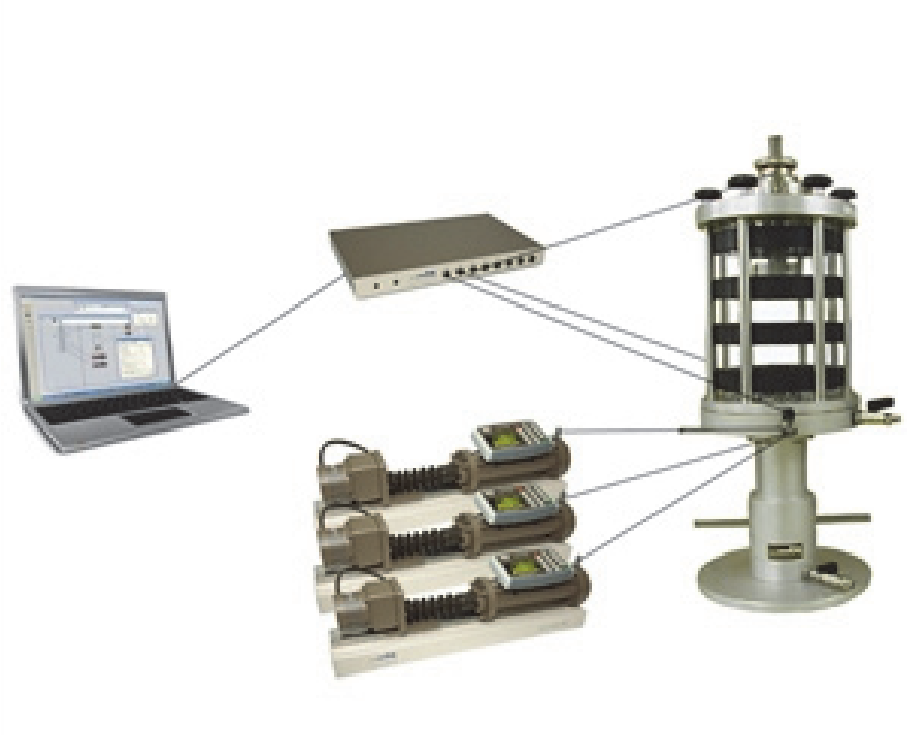

Figure 5.2. Setup of triaxial testing system,GDS Instruments Ltd (2013).

The default test procedure is to consolidate the sample to a prescribed stress state using a ramp loading sequence. Back pressure is also applied to get an appropriate pore pressure in the specimen.

The tests in the present study are mainly consolidated undrained test to describe the yield and failure surface in both compression and extension. The tests are also used to establish e.g. the undrained shear strength and the friction angle.

5.2.4 **Discussion**

In Sweden, typically the oedometer tests are the only tests conducted for establishing the consolidation parameters. There is no measurement of horizontal stresses and therefore no information is obtained regarding the K_0 as a function of stress/strain.

In a Bishop and Wesley triaxial cell there are possibilities of doing both drained and undrained triaxial tests, controlled by either stress or strain. A so-called K_0 test, i.e. oedometric conditions, with these devices is possible

by using either volume control or radial deformation control to keep the radial deformation constant. However, this is controlled by pumps and normally a stress increase is applied continuously. These types of test are very complex, and it is very difficult to keep the vertical stress constant over a relatively long period of time. This is the type of test that would be of interest when looking at creep behaviour and how it affects the overconsolidation ratio over time.

Hence a new K_0-triaxial cell was designed and built were loads could be applied similarly to an IL oedometer test, i.e. incrementally and constant with time.

5.3 Novel K_0-triaxial cell

The new K_0-triaxial cell that was constructed during this project is intended to be used for incremental load steps in either drained or undrained conditions. The new K_0-triaxial cell could easily be extended to handle strain controlled deformation as the oedotriax described by Janbu (1973) and the K_0-triaxial cell described by Campanella & Vaid (1972).

The new K_0-triaxial cell is controlled by a radial deformation gauge to keep the radial deformation constant at the initial value. This differs from the one described by Campanella & Vaid (1972) that only uses a same piston size as the sample.

The main aim of the new K_0-triaxial cell was to study the value of the K_0 with regard to strain and time. The new K_0-triaxial cell also gives the possibilities to study the effect of ring friction when compared to standard oedometer tests. If unloading stages are conducted, the re-/unloading parameters could also be determined.

5.3.1 **Description of the new K_0-triaxial cell**

A schematic sketch of the new K_0-triaxial cell is presented in Figure 5.3. The axial loading ram has the same area as the soil sample to minimize the volume change. The loading ram is guided in its vertical direction by linear ball bearings from SKF type LBCR 60 mm. The loading ram is sealed with Latex folded membrane. The linear ball bearing gives a more or less frictionless vertical movement of the loading ram, and the flexible membrane just extends or compresses as the loading ram moves. As seen in Figure 5.3, the load cell is inside the triaxial cell and the friction that could be developed from the ball bearings is therefore not important since the actual load is being measured inside the triaxial cell.

The medium used to create the cell pressure is paraffin oil and this is controlled by air pressure via oil containers next to the cell.

During consolidation, with the desired stress path, the cell pressure and vertical stress are applied manually by the operator. The cell pressure is controlled by air pressure and the vertical stress by incremental loads i.e. by dead weights.

For K_0-tests, i.e. the oedometer case, where there should be no lateral deformations, the cell pressure is increased or decreased by a computer controlled pump. The feedback of radial deformation gauge is activating the pump when certain conditions are fulfilled. Generally the conditions are set so that when the radial deformation deviates more than +/- 0.3 μm from the initial value the pump will either increase or decrease the cell pressure. The pump is also restricted so that it is only active for a certain time over a time period so it lets the soil sample to respond for the stress change. Normally the active time for the pump to be active is set to 10 s for a period of 100 s.

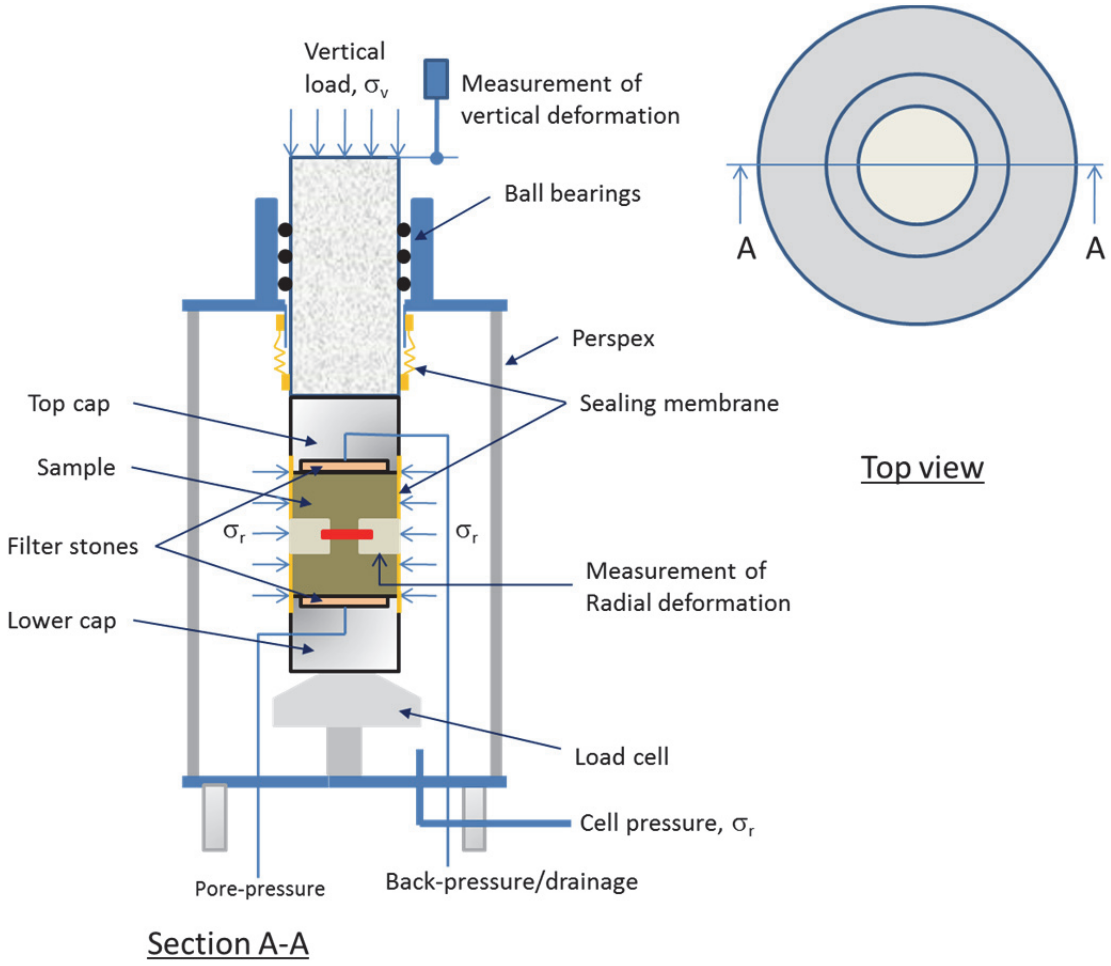

Figure 5.3. A schematic sketch of the new K_0-triaxial cell for sample with a diameter of 50 mm.

5.3.2 **Technical specifications**

In this setup there are six different sensors used to measure the pore pressure, cell pressure, axial load, back pressure, vertical deformation and the radial deformation. The pore- and cell pressure gauges used have a measurement range of 0-300 kPa with an accuracy < 0.1 kPa. The load cell has a measurement range of 0-1 kN, with an accuracy < 1 N and the vertical displacement gauge range was 0-50 mm with an accuracy of < 0.01 mm. The deformation gauge that measures the radial deformation is a SG-DVRT-8 with a signal conditioner model DEMOD-DC from Microstrain Inc. (2013). It has a total stroke length of 8 mm, but in this case it is calibrated within a range of < 1.0 mm in the middle span of the stroke

length resulting in a specified accuracy of 0.1% i.e. 1 μm. The measurements of this calibration gave stable, relative zero displacement, of < 0.3 μm for the two calibration tests, as demonstrated in Figure 5.4 for the relative zero displacement.

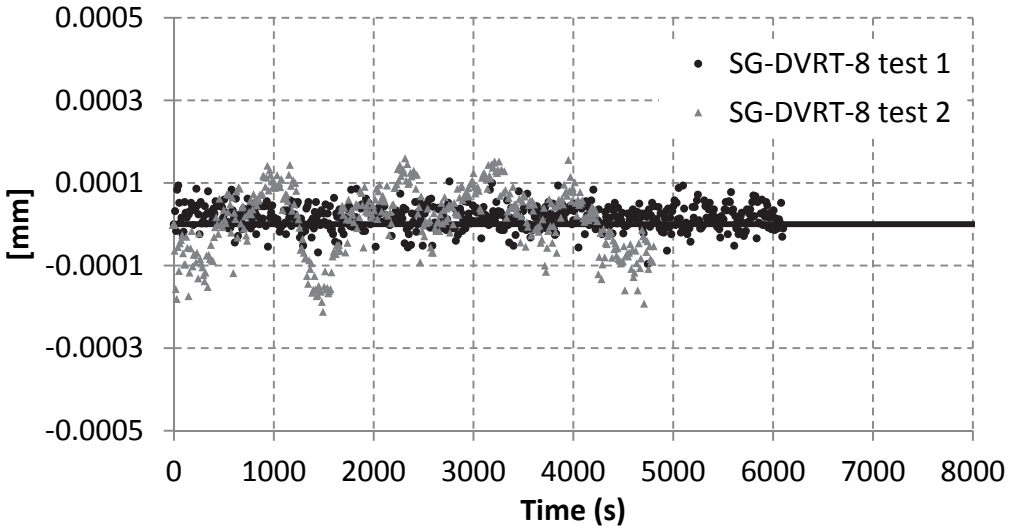

Figure 5.4. Calibration test results of SG-DVRT-8 sensor of relative zero displacement when calibrated for a range of <1.0 mm.

5.3.3 **Experimental procedure**

The soil sample is placed on the lower cap and then the top cap is placed on top of the sample. A latex membrane is then installed and sealed to the top and lower cap by means of O-rings. This procedure is similar to when installing sample in a conventional triaxial test. Subsequently the radial deformation gauge is installed and the loading ram is screwed on to the top cap to ensure full contact and to be able to conduct K_0-consolidation. Finally the cell is filled with paraffin oil and closed.

After the initial stress has been applied the manual cell pressure control is completed and the computer controlled cell pressure pump is activated and configured.

5.3.4 **Experimental tests and Results**

To validate and test the K_0-triaxial cell for different stress ranges two tests on samples from two different depths, 5 and 15 m, were conducted. The sample height was chosen to be 20 mm with a diameter of 50 mm, i.e. the same height and diameter as in the standard tests, i.e. CRS or IL oedometer test. The sample size was chosen so it would be possible to do a direct comparison of the results from the CRS and IL oedometer tests.

The soil samples originate from the central part of Gothenburg, just north east of the Central Railway Station. The average index properties of the soil samples are presented in Table 5.1. The CRS and IL oedometer tests that are used for comparison in stress - strain plots are also presented in Chapter 6.

Table 5.1. Average index properties for the two samples tested in the K_0-triaxial cell.

depth	Density [t/m^3]	w_N [%]	w_L [%]	w_p [%]	c_u^{cone} [kPa]	G_s [t/m^3]	S_t [-]
5 m	1.62	68	67	31	19	2.75	13.5
15 m	1.56	78	70	36	20	2.75	30

The tests performed with the K_0-triaxial cell were conducted in room temperature, i.e. about 21 °C, while the standard tests, i.e. CRS and IL oedometer tests are conducted in a temperature controlled room of about 7 °C. These important differences are corrected for using the relation develop by Tidfors & Sällfors (1989), in this case a factor of 1.1 was used on the effective stresses, and it is assumed not to influence the K_0^{NC} value.

Test 1 – 5 m depth.

For the soil sample from a depth of 5 m a total of 17 load stages were conducted where the first stage was an isotropic consolidation stage to a mean effective stress level of about 15 kPa with an applied back pressure of

40 kPa. The vertical stresses that were applied are presented in Table 5.2. The results from this test are presented in Figure 5.5 to Figure 5.9.

Table 5.2. Actual vertical stress for each stage on a sample from a depth of 5 m, after consolidation, before temperature correction.

Stage	2	3	4	5	6	7	8	9	10	11	12	13	14	15	16	17
σ'_v (kPa)	30	40	50	60	75	115	95	60	36	18	36	56	79	98	117	158

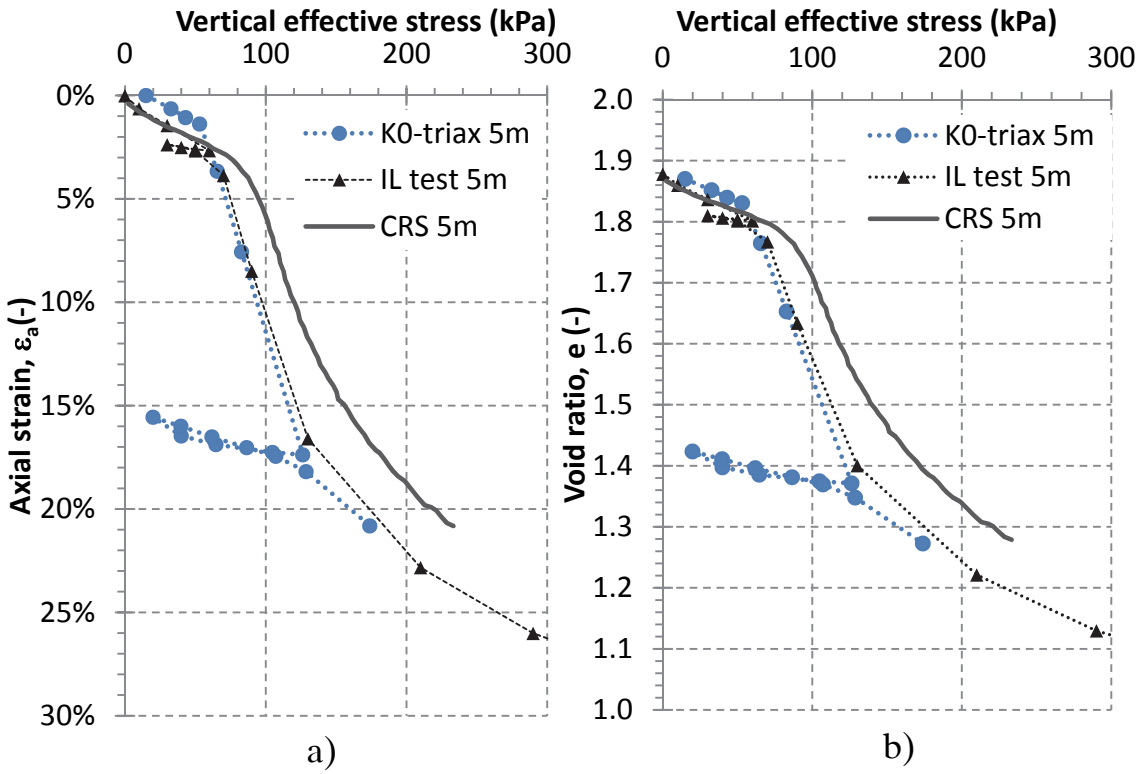

Figure 5.5. Results of the K_0 triaxial test on a sample from a depth of 5 m compared with IL oedometer and CRS results for the same depth. a) σ'_v - ε_a and b) σ'_v - e .

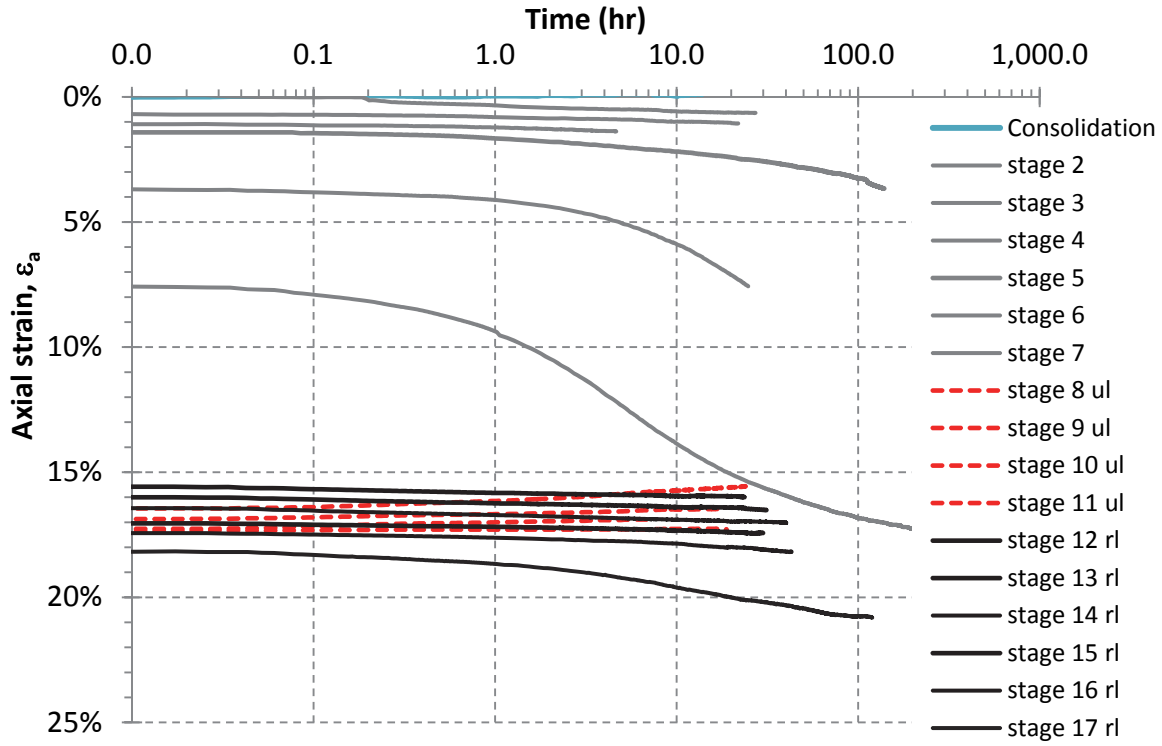

Figure 5.6. Consolidation curves of the K_0 triaxial test on a sample from a depth of 5 m.

The overall stress - strain behaviour for the K_0-triaxial test result is very similar to both the IL oedometer and the CRS tests, as could be seen in Figure 5.5. However, there is a closer match to the IL oedometer. This is most likely due to strain rate effects, i.e. an IL oedometer takes much longer time to reach the same strain as a CRS test, and therefore more strain is measured for the same effective stress. The stiffness parameters evaluated from the K_0-triaxial test are in same order of magnitude as the IL oedometer or CRS test, and this is further discussed in Chapter 6. According to Figure 5.6 the log(time)-ε_a curve also has the same pattern as normally found from IL oedometer tests conducted for these type of clays, see Chapter 6 for more IL oedometer results. The creep parameter evaluated from K_0-triaxial cell is similar to the value evaluated from IL oedometer for the same depth and location. For stage 7 in Figure 5.6 the creep number is evaluated to about $r_s = 150$ ($\mu^* = 0.0067$) which is in the range normally obtained with the empirical relation in Sweden, see Larsson et al. (1997).

In Figure 5.7 the measured K_0 is plotted as a function of time. Based on Figure 5.7 the K_0 value drops from a value of about 1.5 to about 0.4, and then increases to a more or less constant K_0 value with increasing stress and strains. The unloading of the sample is done for the stages 8 to 11, and it is apparent that the K_0 value increases for each unloading stage and almost reaches a K_0 value of 1 for the last stage. As soon as the reloading starts again, i.e. stage 12, the K_0 value drops instantly to a lower value of about 0.6 and keeps on decreasing for each loading stage before increasing, as the first loading sequence, to a more or less constant value of K_0 value. For this test the constant K_0 value at large strain is in a range of about 0.50-0.55.

Figure 5.8 shows the results of the test in the p´-q stress space. The stress path in p´-q space for both loading sequences, i.e. first loading and reloading, is very similar. The stress path response in p´-q space seems to start off at an inclination of about 2:1 and slowly bends off so the inclination goes to 1:2 at increasing stresses, and eventually at larger mean effective stresses the stress ratio seems to go towards a constant value.

The stress path for the unloading sequence in Figure 5.8 is shifted downwards to the mean effective stress axis. However, it seems that is has the same inclination in the beginning of the unloading as the initial part of the loading sequence. For the last two unloading stages, stages 10 and 11, the stress path seems to bend of towards the deviatoric stress axis.

In Figure 5.9 the relative zero lateral deformation, i.e. the change in diameter from start of test, is shown and it could be seen that, except for when the dead weights was changed, the radial deformation is exceptionally small, i.e. less than 0.5 microns.

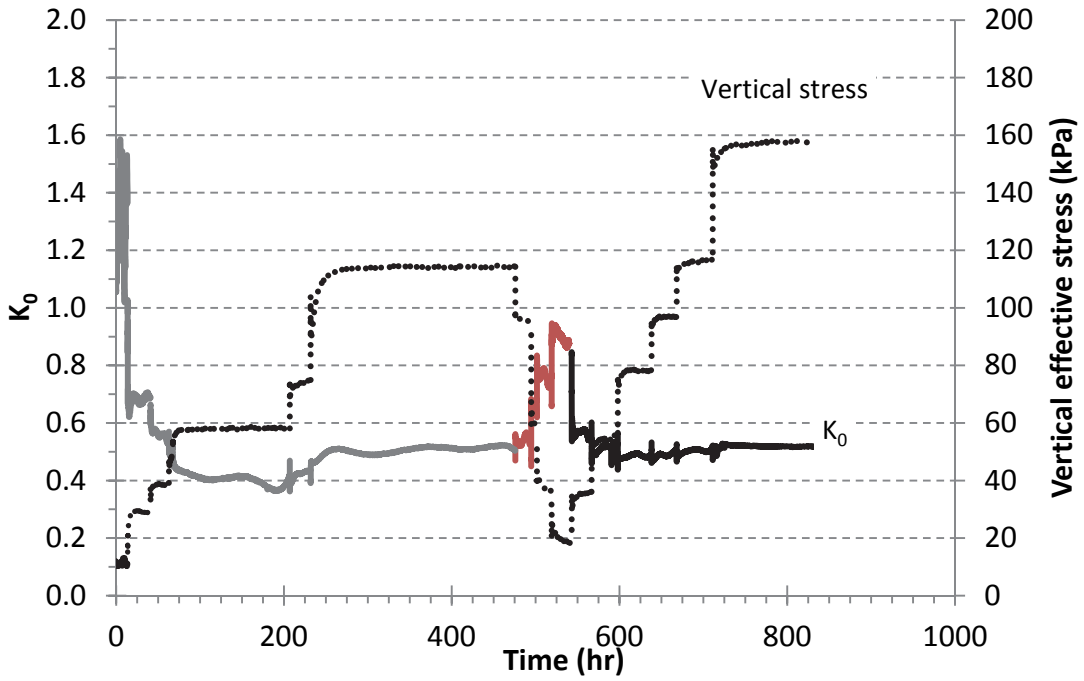

Figure 5.7. Results of the K_0 triaxial test on a sample from a depth of 5 m. K_0 (solid line) and vertical effective stress (dotted line) vs. time (hr).

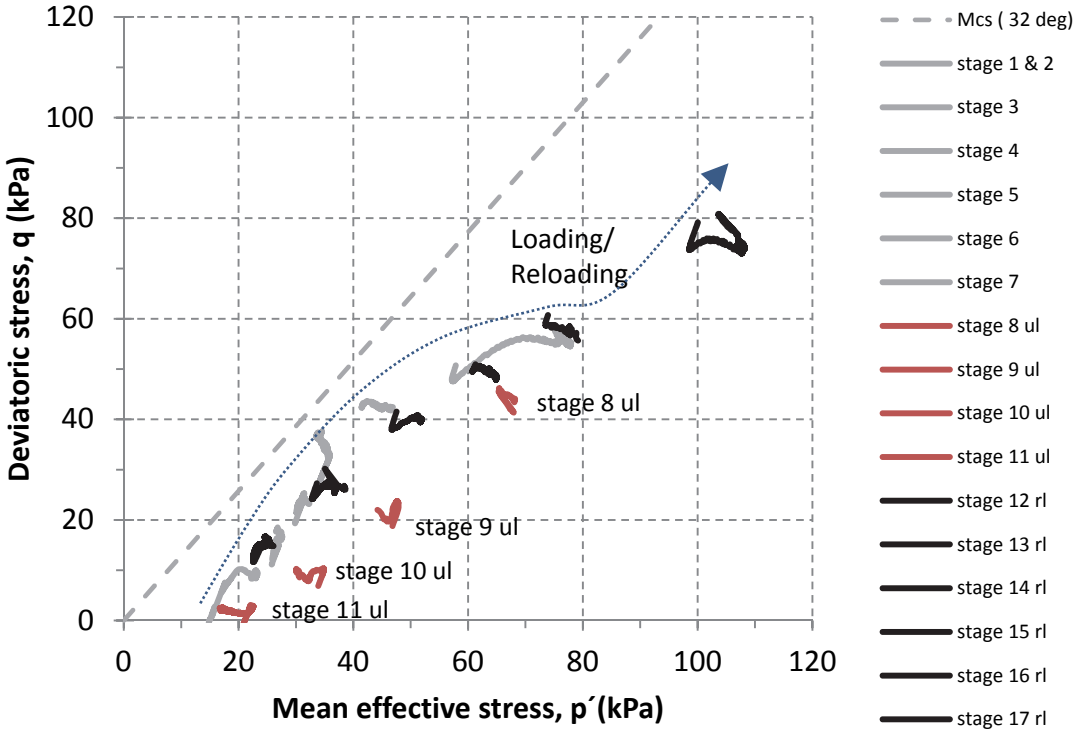

Figure 5.8. Stress path plots on a sample from a depth of 5 m with loading (stages 1-7, black line), unloading (stages 8ul-11ul, red line) and reloading (stages 12rl-17rl, grey line) of the K_0 triaxial test.

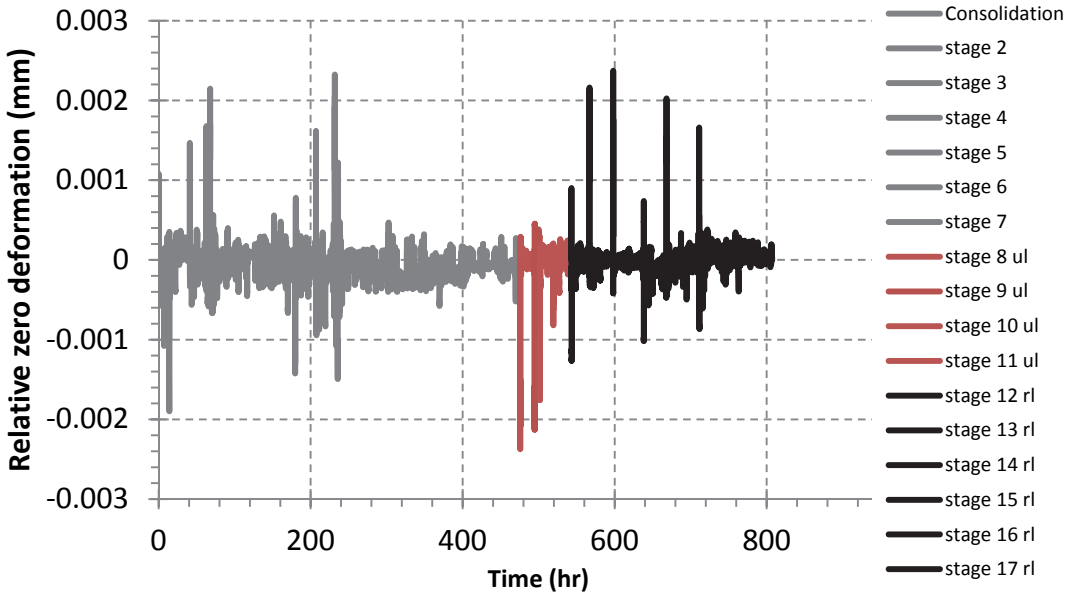

Figure 5.9. Relative zero lateral deformation during the K_0 triaxial test on a sample from 5 m depth.

Just after the change of dead weights, for more or less every stage, the lateral deformation had some peaks according to Figure 5.9. These peaks where only present for a very short time, i.e. less than 5 minutes, before the stress ratio came into equilibrium to zero lateral deformation.

Test 2 – 15 m depth

For the soil sample from a depth of 15 m a total of 8 stages were conducted where the first stage was an anisotropic consolidation stage to a vertical effective stress level of about 40 kPa with a $K_0 = 0.6$ with a applied back pressure of 40 kPa. The vertical stresses that were applied are presented in Table 5.3. The results from this test are presented in Figure 5.10 to Figure 5.14.

Table 5.3. Actual vertical stress for each stage on a sample from a depth of 15 m, after consolidation, before temperature correction.

Stage	2	3	4	5	6	7	8
σ_v (kPa)	50	70	90	105	135	175	250

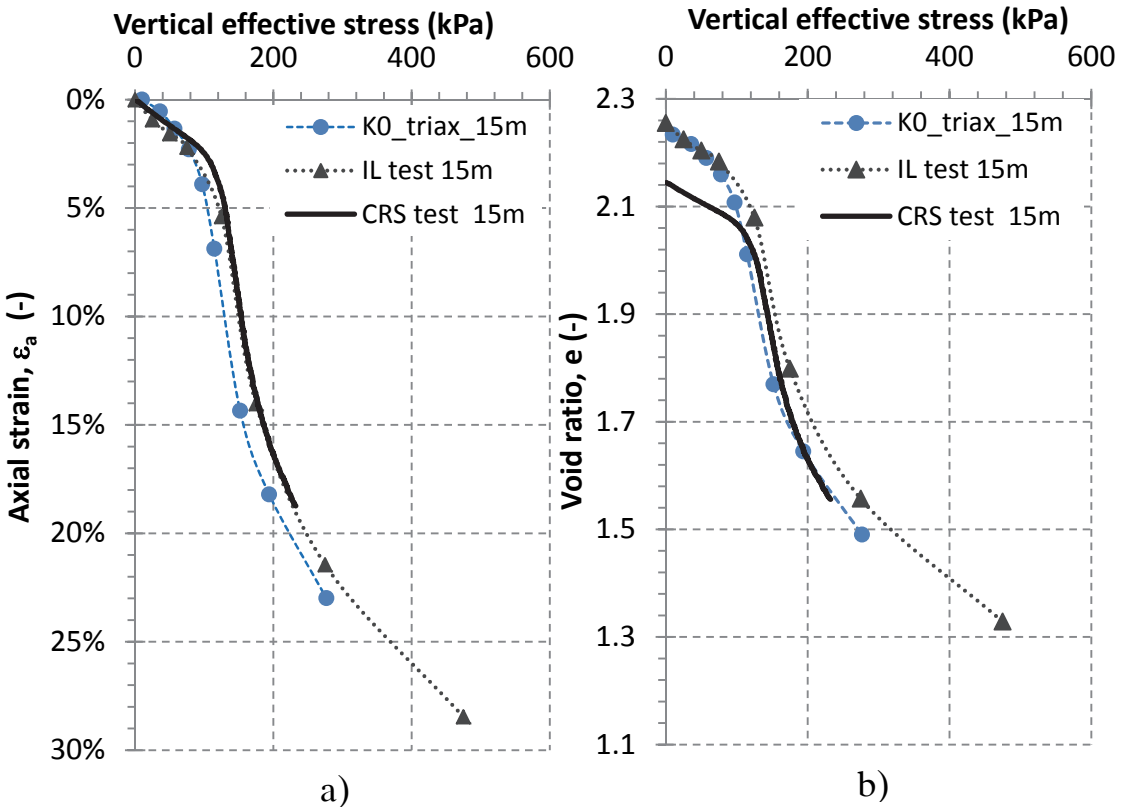

Figure 5.10. Results of the K_0 triaxial test on a sample from a depth of 15 m compared with IL oedometer and CRS results for the same depth. a) σ'_v - ε_a and b) σ'_v - e .

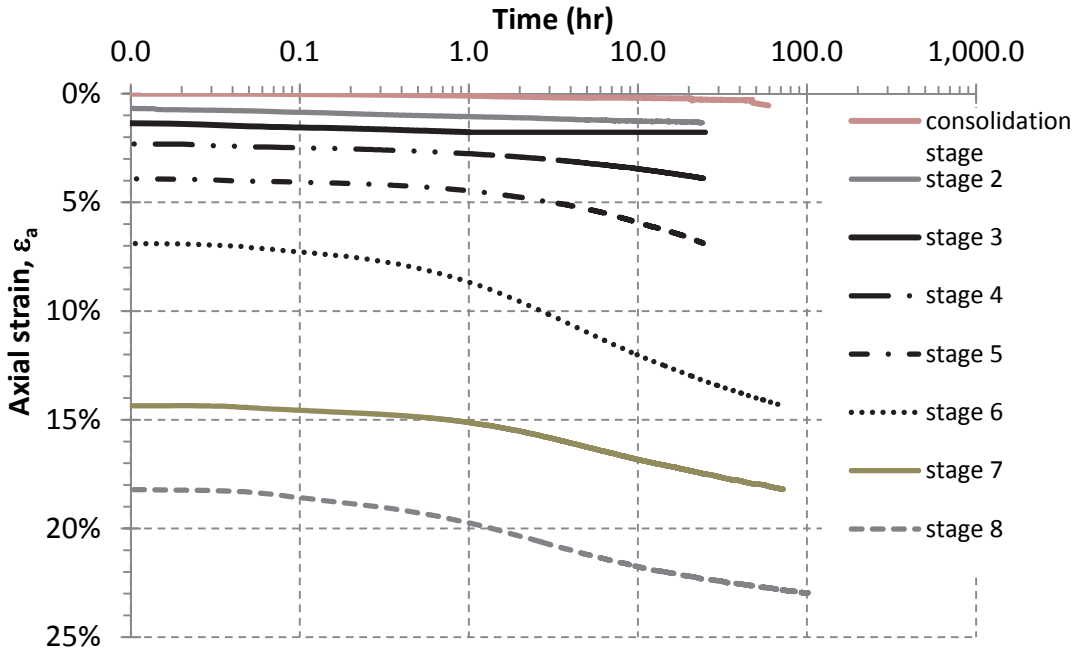

Figure 5.11. Consolidation curves of the K_0 triaxial test on a sample from a depth of 15 m.

The overall stress-strain behaviour for the K_0-triaxial test result for the sample from 15 depth is very similar to both the IL oedometer and the CRS tests, as demonstrated in Figure 5.10. The difference in void ratio for the CRS test compared to the other tests in Figure 5.10 is most likely due to the natural variability of the soil, and that the same mean value of specific gravity has been used for all three tests, see Table 5.1, rather than test specific values.

Since the stress-strain curve of the K_0-triaxial test has the same shape as the IL oedometer and CRS test, the stiffness parameters that would be evaluated from the K_0-triaxial test would be in the same order of magnitude. This is further discussed in Chapter 6.

Based on Figure 5.11 the log(time)-ε_a curve also has the same pattern as normally found from IL oedometer tests conducted for these type of clays, see Chapter 6 for more IL oedometer results. The creep parameter evaluated from K_0-triaxial cell for this sample is in the same order as evaluated from IL oedometer for the same depth and location. For stage 6 in Figure 5.11, the creep number is evaluated to about $r_s = 100$, ($\mu^* = 0.01$) which is in the range normally obtained with this water content, see chapter 6 for more experimental data from conventional tests.

According to Figure 5.12 the K_0 value falls from a slightly higher value to a lower value, about 0.4, and then increases to a K_0 value of about 0.52 for the last stage.

The stress path response in p´-q stress space, as seen in Figure 5.13 seems to start off at an inclination of about 1:1 and slowly bends so the inclination goes to 1:1.5 at increasing stresses, and eventually at larger mean effective stresses the stress ratio seems to go towards a constant value.

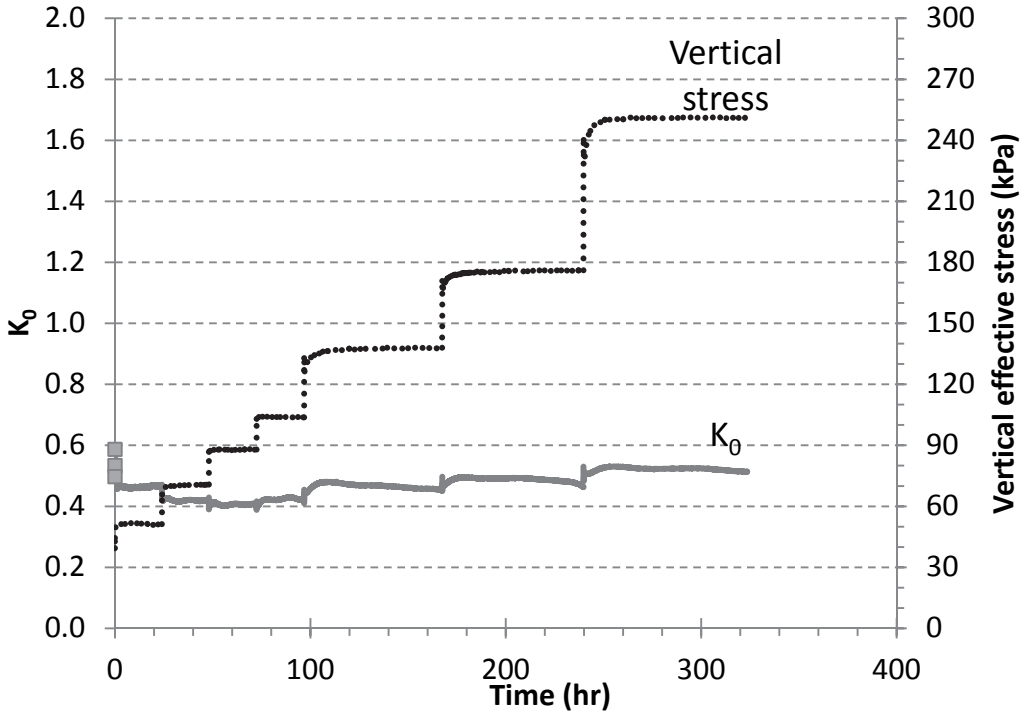

Figure 5.12. Results of the K_0 triaxial test on a sample from a depth of 15 m. K_0 (solid line) and vertical effective stress (dotted line) vs. time (hr).

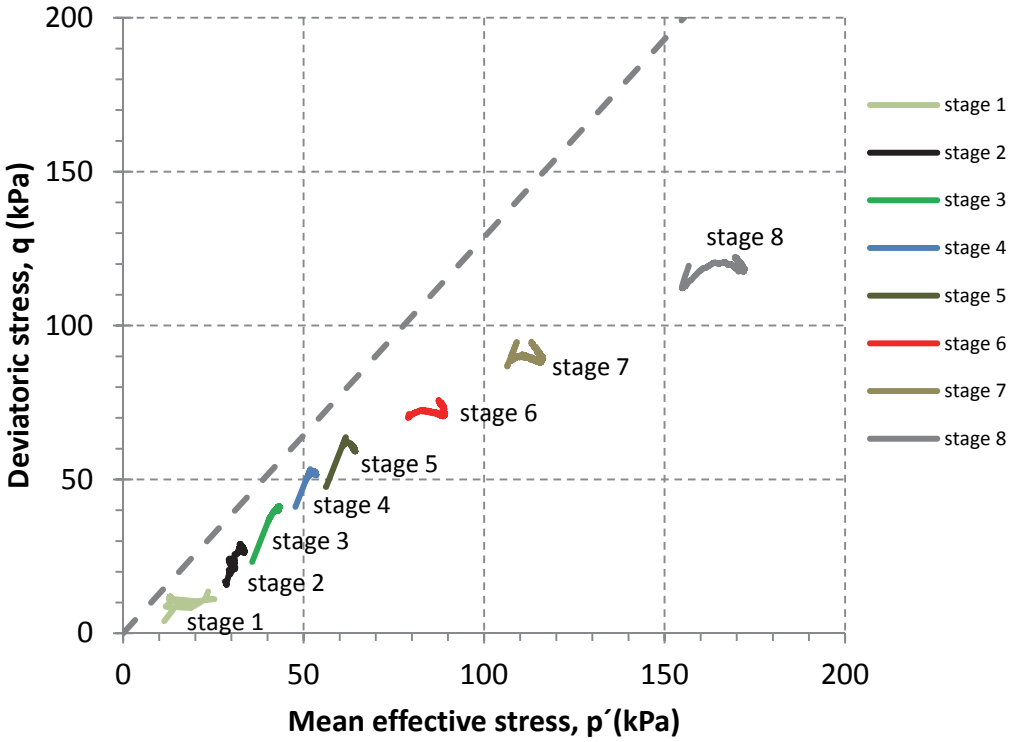

Figure 5.13. Stress path plots on a sample from a depth of 15 m of the K_0 triaxial test.

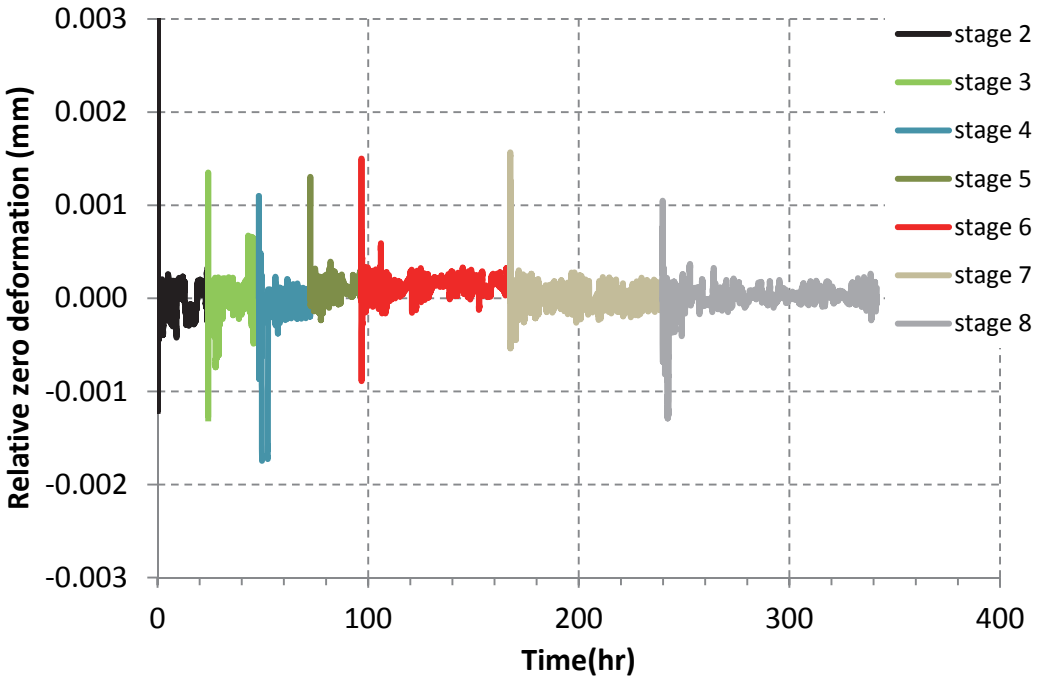

Figure 5.14. Relative zero lateral deformation during the K_0 triaxial test on a sample from 15 m depth.

The relative zero lateral deformation is shown in Figure 5.14 and, except for when the dead weights was changed, the radial deformation is exceptionally small, i.e. less than 0.5 microns.

Just after the change of dead weights, for more or less every stage, the lateral deformation had some peaks as shown in Figure 5.14. These peaks where only present for a very short time, i.e. less than 5 minutes, before the stress ratio came in to equilibrium to zero lateral deformation.

5.3.5 **Discussion**

Based on the results of the two tests presented above, the K_0-triaxial cell seems to work satisfactorily. The lateral deformation of the sample could be said to be constant similar to CRS or IL oedometer tests.

However, care should be taken when comparing the results directly since the loading time for each stage has to be considered, especially when compared in a stress-strain plot.

The main aim of the K_0-triaxial cell was to study the mobilized K_0 values of clays at constant effective stress levels. It could be concluded from the two tests that the K_0 value falls from an initial value to lower value and then increases to a more or less constant K_0 value when stress and strains are increasing, as also shown in Figure 5.15 were K_0 is plotted against normalized stress. For these two tests the constant K_0 values at large strain are in a range of about 0.50-0.55.

A comparison has also been made with earlier laboratory tests of Gothenburg clay by Sällfors (1975) and Kullingsjö (2007) in which horizontal stresses were measured while the lateral deformation was kept constant or controlled. The experimental results from all tests are plotted in Figure 5.15, and the resulting K_0 values at large strains for the tests conducted previously are in the same range as the two tests presented above, i.e. the K_0 value is in a range of 0.50-0.55 for both these tests also.

The K_0 values measured from these results are very different from what would be estimated using the empiric relations by Larsson et al. (2007), were the liquid limit, w_L, is used, as commonly used in Sweden for inorganic soft clays. See eq. (5.1).

$$K_0^{nc} = 0.31 + 0.7 \cdot \left(w_L - 0.2 \right) \tag{5.1}$$

All the tests above had a liquid limit of about 70%, except the tests from Sällfors (1975) that had a liquid limit of 99%. The evaluated K_0^{nc} according to eq. (5.1) for a liquid limit of 70% and 99% would be $K_0^{nc} = 0.65$ and $K_0^{nc} = 0.85$ respectively. This implies that there is very little correlation

between index properties, such as liquid limit, and the K_0^{nc} value, which was also concluded by Kulhawy & Mayne (1990). However, the empirical relation according to eq. 5.1 seems to be defined at a stress level were the apparent preconsolidation pressure is evaluated, and not as considered in this thesis, i.e. at large strains were the soil has reached its normal consolidated state and no significant structure is remaining.

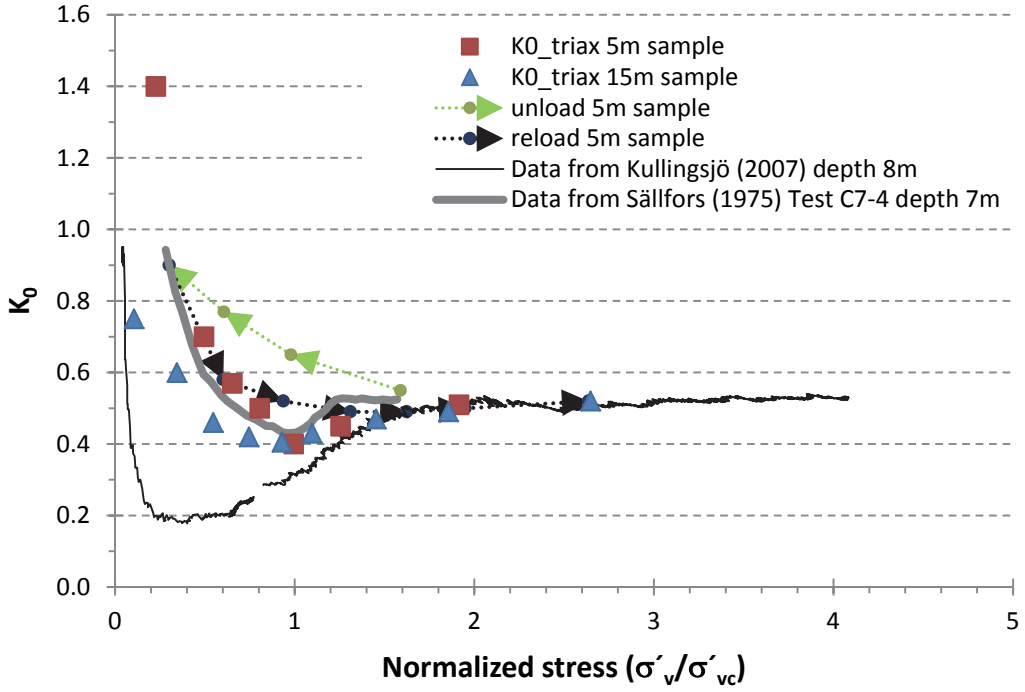

Figure 5.15. Experimental results from the new K_0-triaxial cell compared with previous test results from a depth of 7 m ($\sigma'_{vc} = 75\ kPa$) and 8 m ($\sigma'_{vc} = 130\ kPa$) of Gothenburg clay. Data from Sällfors (1975) and Kullingsjö (2007).

Comparing the results from the laboratory tests by using the Jaky´s formula of K_0^{nc}, see eq. (5.2). it appears that using the Jaky´s formula together with the empirical relations used in Sweden for the friction angle of soft clay (i.e. according to Larsson et al. (2007) the friction angle is 30 degrees for soft clays) a $K_0^{nc} = 0.5$ would be obtained.

$$K_0^{nc} = 1 - \sin\phi'_{cs} \tag{5.2}$$

This implies that Jaky´s formula gives rather good estimate of K_0^{nc} value. However, some modifications are most likely needed, since recent research (see e.g. Chapter 6) has shown that the critical state friction angle is often greater than 30 degrees for soft soils in the Gothenburg area. This would, according to Jaky´s formula, give smaller K_0^{nc} values than measured. It also seems that the friction angle used for Swedish clays according to Larsson et al. (2007) correspond to the peak strength rather than at the critical state.

It could also be argued based on Figure 5.7 and Figure 5.15 that when a soil is first loaded so that the vertical stress exceeds the apparent preconsolidation pressure, the K_0 value seems to drop to a lower value than if a subsequent unloading-reloading sequence had occurred. A reason for this could be that depending on how far above the apparent preconsolidation pressure the new stress state has been, the amount of structure, or bonding, the soil initially had is continuously destroyed.

In the new K_0-triaxial cell there is no ring friction present in contrast to standard oedometer test. According to Sällfors (1975), the frictional loss with a stainless steel oedometer ring lubricated with silicone grease is about 5-10% for a CRS oedometer test. Even though today it is normal to use a Teflon ring instead of a stainless steel ring to minimize the frictional loss, there is still a frictional loss of unknown magnitude. If comparing the IL oedometer test results with the K_0-triaxial test results, they have the same shape but deviate somewhat after reaching the apparent preconsolidation pressure. This would be anticipated if the IL oedometer test had some frictional loss. Comparing these two tests it is probably not enough for conclusions without a systematic study of the time step (duration) for each load step, and conducting more experiments.

Unfortunately, the experiments performed with the new K_0-triaxial cell were conducted in room temperature, due to lack of space in the temperature controlled room. Of course this introduces an additional assumption when comparing the results, since a constant correction factor of 1.1 is applied for the whole stress range due to temperature effects. However, it is not likely that the temperature difference would have any influence on the K_0^{nc} value, which was the main aim of the tests. As the difference between the results, after temperature correction, is very small, it could also be attributed to natural variability of the soil and/or different handling during installation of the samples.

6 EXPERIMENTAL RESULTS AND SIMULATIONS

This chapter consist of two parts. The first part consists of experimental results and the second part consists of simulation of some selected experimental results to validate and test the performance of the MAC-s model.

6.1 Laboratory experiments

The objective of the laboratory study was to investigate the creep behaviour with focus on the clay in the Gothenburg area. All the experiments were conducted at GeoEngineering laboratory at Chalmers, if not stated otherwise, and the samples were taken with the Swedish standard II piston sampler, St II, with a sample diameter of 50 mm.

In this work focus is on the creep behaviour of soft clays, and all laboratory experiments that have been performed in this study are fully presented in the report by Olsson et al. (2013). The laboratory experiments in this report investigate four different locations in the Gothenburg City area, see Figure 6.1, and in this work focus is mainly on one, i.e. the area around the main train station in the Gothenburg City, called CC5001. However, some of the evaluated parameters from the other locations are combined in graphs that are presented in the following.

Figure 6.1. Location of the four different investigation sites in the Gothenburg city area, picture from www.eniro.se.

6.1.1 Test program

The laboratory test programme consists of 20 Incremental Loading (IL) oedometer tests, 26 Constant Rate of Strain (CRS) tests and 7 triaxial tests. In addition to these tests 35 index tests were made to determine water content, liquid limit, plasticity limit, density, sensitivity and undrained shear strength from fall cone tests. In addition, some other experimental results, including undrained triaxial tests, from other projects in the same area are used for both evaluating parameter evaluation and comparisons.

6.1.2 Index properties

In this section some of the index properties of clay in the area of the Gothenburg train station are presented. In Figure 6.2 the density and sensitivity is presented as a function of depth, and in Figure 6.3 the natural

water content, liquid limit and plasticity limit are presented in the same manner.

Based on Figure 6.2 the top part of the clay layer has a density of about 1.65 t/m^3 and this drops to about 1.5 t/m^3 at a depth of 10-15 m. Thereafter, the density seems to increase with depth. The sensitivity is ranging between 5-35 as could be seen from Figure 6.2, with the highest values at the depth of about 10-15 m. The scatter is, however, significant.

The natural water content and the liquid limit are more or less of the same order, as can be seen in Figure 6.3. Deeper down the liquid limit is slightly higher than the natural water content. The plasticity limit is in a range of about 30-40 for the entire soil profile, with the highest values at the depths of about 10-15 m.

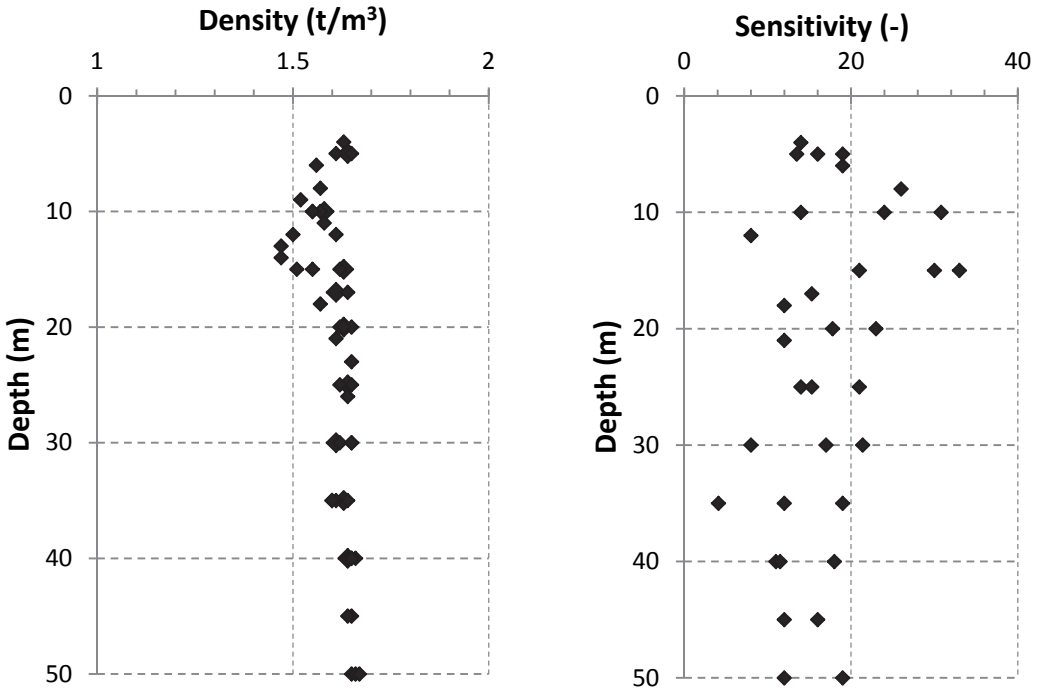

Figure 6.2. Density and sensitivity versus depth for the CC5001 area.

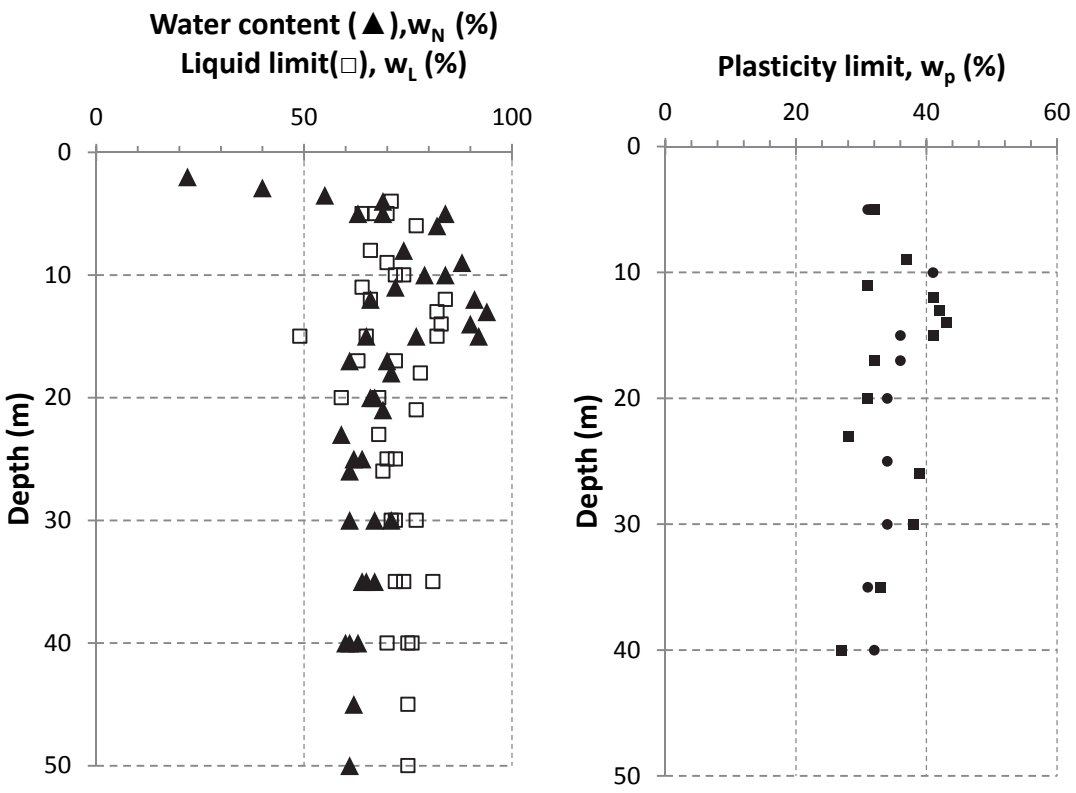

Figure 6.3. Water content, liquid limit and plasticity limit versus depth for the CC5001 area.

The hydraulic conductivities evaluated from the results of the CRS oedometer tests are in a range of about $5\text{-}20 \cdot 10^{-10}$ m/s for the whole soil profile without any specific trend. The change of hydraulic conductivity with strain, called β_k, is also evaluated from the CRS oedometer tests and the β_k value was found to be in a range of 2-4, see e.g. Larsson et al. (1997) for definition.

6.1.3 1-D compression properties

In Figure 6.4 and Figure 6.5 the results for IL oedometer and CRS oedometer tests are plotted with respect to normalized stress (i.e. vertical effective stress divided by evaluated preconsolidation pressure) and volumetric strain, respectively, for different depths. The apparent preconsolidation pressure is stated in the legend for each test.

In Figure 6.6 and Figure 6.7 the IL oedometer and CRS oedometer tests are plotted with respect to vertical effective stress (in logarithmic scale) against void ratio.

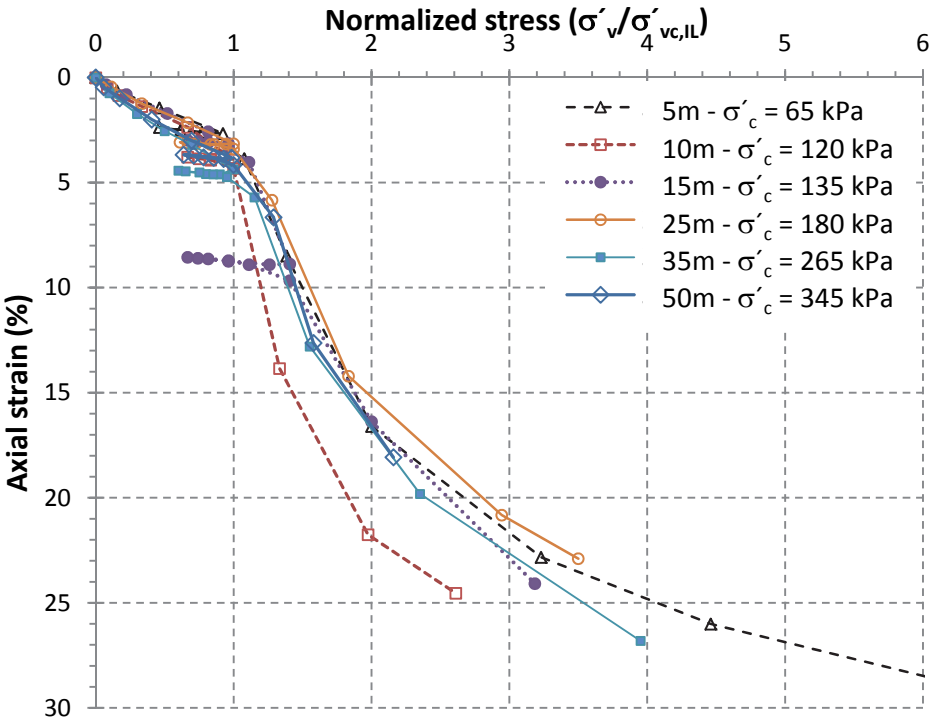

Figure 6.4. Normalized stress-strain plot of IL oedometer tests for the CC5001 area.

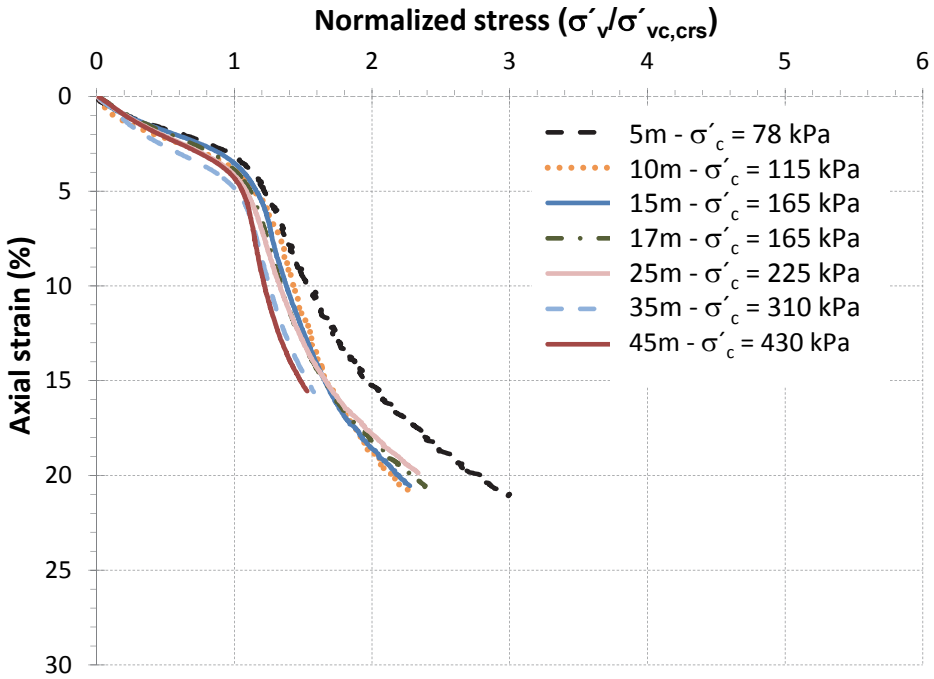

Figure 6.5. Normalized stress-strain plot of CRS oedometer tests for the CC5001 area.

Based on Figure 6.4 and Figure 6.5, the normalized stress-strain curves fall in to a relatively small band. A small deviation could be seen for the 10 m IL oedometer test in Figure 6.4 and the 5 m CRS oedometer test in Figure 6.5.

It is also apparent from Figure 6.4 and Figure 6.5 that when comparing the evaluated preconsolidation pressures from the two different tests, i.e. IL and CRS oedometer, the preconsolidation pressure for IL oedometer results is systematically smaller than in the CRS oedometer tests, except for the depth 10m were it is more or less the same. The former is to be expected since the IL oedometer is taking normally several days to reach the preconsolidation pressure, while the CRS oedometer only takes a few hours.

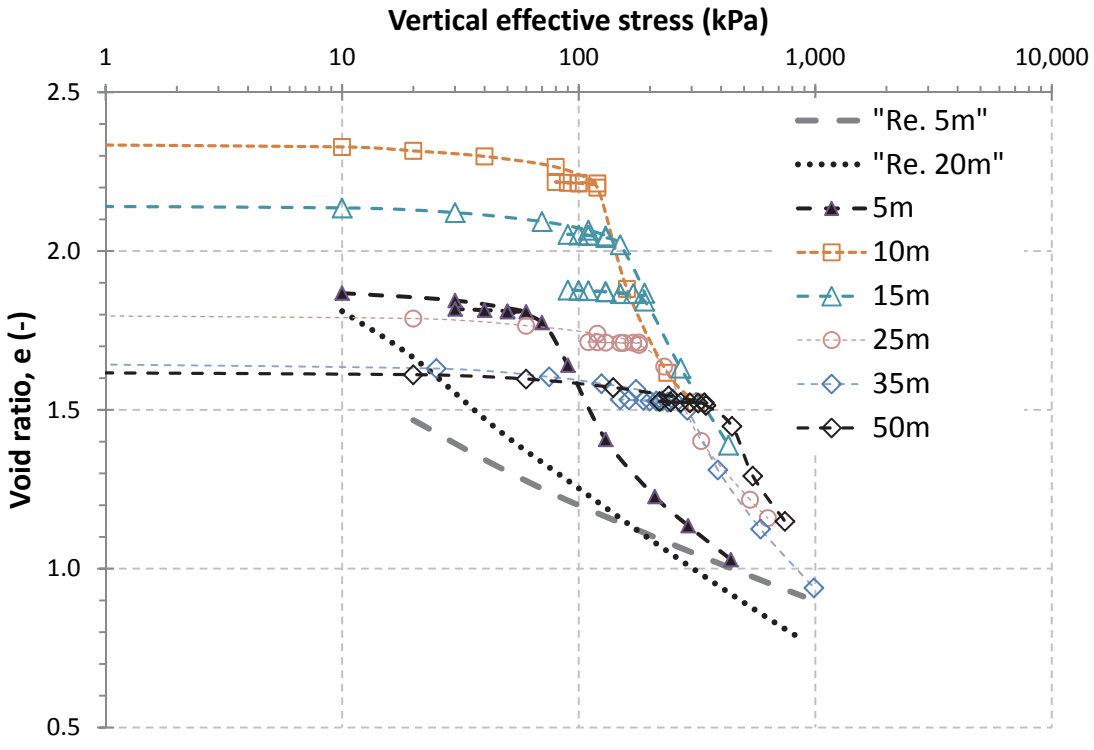

Figure 6.6. IL oedometer tests in semi-log scale for the CC5001 area. Also included tests on two reconstituted samples giving the intrinsic compression lines.

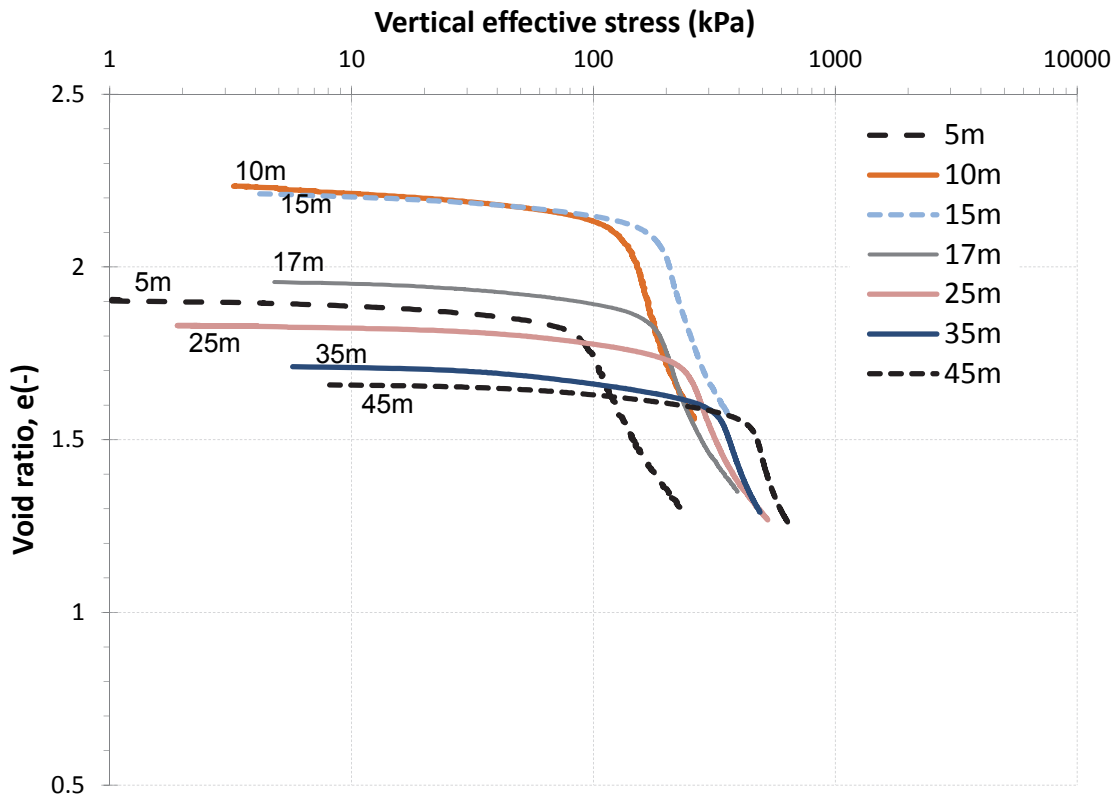

Figure 6.7. CRS oedometer tests in semi-log scale for the CC5001 area.

Based on Figure 6.6 and Figure 6.7, when the results are plotted with respect to vertical effective stress (in logarithmic scale) against void ratio the stress–strain curve seems to fall over to each other at the different void ratios, except for the 5 m depth. This would imply that all the samples seem to eventually head to the same compression line.

In Figure 6.6 results on two reconstituted samples are also plotted for the depths 5 m and 20 m, which also give the intrinsic properties of the soil. It can be seen that the results on the undisturbed sample from 5 m depth seems to converge on to those of the corresponding reconstituted sample, i.e. intrinsic compression line (ICL), after relatively large strain. The other undisturbed samples seem to converge to the intrinsic compression line corresponding to 20 m depth for greater strains. Since the oedometer curves are much steeper than ICL this implies that the soil has a lot of structure which is consistent with the measured values of sensitivity.

In Figure 6.8 and Figure 6.9 the evaluated creep index, $C_{\alpha e}$, and creep number, r, are plotted, against normalized stress. Based on Figure 6.8, when the stresses are reaching the preconsolidation pressure the creep index is increasing drastically. For higher stress levels, also corresponding to larger strains, the creep index are decreasing and seem to, slowly, converge to the intrinsic value evaluated from the test on reconstituted samples. The same behaviour is also observed for the creep number, r, in Figure 6.9. The relationship between the creep index, $C_{\alpha e}$, and the creep number, r, is according to eq. (6.1).

$$r = \frac{2.3 \cdot (1 + e_0)}{C_{\alpha e}} \tag{6.1}$$

As seen from Figure 6.8, the highest value of the creep index, $C_{\alpha e}$, is not corresponding to the apparent preconsolidation pressure, but at a stress state 1.2-1.4 times higher than the apparent preconsolidation pressure evaluated from the CRS oedometer tests. Similar findings was reported by Claesson (2003). The stress state at which the maximum creep index is found coincide more or less, with the steepest part of the stress-strain curve, and this would correspond to the lowest value of the oedometer modulus or the highest value of the compression index.

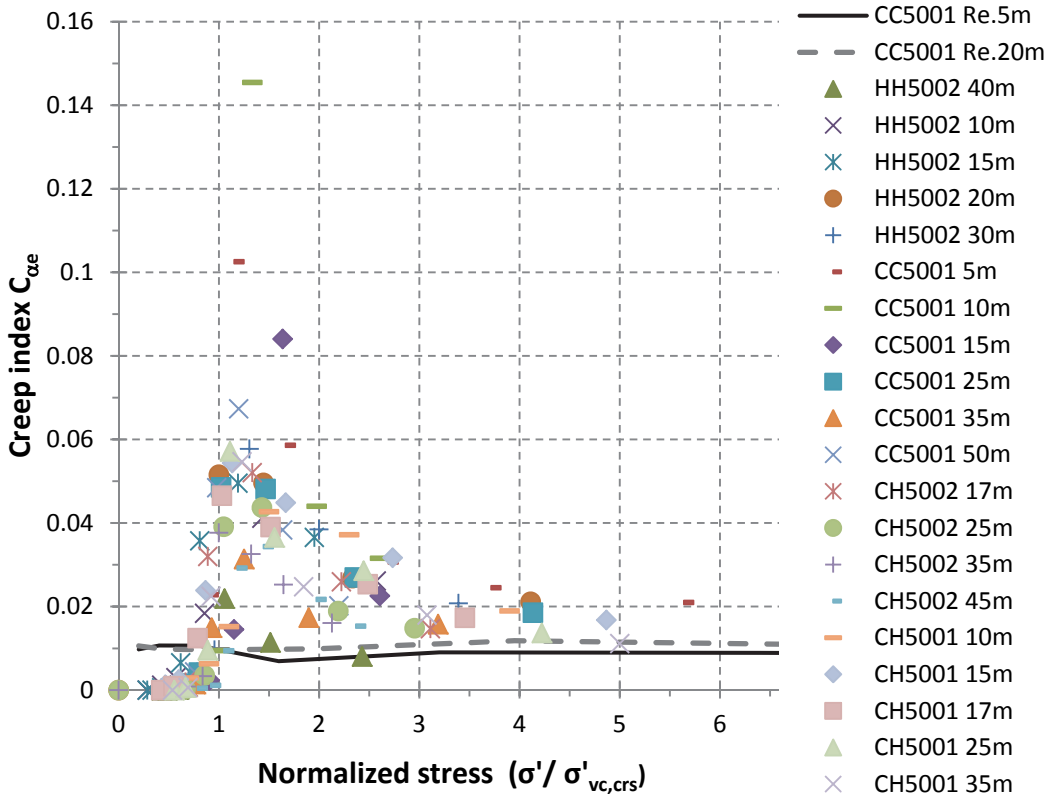

Figure 6.8. Evaluated values of the creep index, C_{ae}, for all four locations.

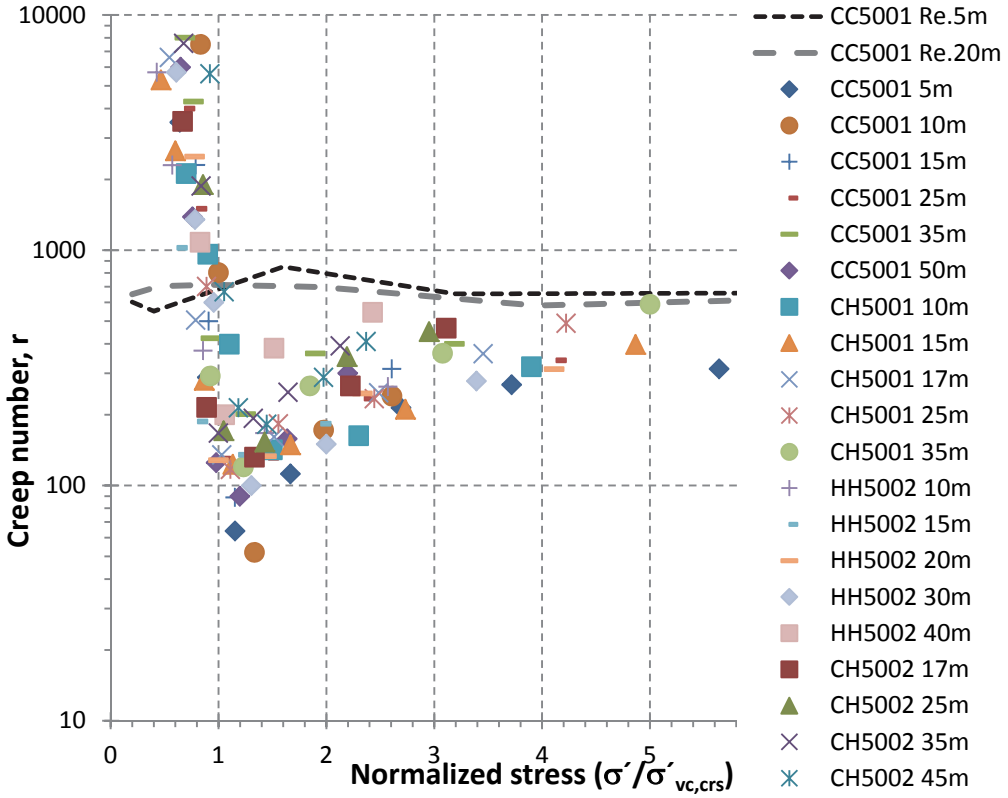

Figure 6.9. Evaluated values of the creep number, r, for all four locations.

Similarly to the creep index, $C_{\alpha e}$, the compression index, C_c, is not a constant value. In the following, the C_c values have been defined at the steepest section of the stress–strain curve, corresponding to the peak value of the $C_{\alpha e}$. The evaluated values for the compression indices, C_c, from the CC5001 area from both the IL oedometer and the CRS oedometer tests are plotted in Figure 6.10 against depth, together with the $C_{\alpha e}/C_c$ for the peak values as suggested by Mesri & Godlewski (1977).

Based on Figure 6.10a the C_c-value for the IL oedometer tests are more or less constant with depth giving a C_c-value of about 1.5, except at 10 m depth were the C_c-value is about 2.4. The values evaluated from the CRS oedometer tests show more or less the same trend as the IL oedometer, but the C_c-values vary between 1.5-2 with a higher value of C_c at 10 m depth. The intrinsic values from the two reconstituted tests are also shown. The evaluated intrinsic values of C_c are about $C_c = 0.3$ and $C_c = 0.5$ for 5 m and 20 m depth, respectively.

The $C_{\alpha e}/C_c$ relation that is plotted in Figure 6.10b are in the range of about 0.02 - 0.07, with the higher values at the top layers and decreasing towards the depth, until for a sample from 50 m depth it increases again. The evaluated intrinsic values, $C_{\alpha ei}/C_{ci}$, from the reconstituted tests are also plotted, and are in the range of 0.015-0.025.

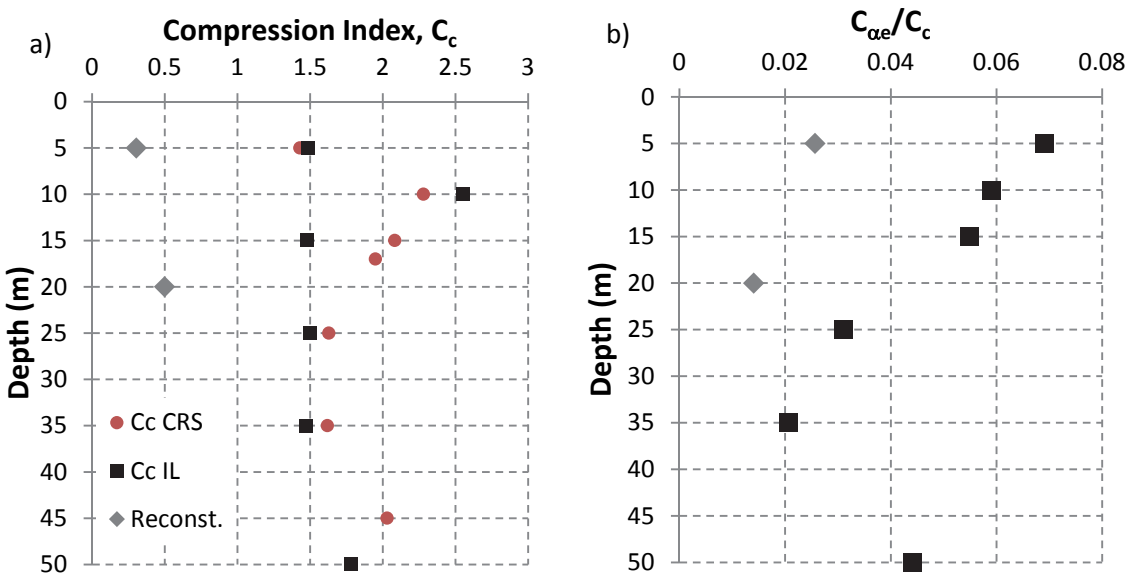

Figure 6.10. a) Evaluated compression index, C_C, b) the ratio between $C_{\alpha e}$ and C_C. for the CC5001 area, also including the two reconstituted tests.

6.1.4 Strength and yield properties from triaxial testing

The undrained triaxial test results presented in Figure 6.11 to Figure 6.14 were conducted by a different project, Wood & Karstunen (2013), in the same area as the CC5001, i.e. at the Gothenburg train station area. The undrained triaxial tests presented in p´-q space in Figure 6.11 were first consolidated to an estimated in-situ stress and then sheared undrained with a deformation rate of 0.01 mm/min. The samples had a diameter of 50 mm and a height of 100 mm. The results from the undrained compression tests in Figure 6.11 indicate a critical friction angle in a range of 31°-34° for the compression side, i.e. a M_c = 1.25-1.36, and in a range of 34°-37 ° for the extension side, i.e. M_e = 0.95-1.0, with the lowest critical state friction angle for the samples at the 45 m depth. The results in Figure 6.12 to Figure 6.14 indicate that the peak strength is reached at a axial strain level of about 1% for all compression tests and about 3-4% for all the extension tests.

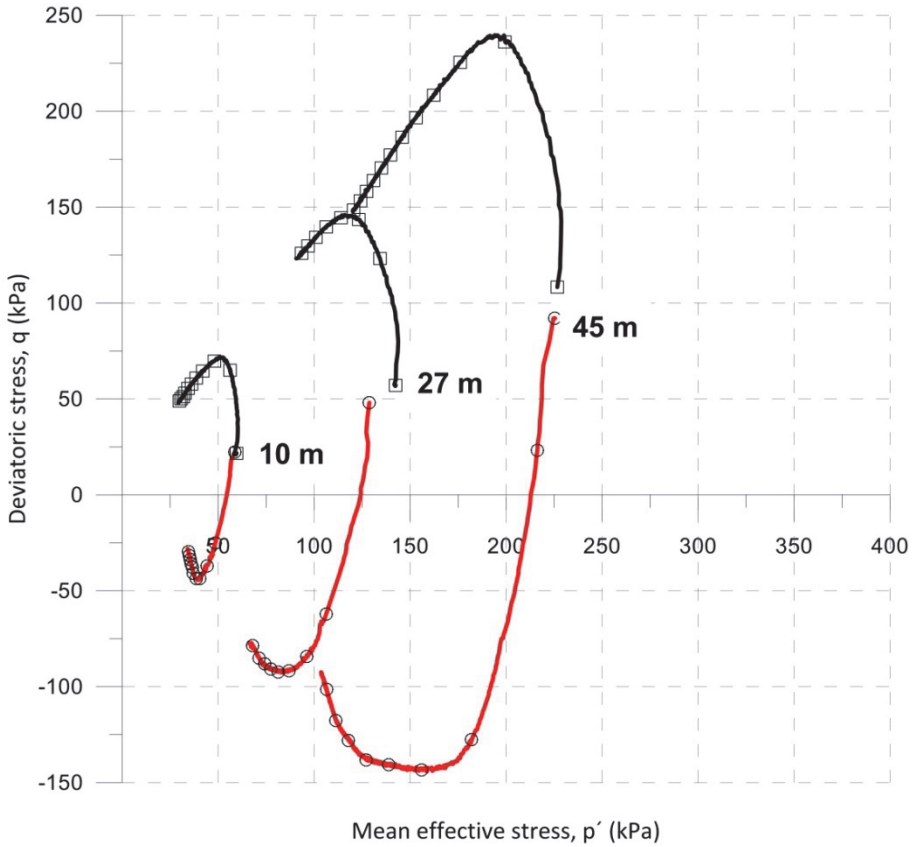

Figure 6.11. Undrained triaxial test at the depths 10m, 27m and 45m, both compression and extension, conducted at the train station area.

Based on Figure 6.12 to Figure 6.14 all compression tests are showing softening behaviour after reaching the peak. However, the evaluated effective stress is based on the measured pore pressure response in the bottom of the sample, and therefore it is difficult to predict the real effective stress path when the sample is developing some type of failure mechanism.

For the extension tests, the vertical effective stress is first decreasing, as expected, and then after rather large strain the vertical effective stress starts to increase. This is probably due to the failure mechanism, the so-called necking of the sample, and this would be consistent with the p´-q stress path in Figure 6.11.

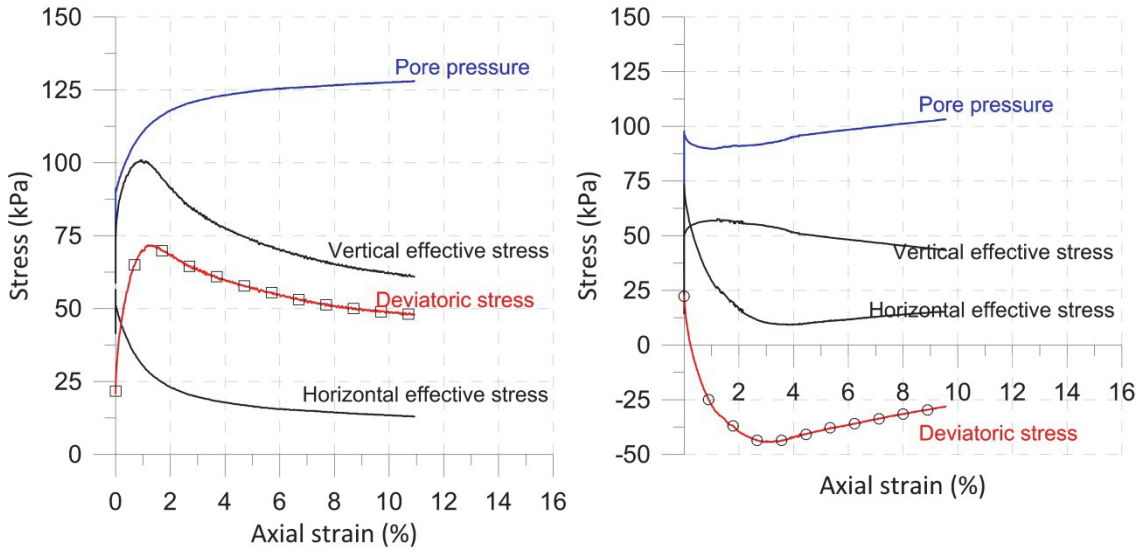

Figure 6.12. Stress-strain curve for the undrained triaxial test at a depth 10 m for compression (left) and extension (right). Note the different scales for the y-axis.

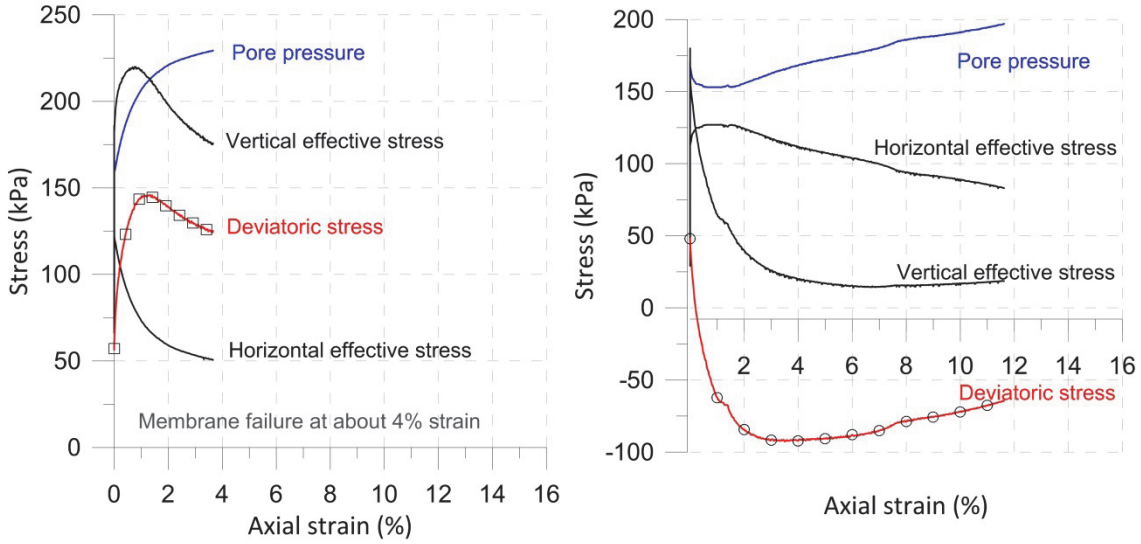

Figure 6.13. Stress-strain curve for the undrained triaxial test at a depth 27 m for compression (left) and extension (right). Note the different scales for the y-axis.

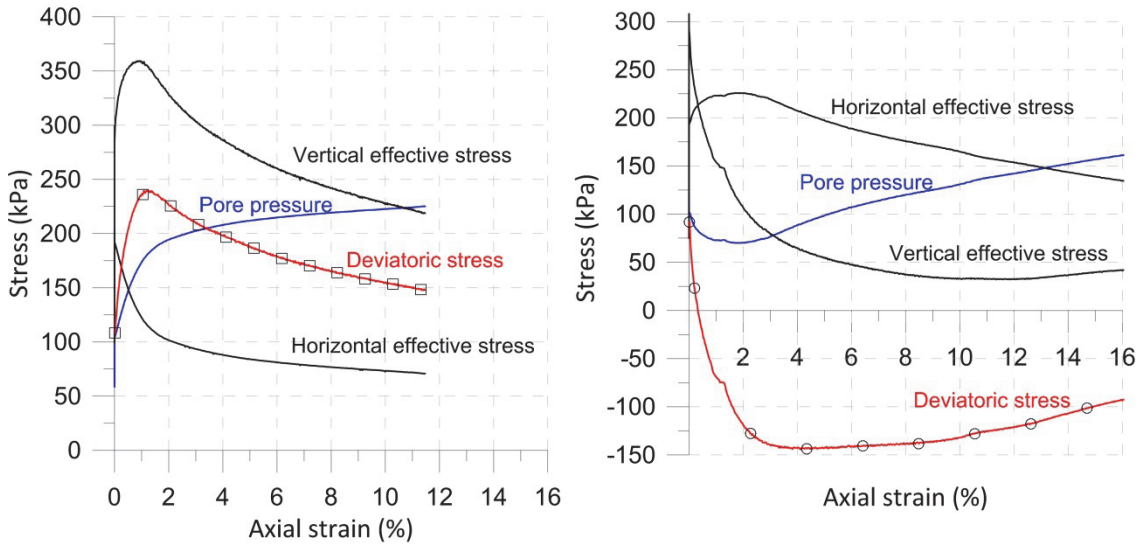

Figure 6.14. Stress-strain curve for the undrained triaxial test at a depth 45 m for compression (left) and extension (right). Note the different scales for the y-axis.

The undrained triaxial test presented in Figure 6.15 had a sample diameter of 50 mm and a height of 100 mm and consists of three stages. First stage was a drained p´-q stress path, corresponding to a K_0 value of about 0.55, to a vertical effective stress of about 510 kPa and then unloaded to an overconsolidation ratio of about four. This was done in order to create a soil with a significant overconsolidation ratio. The third stage was an undrained shearing stage that is presented in Figure 6.15 together with two of the undrained triaxial compression tests from Figure 6.11, i.e. 27 m and 45 m depths. Unfortunately the test was stopped when reaching the maximum possible axial deformation for the triaxial equipment, due to the first consolidation stage creating about 20% axial strain.

It is apparent from Figure 6.15 that the stress path for the overconsolidated sample has a more pronounced inclination, i.e. an increase in mean effective stress, in the beginning of the undrained shearing compared to the other two tests. This would imply that the elastic response is not isotropic and in this case the vertical stiffness appears to be greater than the horizontal.

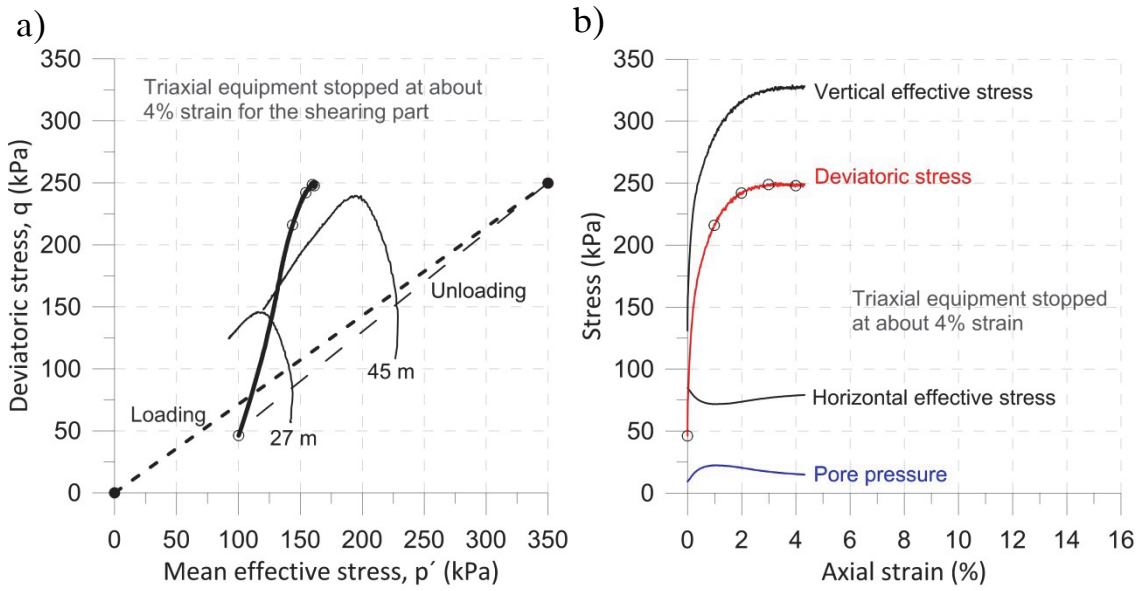

Figure 6.15. Triaxial test with loading and unloading before undrained shearing. a) Stress path and b) the stress-strain relations are presented for the undrained shearing part for the overconsolidated test. In a) is also included the 27 m and 45 m undrained triaxial tests from Figure 6.11

The stress path is over shooting the evaluated critical state line from the 27 m and 45 m tests, i.e. entering the dry side, before reaching failure. The peak strength of the sample seems to correspond to around 3% axial strain and there was no tendency for strain softening before the test was stopped. The excess pore pressure shown in Figure 6.15b are increasing at the start of the undrained shearing of the sample and after passing the evaluated critical state line the excess pore pressure is decreasing. After further straining the excess pore pressure seems to level out which is assumed to correspond to a critical state.

In Figure 6.16 the yield points evaluated from five drained triaxial tests are shown, additionally there are also the yield points from two K_0-triaxial tests presented in Chapter 5 and the normal compression surface (NCS) of the MAC-s model is also plotted. These tests were conducted with a sample height of 20 mm to represent the same size as in an oedometer test. The

tests were performed with a constant effective stress ratio and with same deformation rate as the CRS oedometer test, i.e. 0.0024 mm/min. The evaluation procedure to obtain the yield points in p´-q space are presented in detail in Appendix A.1.

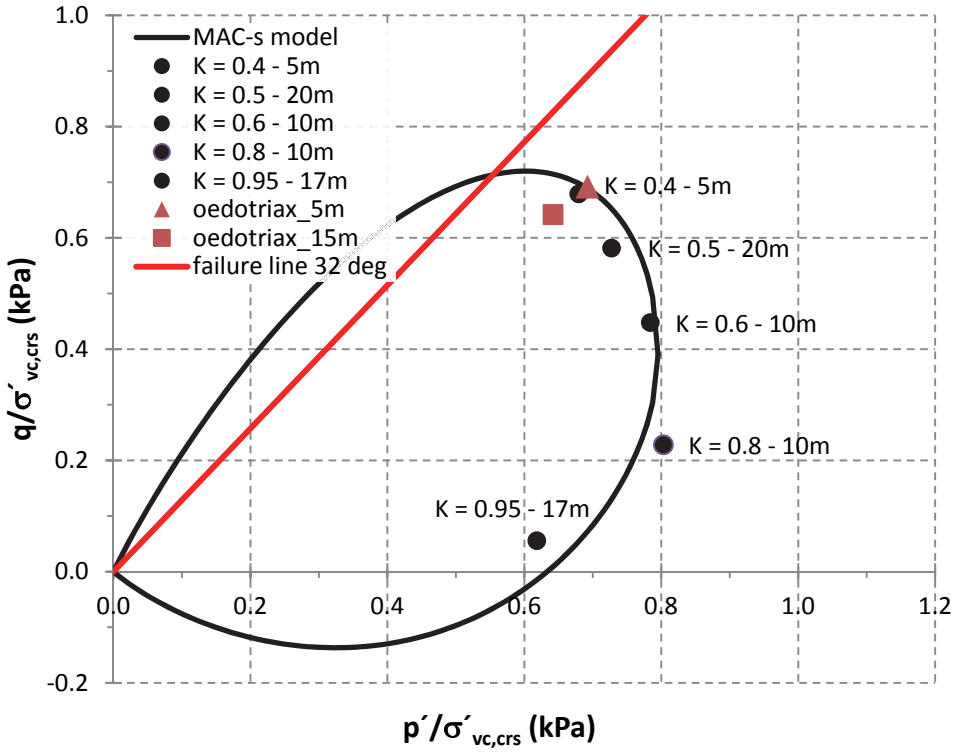

Figure 6.16. Evaluated yield points from drained triaxial tests with different p´-q stress paths. Also included the yield points from the two K_0-triaxial tests presented in Chapter 5 and the NCS of the MAC-s model with input parameters as Table 6.1.

Figure 6.16 demonstrates that the yield surface is inclined implying significant initial anisotropy. This is probably due to the deposition process and subsequent loading history. It can also be seen that the formulation of the normal compression surface for the MAC-s model is in very good agreement with the laboratory results. The results in Figure 6.16 have a similar shape and size as other reported natural clays, see e.g. Larsson (1981) and Leroueil (2006).

In Figure 6.17 the normalized vertical effective stress against axial strain is plotted. Based on Figure 6.17 all the drained stress path controlled tests performed give the same shape for the normalized stress-strain curve, except for the test conducted with a K_0 value of 0.95. For the tests with a K_0=0.95 the transition when passing the preconsolidation pressure is much less pronounced. This is, however, to be expected since this stress path is far from what the soil has consolidated for and hence forcing a rotation of the normal compression surface as the soil wants to become more or less isotropic. This would probably destroy much of the structure the soil has developed during the sedimentation history of the soil, including both temperature and other effects such as chemical reaction etc.

According to Figure 6.17 there is a change in the inclination for the K = 0.6 and K = 0.8 test at an axial strain of about 11%. In the determination of the yield points it is assumed that this effect, which is most likely caused by one of the boundaries in the triaxial test, did not significantly affect the obtained results.

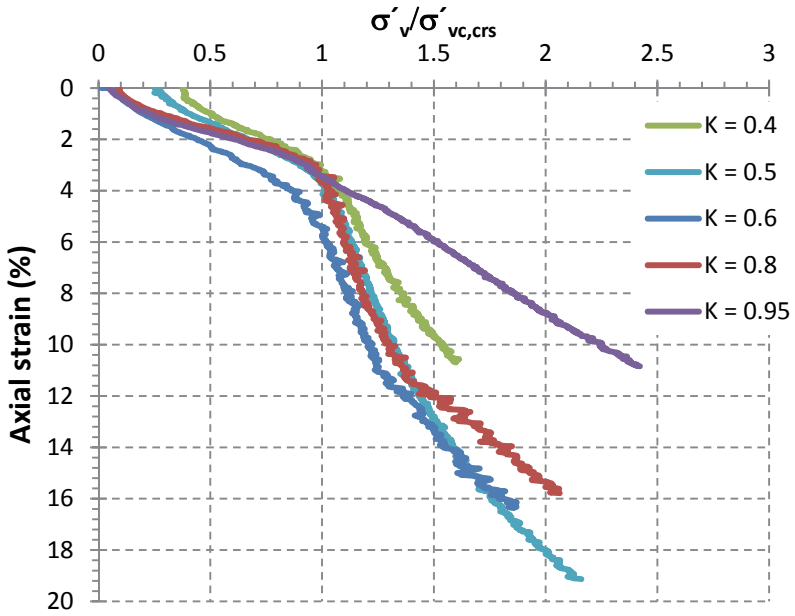

Figure 6.17. Normalized vertical effective stress versus axial strain for all five drained triaxial tests conducted with K constant stress paths.

6.2 Simulations

In order to see how well the MAC-s model, presented in Chapter 4, represents real soil behaviour, a number of simulations are conducted as boundary value problems modelled with COMSOL Multiphysics v.4.3 finite element software. The methodology used to evaluate the input parameters was described in Chapter 4, if not stated otherwise.

The common input parameters for all the simulations are summarized in Table 6.1. However, some of the input parameters differ due to depth and location and are then stated for that test.

The vertical preconsolidation pressure, used in the simulations, was set to 120 kPa and 100 kPa for the oedometer tests and triaxial test, respectively, for the 10 m depth. The vertical preconsolidation pressure was set to 350 kPa in the simulation of the triaxial test of 45 m depth. The input values of K_0^{nc}, α_0 and ω_d is calculated as described in Chapter 4. The hydraulic conductivity, k, is set to $8 \cdot 10^{-10}$ m/s for both the 5 m and 10 m depth and the β_k value is set to 3.

Table 6.1. Input parameters for simulations.

ν_{ur}	ϕ'	κ^*	λ_i^*	r_{si}	τ	ω_v	ω_d^*
0.2	32°	0.016	0.075	700	1 day	200	170

χ_0	ξ_v	ξ_d	M_e	M_c	α_0	m
20	13	5	1	1.287	0.491	0.4

Note: Input parameters M_c, α_0 and ω_d^* is a function of friction angle ϕ' cf. Chapter 4.

The results of the simulations are presented in Figure 6.18 to Figure 6.26, and are compared with the corresponding laboratory result.

In Figure 6.18 and Figure 6.19 the results from an IL oedometer simulation are presented and compared with the experimental results. The simulation has been conducted on a clay sample from 10 m depth. The initial stress of the soil is assumed to be 10 kPa to represent that some negative pore pressure is still left from the extraction. Figure 6.18 demonstrates a very good match between the experimental and simulation. However, as shown in Figure 6.19 the time it takes for the simulation to reach full consolidation is much faster in the simulations than the laboratory result. This discrepancy could not only be explained by calibrating some of the material parameters used in the MAC-s model further, within reasonably limits.

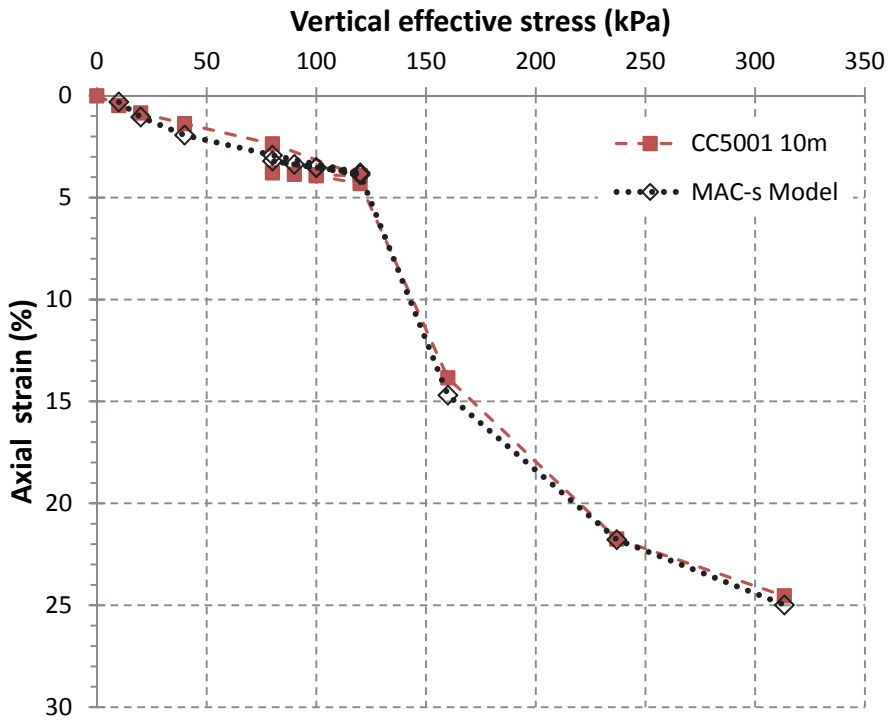

Figure 6.18. Stress-strain curves of simulation result compared with laboratory result of an IL oedometer test at the depth of 10 m.

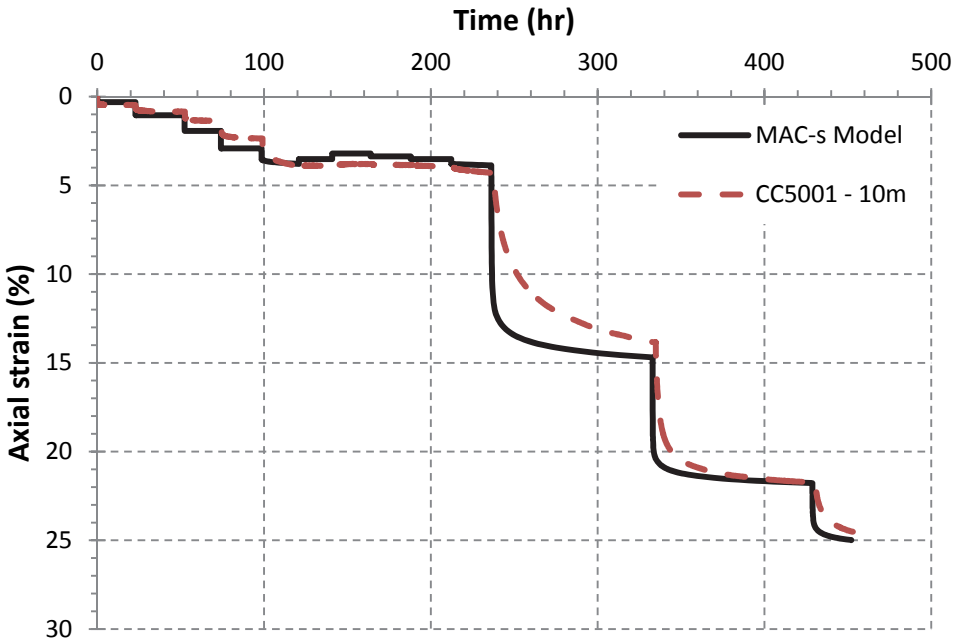

Figure 6.19. Vertical stress versus time curves of simulation result compared with laboratory result of an IL oedometer test at the depth of 10 m.

In Figure 6.20 a CRS oedometer test is simulated and compared with laboratory results for a clay sample from 10 m depth. The initial stress of the soil is assumed to be 10 kPa to represent that some negative pore pressure is still left from the extraction. The simulated stress–strain curve has a relatively good agreement with the laboratory results, except around the preconsolidation pressure, where the simulation predicts a much more sudden transition than the laboratory curve.

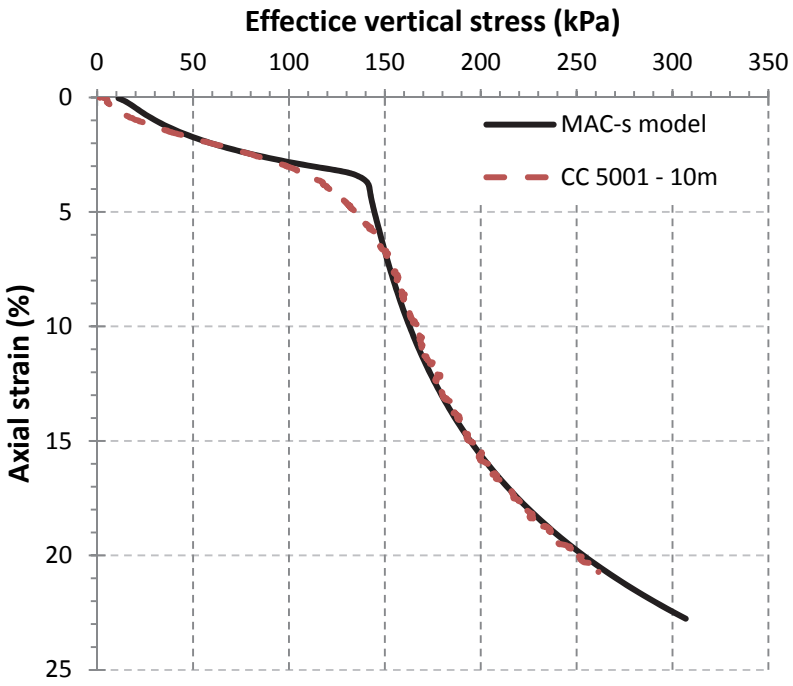

Figure 6.20. Stress-strain curve of simulation result compared with laboratory result of a CRS oedometer test at the depth of 10 m.

In Figure 6.21 and Figure 6.22 four K_0-consolidated undrained triaxial tests are simulated and compared with the corresponding laboratory test, in p´-q stress space plot and q-axial strain plot, respectively. As shown in Figure 6.21 the MAC-s model is in good agreement with experimental results in p´-q stress space. However, it seems that for compression test on a sample from 10 m depth a slight underestimation is done with the selection of value for the critical state friction angle. With a slightly larger value of the critical state friction angle than assumed a better fit would have been obtained for this specific test. The critical state friction angle chosen is based on an average critical state friction angle from all the undrained triaxial compression tests presented in Figure 6.11. For compression test on a sample from 45 m depth better comparison is obtained for the stress path. For the extension tests the simulated stress paths are in good agreement with experimental results, i.e. following the stress path until a certain stress level where the experimental results decrease faster in mean effective stress than predicted by the model.

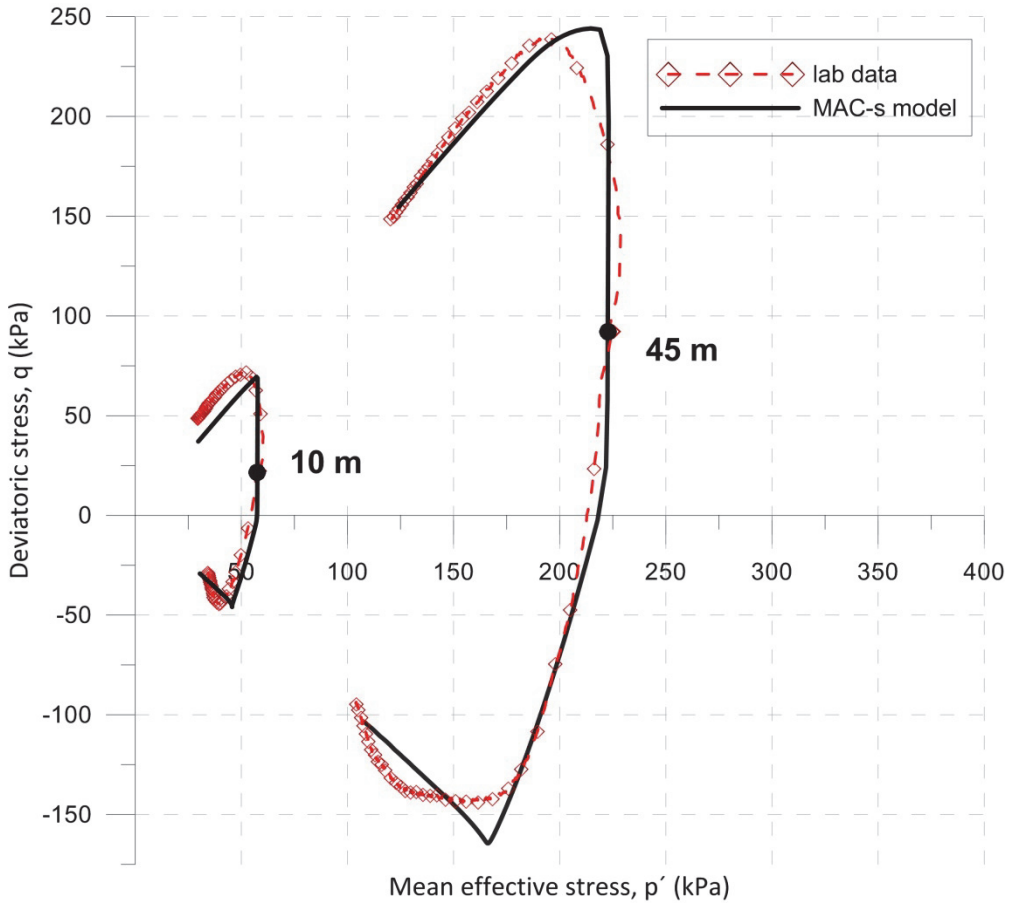

Figure 6.21. Simulations results (solid black lines) compared with laboratory results (dashed red lines with squares) of the K_0-consolidated undrained triaxial test from 10 m and 45 m from CC5001 area in terms of stress path. Black dots indicate the K_0-conslidated stress state just before the undrained shearing.

Based on Figure 6.22 the predicted deviatoric stress versus axial strain is in good agreement with the experimental data. However, the sample from the depth of 45 m seems to behave in stiffer manner in the simulation compared with the experimental data when approaching the peak strength.

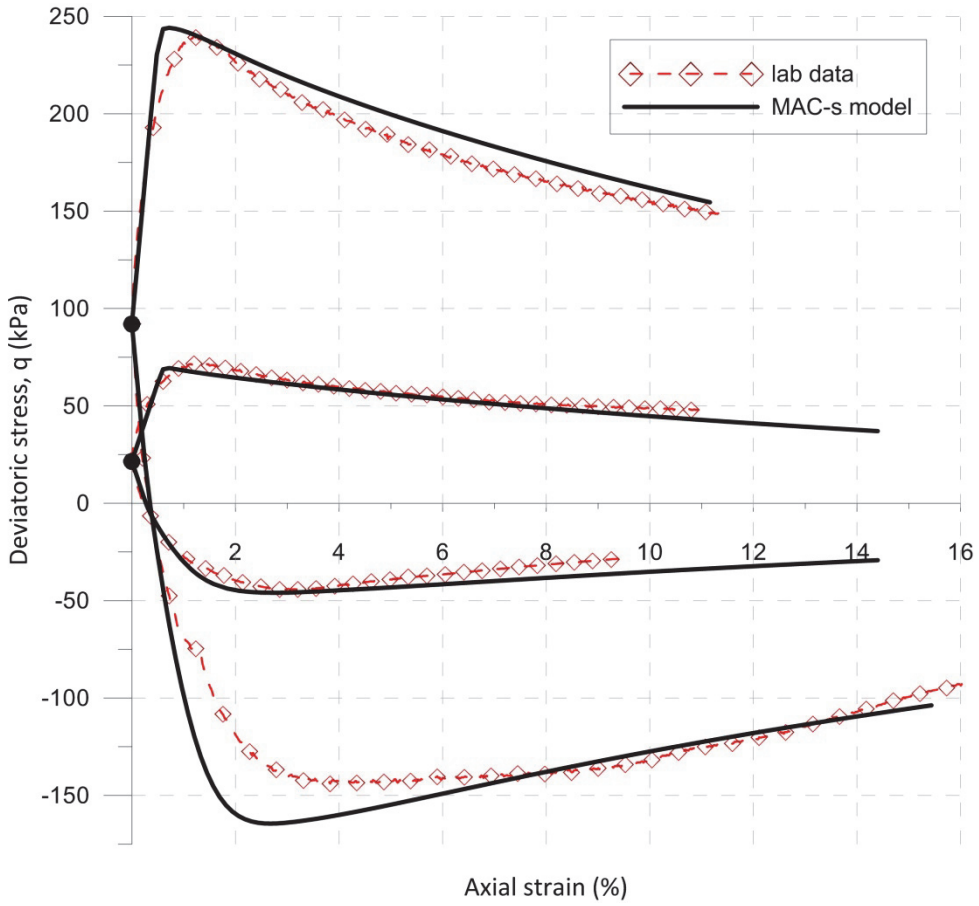

Figure 6.22. Simulation results (solid black lines) compared with laboratory results (dashed red lines with squares) of the K_0-consolidated undrained triaxial test from 10 m and 45 m from CC5001 area in terms of stress-strain curves. Black dots indicate the K_0-conslidated stress state just before the undrained shearing.

In Figure 6.23 a K_0-consolidated undrained triaxial test is simulated, where an overconsolidated stress state has been accomplished as with a drained loading and unloading stage as shown in the figure. The same parameter set up has been used with the exception that the shape parameter m is set to 0.25 and initial structure has been reduced to $\chi_0 = 1$ when undrained shearing phase starts. This was due to all the creep strains that had occurred during the consolidation phase. Additionally, the elastic parameter, α_e, is set to 0.5 evaluated from the p´-q stress plot in Figure 6.23. This would imply that the vertical stiffness is much greater than the horizontal.

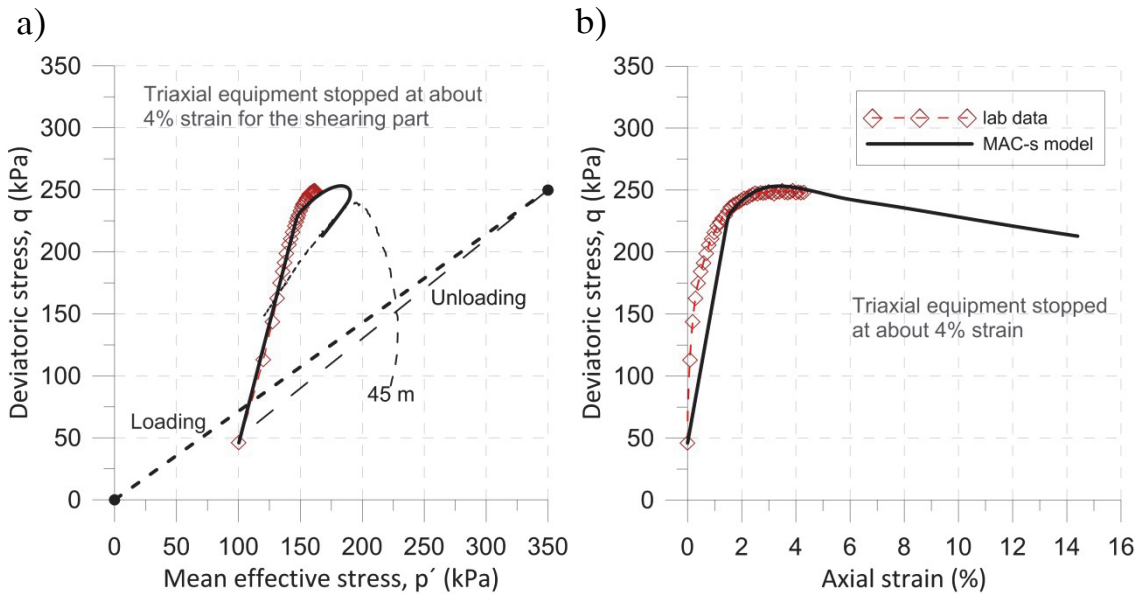

Figure 6.23. Simulation results (solid black lines) compared with laboratory results (dashed red lines with squares) plotted in a) stress space and b) deviatoric stress versus axial strain.

According to Figure 6.23 the simulated p´-q stress path is in very good agreement with experimental result. However, it seems that the initial stiffness in the experimental results is much stiffer than the stiffness predicted by the model. In the p´-q stress plot the predicted p´-q stress path continues to increase in mean effective stress until a stress level at which it turns and starts to decrease. This is associated with reaching the critical state line.

Figure 6.24 presents a simulation of the sample from 5 m depth from the K_0-triaxial test presented in Chapter 5. This test make use of the same input parameters as described in Table 6.1, except for the intrinsic compression index, λ_i^*, and the intrinsic creep number, r_{si} has been calibrated against the IL oedometer results for the same depth. The intrinsic compression index was set to λ_i^*=0.069, the intrinsic creep number r_{si}=500 and the preconsolidation pressure was set to 63 kPa.

Based on Figure 6.24 the predicted stress-strain curve is in very good agreement with the experimental results. However, in the reload curve, the axial strain is marginally under predicted.

In Figure 6.25 the predicted volumetric strain versus time is presented together with the experimental results. Observe that only some selected stages are presented in Figure 6.25, for the sake of clarity.

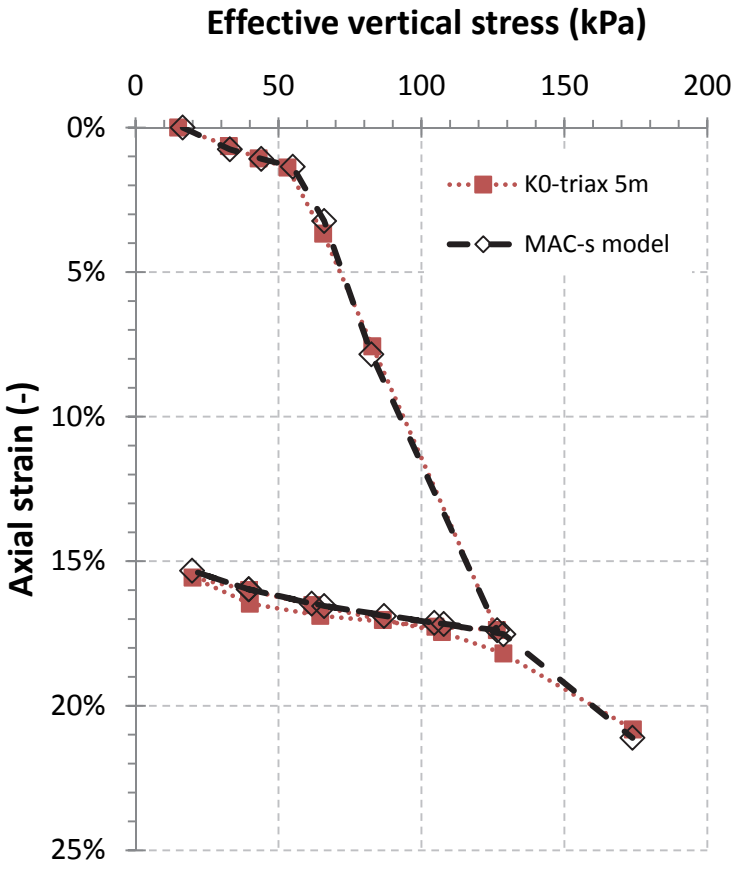

Figure 6.24. Simulations results of K_0 triaxial test for the sample from a depth of 5m compared with laboratory results.

From Figure 6.25 it is apparent that the predicted consolidation time is different from the measured, especially stage 6 and 7. The predicted consolidation seems to be in the order of 50-100 times faster than observed consolidation time, when stresses are above the apparent preconsolidation pressure. Figure 6.26 presents the p´-q stress plot. The predicted stress path follows the experimental data for the first and second loading (stage 1-7

and 12-17). However, the predicted stress path of the un-/reload curve differ from the experimental results, i.e. the experimental results makes a small loop while the predicted un-/reload curve is following a straight line back and forth.

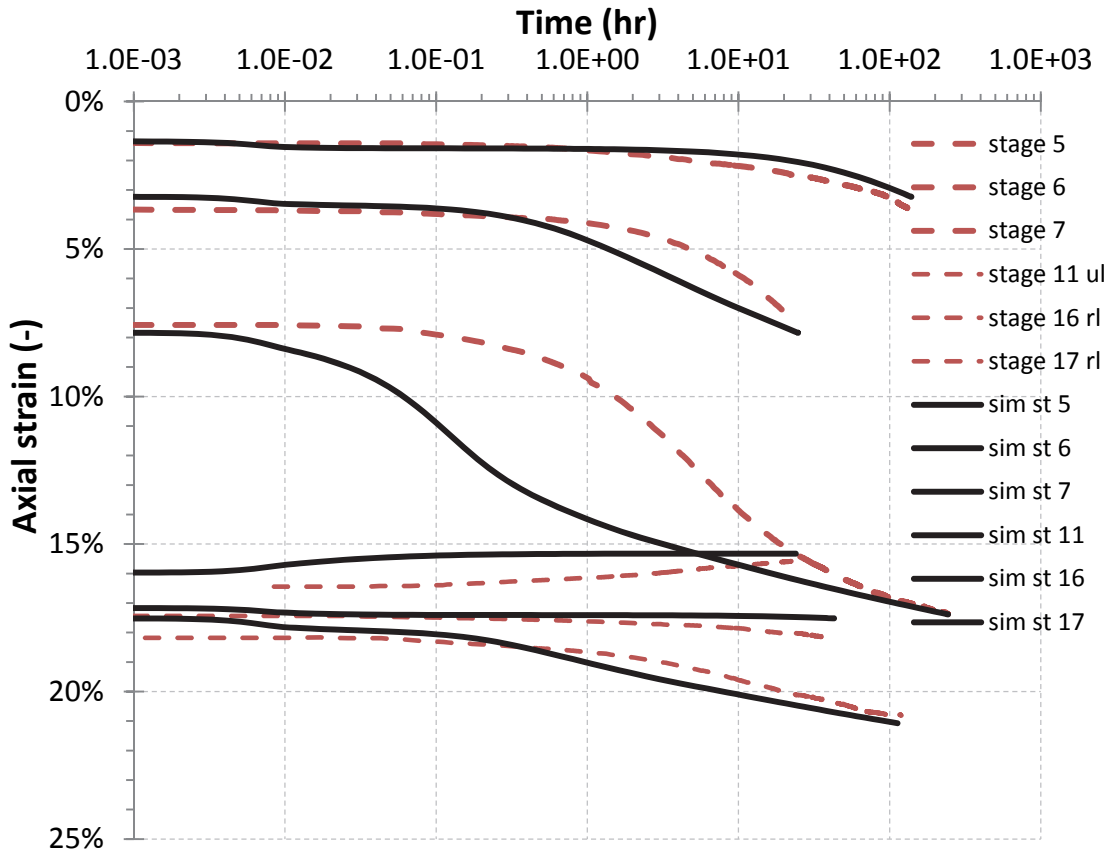

Figure 6.25. Simulation results of K_0 triaxial test (solid black lines) of axial strain versus log(time) for some selected stages from the sample from a depth of 5 m compared with laboratory results (dashed red lines).

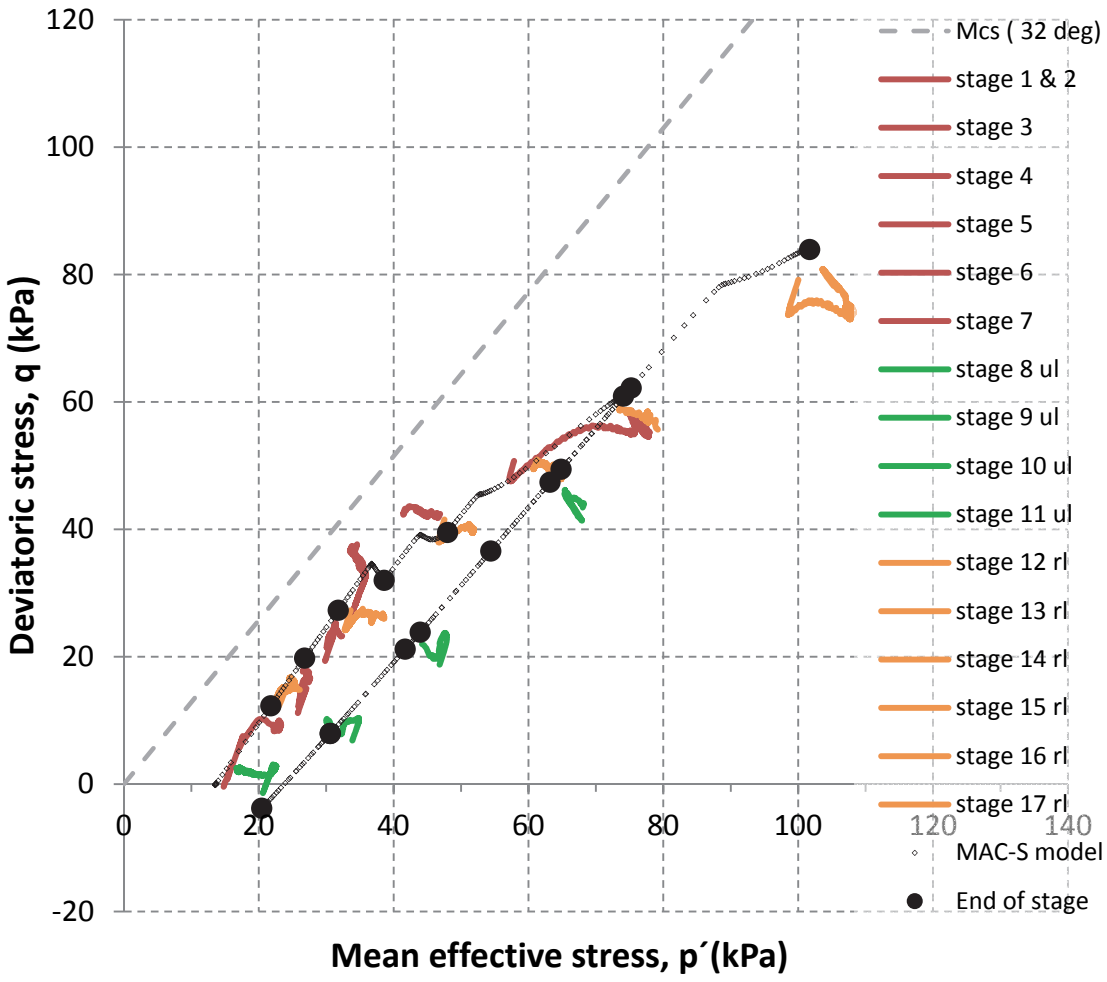

Figure 6.26. Simulation results of K_0 triaxial test in stress space of the sample from a depth of 5 m compared with the laboratory results. The filled dots represent the stress state at end of each stage.

It is also apparent from Figure 6.26 that the stress ratio (q/p´) is over predicted when passing the preconsolidation pressure, i.e. reaching the normal consolidated state. This would imply that the K_0^{nc} value would be under predicted by the model. This is also shown in Figure 6.27 where the predicted K_0 of the MAC-s model is plotted against normalized stress and compared with laboratory results presented in Chapter 5.

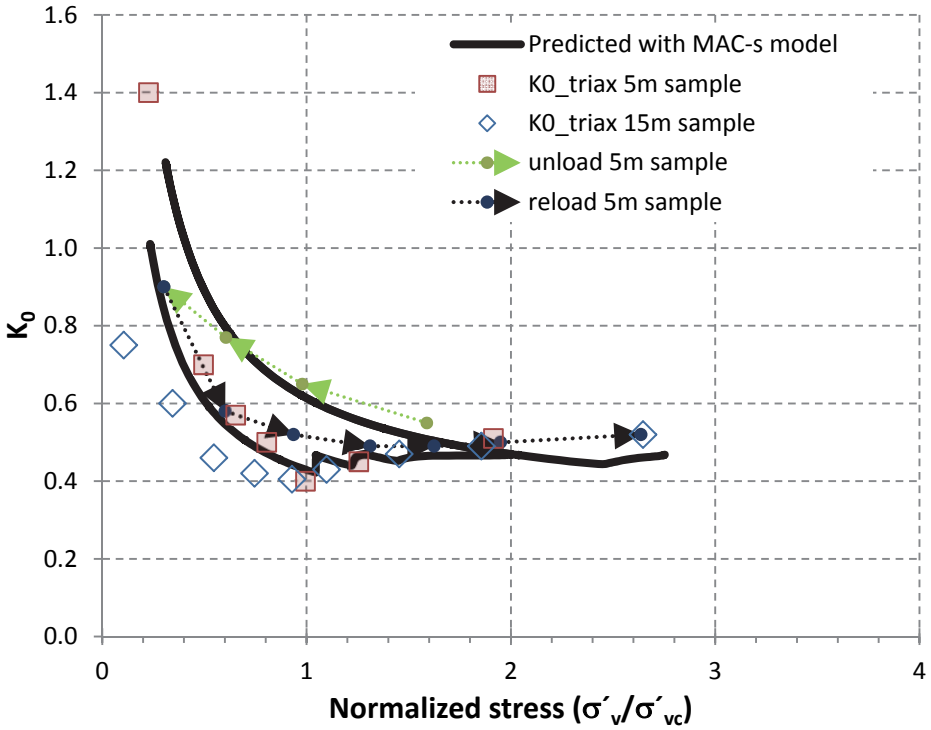

Figure 6.27. K_0 predicted with the MAC-s model for the sample from a depth of 5m compared with laboratory results.

Based on Figure 6.27 the K_0 prediction of the MAC-s model is matching the first loading curves of the laboratory results, but the K_0 on load reversals is not, as expected, properly captured. This suggests that the elastic part of the model might need further consideration.

6.3 Conclusions

The experimental results presented in the previous section are in line with previous findings for Gothenburg clay, e.g. Alte et al. (1989) and Claesson (2003).

From the simulation results presented above, the MAC-s model is able to capture many of the important features on rate-dependency of Gothenburg clay. However, in its current form, the model does not capture, as expected, the load reversal properly and furthermore the model underestimates the K_0^{nc} value at large strain.

7 CONCLUSIONS AND RECOMMENDATIONS

7.1 Conclusions

The objective of this project was to investigate and provide a deeper understanding in the constitutive behaviour of soft clay. Focus has been on the rate-dependency of natural clay deposits. The research comprised of development of a new rate-dependent model, and in order to help estimate K_0^{nc} value a novel K_0-triaxial cell was developed and tested on samples of soft Gothenburg clay. The K_0^{nc} value is a crucial input parameter that governs the accuracy of boundary value level simulations for constitutive models for soft soils.

This thesis introduces the MAC-s model, a new anisotropic creep model with a new reference surface combined with plastic potential from the S-CLAY1S model, see Chapter 4. The reference surface of the MAC-s model aims to increase the accuracy for predictions of overconsolidated clays by allowing the user to more accurately define the shape of the reference surface in that region in stress space. This is achieved by introducing one additional model parameter compared to similar creep models. This parameter is easily obtained from standard laboratory tests combined with model simulations. The simulations with the new model of IL oedometer, CRS oedometer and undrained triaxial tests are in good agreement with experimental data, as shown in Chapter 6. However, in its current form, the model is, as expected, not capable of accurately capturing load reversals.

The novel K_0-triaxial cell, presented in Chapter 5, is designed to measure the lateral stress component on the boundary of the soil sample, whilst maintaining zero lateral deformation. Hence, as opposed to standard IL tests the evolution of the K_0 value is measured. The test results on soft Gothenburg clay indicate that the ratio between the horizontal and vertical

effective stress at normal consolidated conditions, i.e. the K_0^{nc} value, is in the range of 0.50-0.55. This is in accordance with previous measurements, which contradict the empirical relations commonly used in Sweden. These results imply that the commonly used empirical relations, based on the index properties, of the clay should be used with care.

7.2 Recommendations

More experimental tests should be performed to validate the model formulation and gather more comprehensive data on K_0^{nc} values for soft soils. This implies application of non-standard stress or strain paths testing e.g.:

- Experimentally probe along different stress paths for the normal compression surface in drained conditions. The latter will also allow for validation of the hardening laws controlling the evolution of anisotropy and the destructuration of bonds in the context of creep models.
- K_0-triaxial tests with measurement of radial deformation and with load reversals to capture the soils unload and reload behaviour. The incremental loading of the sample in the current design should be extended with an actuator to load the sample using either displacement- and/or load control. The latter would enable to apply the required stress or strain path for obtaining the non-standard parameters for advanced constitutive models.
- IL oedometer on reconstituted or remoulded clay samples to establish the intrinsic properties of the Gothenburg clay.

For natural soils this implies that a sufficient number of samples, following best international practice in sampling, handling and storage, should be obtained for each representative soil layer. These tests should be

performed in proper controlled conditions, such as e.g. temperature, humidity and vibrations.

Using the data obtained from the tests suggested above would help to improve the MAC-s model. The following components are suggested as a starting point for further developments:

- The hardening laws of the model need further validation and possible reformulation.
- In order to improve performance in the small strain domain (e.g. shear strains < 10^{-5}), which is very relevant to excavation and tunnel problems, a small strain formulation should be implemented.

In it is current form the MAC-s model is a valuable tool in engineering with the intention to increase the accuracy of long-term deformation predictions of soft soils. This is, however, only applicable when the input data is based on site specific high quality experimental data. The use of the novel K_0-triaxial cell gives valuable additional information of the stress state of the sample compared to standard IL or CRS oedometer tests. When embedded in engineering practice it will assist in the use of advanced constitutive models, such as the MAC-s model.

REFERENCES

Adachi, T. and Oka, F. (1982). Constitutive equations for normally consolidated clay based on elasto-viscoplasticity Soils and Foundations 22(4), pp. 57-70.

Alte, B., Olsson, T., Sällfors, G. and Bergsten, H. (1989). Study of the Gothenburg clay" Geological - geotechnical study of clay from great depths in kv. Guldet, Bo Alte AB & Chalmers University of Technology, Gothenburg. (In Swedish)

Bardet, J. P. (1990). Lode dependences for isotropic pressure-sensitive elastoplastic materials Journal of Applied Mechanics 57(3), pp. 498-506.

Bjerrum, L. (1967). Engineering geology of Norwegian normally-consolidated marine clays as related to settlements of buildings (Seventh Rankine Lecture) Géotechnique 17(2), pp. 83-118.

Boudali, M. (1995). Comportement tridimensionel et visqueux des argiles naturelles, Université Laval. Québec. Phd. Thesis

Brinkgreve, R. B. J., Swolfs, W. M. and Engin, E. (2011). PLAXIS Manual 2D 2011. Netherlands.

Buisman, K. (1936). Results from long duration settlement tests. Proc. 1st International Conference on Soil Mechanics and Foundation Engineering, Cambridge, Vol. 1, pp. 103-107.

Burland, J. B. (1990). On the compressibility and shear strength of natural clays Géotechnique 40(3), pp. 329-378.

Burmister, D. M. (1951). The application of controlled test methods in consolidation testing. Symp. on Consolidation Testing of Soils, Philadelphia, Pennsylvania, 126, ASTM (Spec. Tech. Publ.), pp. 83.

Callisto, L. and Calabresi, G. (1998). Mechanical behaviour of a natural soft clay Géotechnique 48(4), pp. 495-513.

Campanella, R. G. and Vaid, Y. P. (1972). A Simple Ko Triaxial Cell Canadian Geotechnical Journal 9(3), pp. 249-260.

Casagrande, A. (1936). The determination of the preconsolidation load and its practical significance. Proc. 1st International Conferens in Soil Mechanics and Foundation Engineering, Cambridge, Vol. 3, pp. 60.

Claesson, P. (2003). Long term settlements in soft clays, Chalmers University of Technology. Gothenburg. Phd. Thesis

Dafalias, Y. F. (1986). Anisotropic critical state clay plasticity model Mechanics research communications vol. 13(6), pp. 341-347.

GDS Advanced Digital Controller Handbook (2000). GDS Instruments Ltd, Hampshire, UK.

GDS Instruments Ltd (2013). Triaxial Testing System. from www.gdsinstruments.com.

Gens, A. and Nova, R. (1993). Conceptual bases for a constitutive model for bonded soils and weak rocks. Proc. of Int. Symp. on Hard soils - Soft Rocks, Athens, pp. 485-494.

Graham, J. and Houlsby, G. T. (1983). Anisotropic elasticity of a natural clay Géotechnique 33(2), pp. 165-180.

Graham, J., Noonan, M. L. and Lew, K. V. (1983). Yield states and stress–strain relationships in a natural plastic clay Canadian Geotechnical Journal 20(3), pp. 502-516.

Grimstad, G. (2009). Development of effective stress based anisotropic models for soft clays, Norwegian University of Science and Technology (NTNU). Trondhiem. Phd. Thesis

Grimstad, G. and Degago, G. (2010). A non-associated creep model for structured anisotropic clay (n-SAC). Numerical Methods in Geotechnical Engineering (NUMGE 2010), CRC Press, pp. 3-8.

Grimstad, G., Degago, S., Nordal, S. and Karstunen, M. (2008). Modelling creep and rate effects using the time resistance concept in a model for anisotropy and destructuration. Nordic Geotechnical Meeting, Sandefjord, Norway, pp. 195-202.

Jaky, J. (1944). The coefficient of earth pressure at rest J. Soc. Hung. Eng. Arch., pp. 355-358.

Jaky, J. (1948). Pressure in silos. Proc. 2nd Int. Conf. on Soil Mechanics and Foundation Engineering, Rotterdam, The Netherlands, pp. 103-107.

Janbu, N. (1973). Shear Strength and Stability of Soils. NGF-Foredraget 1973. Oslo.

Karstunen, M. and Koskinen, M. (2008). Plastic anisotropy of soft reconstituted clays Canadian Geotechnical Journal 45(3), pp. 314-328.

Karstunen, M., Krenn, H., Wheeler, S. J., Koskinen, M. and Zentar, R. (2005). Effect of Anisotropy and Destructuration on the Behaviour of Murro Test Embankment International Journal of Geomechanics 5(2), pp. 87-97.

Kirkgard, M. M. (1988). An experimental study of the three-dimensional behavior of natural normally consolidated anisotropic clay, University of California, Los Angeles. United States -- California. PhD. Thesis

Kirkgard, M. M. and Lade, P. V. (1993). Anisotropic three-dimensional behavior of a normally consolidated clay Canadian Geotechnical Journal 30(5), pp. 848-858.

Koskinen, M., Karstunen, M. and Wheeler, S. (2002). Modelling destructuration and anisotropy of a soft natural clay. 5th European Conference on Numerical Methods in Geotechnical Engineering. Paris, France, Presses de l'ENPC, pp. 11-20.

Kulhawy, F. H. and Mayne, P. W. (1990). Manual on estimating soil properties for faoundation design. Final Report, Project 1496-3, EL-6800, Eletric Power Research Insitute Palo Alto, CA.

Kullingsjö, A. (2007). Effects of deep excavations in soft clay on the immediate surroundings, Chalmers University of Technology. Gothenburg. Phd. Thesis

Lade, P. V. (1977). Elasto-plastic stress-strain theory for cohesionless soil with curved yield surfaces International Journal of Solids and Structures 13(11), pp. 1019-1035.

Lade, P. V. and Duncan, J. M. (1975). Elastoplastic stress-strain theory for cohesionless soil J. Geotechnical Engineering Division, ASCE, 101, pp. 1037-1053.

Larsson, R. (1981). Drained behaviour of Swedish clays. Report No. 12, Swedish Geotechnical Institute, Linköping.

Larsson, R. (1986). Consolidation of soft soils. Report No. 29, Swedish Geotechnical Institute, Linköping.

Larsson, R., Bengtsson, P.-E. and Eriksson, L. (1997). Prediction of settlements of embankments on soft, fine-grained soils. Information 13E, Swedish Geotechnical Institute, Linköping.

Larsson, R., Sällfors, G., Bengtsson, P.-E., Alén, C., Bergdahl, U. and Eriksson, L. (2007). Shear strength - evaluation of cohesion soil. Information 3, Swedish Geotechnical Institute, Linköping. (In Swedish)

Leoni, M., Karstunen, M. and Vermeer, P. A. (2008). Anisotropic creep model for soft soils Géotechnique 58(3), pp. 215-226.

Leroueil, S. (2006). The isostache approach. Where are we 50 years after its development by professor Suklje? Proc. 13th Danube Eur. conf. on Geotechnical Engineering, Ljubljana, pp. 55-88.

Leroueil, S., Kabbaj, M., Tavenas, F. and Bouchard, R. (1985). Stress-strain-strain rate relation for the compressibilty of sensitive natural clays Géotechnique 35(2), pp. 159-180.

Leroueil, S. and Marques, M. E. S. (1996). Importance of Strain Rate and Temperature Effects in Geotechnical Engineering ASCE Geotechnical special publication no.61, pp. 1-60.

Liingaard, M., Augustesen, A. and Lade, P. V. (2004). Characterization of Models for Time-Dependent Behavior of Soils International Journal of Geomechanics 4(3), pp. 157-177.

Länsivaara, T. (1999). A study of the mechanical behavior of soft clays, Norwegian University of Science and Technology (NTNU). Trondheim. Phd. Thesis

Matsuoka, H. and Nakai, T. (1974). Stress-deformation and strength characteristics of soil under three difference principal stresses Proceedings of the Japan Society of Civil Engineers (JSCE) 232, pp. 59-70.

Menzies, B. K. (1988). A Computer Controlled Hydraulic Triaxial Testing Sytem ASTM Special Publication 977, pp. 82-94.

Mesri, G. and Godlewski, P. M. (1977). Time and stress-compressibility interrelationship American Society of Civil Engineers, Journal of the Geotechnical Engineering Division 103(5), pp. 417-430.

Microstrain Inc. (2013). SG-DVRT sensor. 2013, from http://www.microstrain.com/displacement/sg-dvrt.

Mitchell, J. K. and Soga, K. (2005). Fundamentals of Soil Behavior (3rd Edition), John Wiley & Sons.

Nadarajah, V. (1973). Stress-strain properties of lightly overconsolidated clays, Cambridge University. PhD. Thesis

Nakai, T., Matsuoka, H., Okuno, N. and Tsuzuki, K. (1986). True triaxial tests on normally consolidated clay and analysis of the observed shear behavior using elastoplastic constitutive models Soils and Foundations 26(4), pp. 67-78.

Nordal, S. (2008). Soil modeling - PhD course BA8304. Trondheim, NTNU - Geotechnical Division.

Olsson, M. (2010). Calculating long-term settlement in soft clays - with special focus on the Gothenburg region, Chalmers University of Technology. Gothenburg. Licentiate thesis

Olsson, M. (2013). Implementation of a anisotropic creep model into COMSOL Multiphysics v.4.3b. (In preperation), Chalmers University of Technology, Division of GeoEngineering, Gothenburg.

Olsson, M., Alén, C. and Karstunen, M. (2013). En studie om pågående sättningar i centrala Göteborg (under bearbetning), Chalmers tekniska högskola, Avd. Geologi och Geoteknik, Göteborg. (In Swedish)

Persson, J. (2004). The Unloading Modulus of Soft Soil: A Field and Laboratory Study, Chalmers tekniska högskola. Licentiate thesis

Perzyna, P. (1963). The constitutive equations for workhardening rate sensitive plastic materials. Proc. of Vibrational Problems, Warzaw, Vol.4, pp. pp. 281-290.

Pestana, J. M. (1994). A unified constitutive model for clays and sands, Massachusetts Institute of Technology. Massachusetts. PhD. Thesis

Pestana, J. M. and Whittle, A. J. (1999). Formulation of a unified constitutive model for clays and sands International Journal for Numerical and Analytical Methods in Geomechanics 23(12), pp. 1215-1243.

Potts, D. M. and Zdravkovic, L. (1999). Finite element analysis in geotechnical engineering - Theory. London, Thomas Telford Publishing.

Roscoe, K. H. and Burland, J. B. (1968). On the generalised stress-strain behaviour of wet clay. Engineering plasticity (Cambridge: Cambridge University Press), in Heyman. J. and Leckie. F.A. (eds.), pp. 535-609.

Roscoe, K. H. and Schofield, A. N. (1963). Mechanical behaviour of an idealised wet clay. Proc. European Conf. on Soil Mechanics and Foundation Engineering, Weisbaden, Vol. 1, pp. pp. 47-54.

Roscoe, K. H., Schofield, A. N. and Wroth, C. P. (1958). On the yielding of soils Géotechnique 8(1), pp. 22-53.

Runesson, K. (1978). On non-linear consolidation of soft clay, Chalmers University of Technology. Gothenburg. Phd. Thesis

Schmertmann, J. H. (1953). Estimating the true consolidation behaviour of clay from laboratory test results Proceedings ASCE 79(separate No. 311), pp. 1-26.

Schmidt, B. (1966). Earth pressures at rest related to stress history. Discussion Can. Geotech. J. 3, pp. 239-242.

Schofield, A. N. and Wroth, C. P. (1968). Critical state soil mechanics. London, McGraw-Hill.

Sekiguchi, H. and Ohta, H. (1977). Induced anisotropy and time dependency in clays. 9th ICSMFE. Tokyo. Constitutive equations of soils, pp. 229-238.

Sheahan, T., Ladd, C. and Germaine, J. (1996). Rate-Dependent Undrained Shear Behavior of Saturated Clay Journal of Geotechnical Engineering 122(2), pp. 99-108.

Sheng, D., Sloan, S. W. and Yu, H. S. (2000). Aspects of finite element implementation of critical state models Computational Mechanics 26(2), pp. 185-196.

Sivasithamparam, N. (2012). Development and Implementation of Advanced Soft Soil Models in Finite Elements, University of Strathclyde. Glasgow. PhD. thesis

Sivasithamparam, N., Karstunen, M., Brinkgreve, R. B. J. and Bonnier, P. G. (2013). Comparison of two anisotropic rate dependent models at element level. Proc. International Conference on Installation Effects in Geotechnical Engineering, Rotterdam, NL, Taylor & Francis Group, London, pp. 43-50.

Stolle, D. F. E., Bonnier, P. G. and Vermeer, P. A. (1997). A soft soil model and experiences with two integration schemes. Proc. NUMGO VI, Montreal, pp. 123-128.

Stolle, D. F. E., Vermeer, P. A. and Bonnier, P. G. (1999). Time integration of a constitutive law for soft clays Communications in Numerical Methods in Engineering 15(8), pp. 603-609.

Sällfors, G. (1975). Preconsolidation pressure of soft, high-plastic clays, Chalmers University of Technology. Göteborg. Phd. Thesis

Terzaghi, K. (1954). Theoretical soil mechanics. New York, John Wiley and sons. 7th printing.

Tidfors, M. (1987). Temperature effects on deformations properties on clay - A laboratory study, Chalmers University of Technology, Gothenburg. (In Swedish)

Tidfors, M. and Sällfors, G. (1989). Temperature effect on preconsolidation pressure Geotechnical Testing Journal 12(1), pp. 93-97.

Vermeer, P. A. and Neher, H. (1999). Beyond 2000 in Computational Geotechnics - A soft soil model that accounts for creep. Rotterdam, A.A. Balkema.

Vermeer, P. A., Stolle, D. F. E. and Bonnier, P. G. (1998). From the classical theory of secondary compression to modern creep analysis. Proc. Computer Methods and advances in Geomechanics, Wuhan, China, Rotterdam: Balkema, pp. 2469-2478.

Wheeler, S. J. (1997). A rotational hardening elasto-plastic model for clays. Proc. 14th Int. Conf. on Soil Mechanics and Foundation Engineering, Hamburg, Vol. 1, A.A. Balkema, pp. 431-434.

Wheeler, S. J., Karstunen, M. and Naatanen, A. (1999). Anisotropic hardening model for normally consolidated soft clays. In Proceedings of the 7th International Symposium on Numerical Models in Geomechanics (NUMOG), Graz, Austria, A.A. Balkema, Rotterdam, pp. 33-40.

Wheeler, S. J., Näätänen, A., Karstunen, M. and Lojander, M. (2003). An anisotropic elastoplastic model for soft clays Canadian Geotechnical Journal 40(2), pp. 403-418.

Wood, D. M. (1990). Soil behaviour and critical state soil mechanics. Cambridge, Cambridge University Press.

Wood, T. and Karstunen, M. (2013). Forskningsrapport: Fas 1 Geoteknik/MUR, Jernhusen, Region City., Chalmers tekniska högskola, Avd. Geologi och Geoteknik, Göteborg. (In Swedish)

Yin, Z.-Y. and Karstunen, M. (2011). Modelling strain-rate-dependency of natural soft clays combined with anisotropy and destructuration Acta Mechanica Solida Sinica 24(3), pp. 216-230.

Zentar, R., Karstunen, M. and Wheeler, S. J. (2002). Influence on anisotropy and destructuration on undrained shearing of natural clays. 5th European Conference on Numerical Methods in Geotechnical Engineering (NUMGE 2002), Paris, ENPC/LCPC Press, pp. 21-26.

Appendix A.1

Evaluation of parameters from drained triaxial tests.

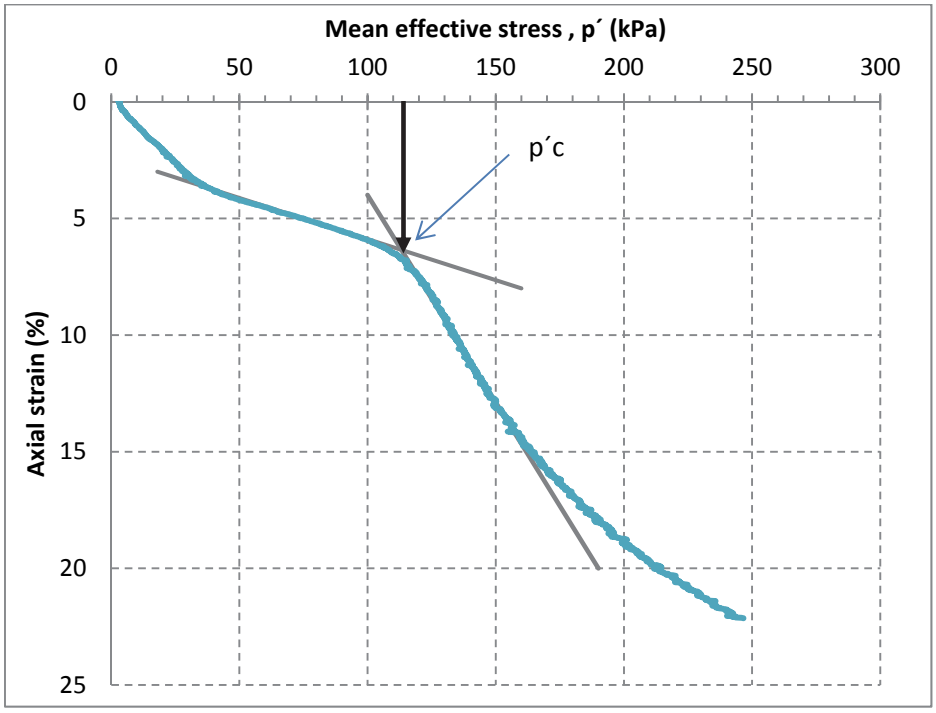

Figure A.1.1. Description on how to evaluate the p´c value with respect to axial strain.

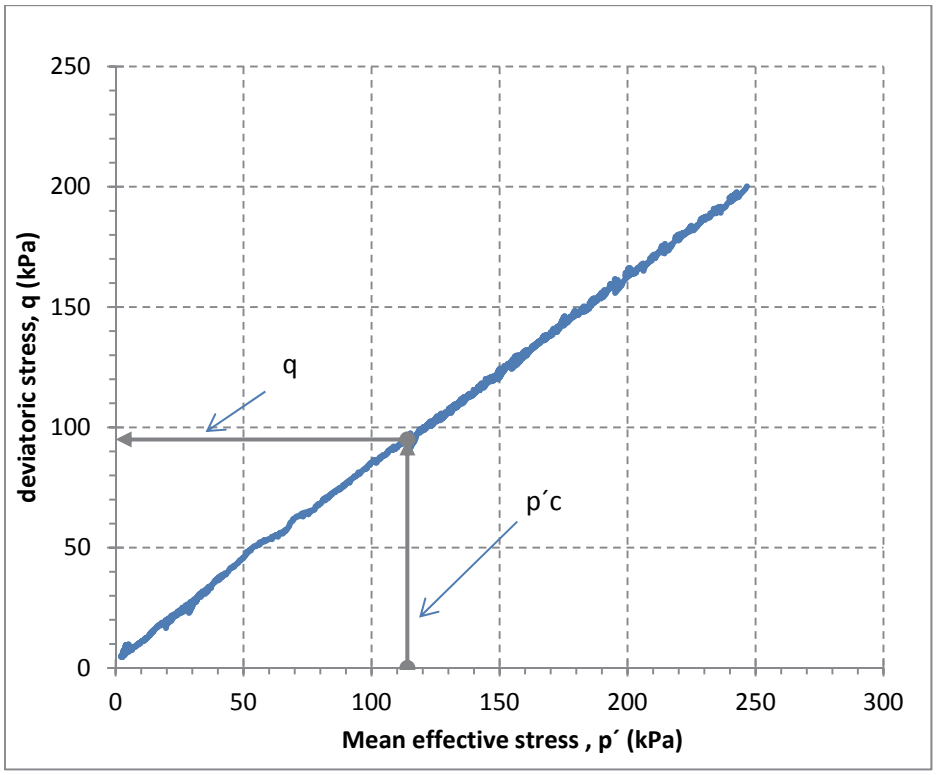

Figure A.1.2. Description on how to evaluate the q value with respect to p´c value.)c